LA-10114-PR
Progress Report

Los Alamos National Laboratory is operated by the University of California for the United States Department of Energy under contract W-7405-ENG-36.

Radiation Transport

October 1, 1982—March 31, 1983

Los Alamos Los Alamos National Laboratory
Los Alamos, New Mexico 87545

The four most recent reports in this series, unclassified, are LA-9336-PR, LA-9451-PR, LA-9533-PR, and LA-9629-PR.

LA-10114-PR
Progress Report

UC-80
Issued: May 1984

Radiation Transport

October 1, 1982—March 31, 1983

R. D. O'Dell

Los Alamos National Laboratory
Los Alamos, New Mexico 87545

CONTENTS

ABSTRACT 1

I. INTRODUCTION 1

II FISSION REACTOR NEUTRONICS 2

A. ONEDANT Code Release (F. W. Brinkley and D. R. Marr) 2
B. ONEDANT/TWODANT Input Module Improvements (F. W. Brinkley, D. R. Marr, and R. D. O'Dell) 3
C. ONEDANT/TWODANT Improvements (D. R. Marr) 4
D. TWODANT Code Improvements (D. R. Marr and F. W. Brinkley) 4
E. Validation Testing of the Preliminary Production Version of TWODANT (D. R. McCoy) 6
F. Export of TWODANT to Argonne National Laboratory (F. W. Brinkley, Jr.) 12
G. DIF3D Implementation at Los Alamos (F. W. Brinkley, Jr., and D. R. McCoy) 14
H. TWOHEX Development (W. F. Walters) 14

III. DETERMINISTIC TRANSPORT METHODS 19

A. Diffusion Synthetic Acceleration for the Diamond Differenced Discrete Ordinates Equation in Spherical Geometry (R. E. Alcouffe and E. W. Larsen) 19
B. A Linear Discontinuous Scheme for the Two-Dimensional General Geometry Transport Equation (R. E. Alcouffe) 28
C. Rapidly Converging Iterative Methods for Numerical Transport Problems (E. W. Larsen) 35
D. Modified One-Group Acceleration of the Frequency-Dependent Diffusion Equation (E. W. Larsen) 41
E. A Modal Acceleration Method for Frequency-Dependent Diffusion Equations (E. W. Larsen) 44
F. Behavior of DSA Methods for Time-Dependent Transport Problems with Unaccelerated Diffusion Iterations (E. W. Larsen) 55
G. New Diffusion-Synthetic Acceleration Strategies for Frequency-Dependent Transport Equations (E. W. Larsen) 59
H. Thermal Radiation Transport (B. A. Clark) 66
I. A Sharper Version of the Cauchy-Schwarz Inequality for Real-Valued Functions (E. W. Larsen) 67

IV. MONTE CARLO RADIATION TRANSPORT 72

A. MCNP Version 3 (T. N. K. Godfrey) 72
B. Portability Techniques used in MCNP Version 3 (T. N. K. Godfrey) 73
C. MCNP Version 3 Implementation (J. T. West) 76
D. MCNP, A New Surface Source Capability (J. T. West) 77
E. Generalization of MCNP Standard Sources (R. G. Schrandt) 83
F. A New Biasing Technique for MCNP (T. E. Booth) 83
G. A New Weight Window Generator for MCNP (T. E. Booth) 84

CONTENTS (cont)

H. Cyltran Calculations for Two Electron-Gamma Converters (H. G. Hughes and J. M. Mack) 87
I. MCMG Update (D. G. Collins and W. M. Taylor) 88
J. MCMG Utilization and Adjoint Calculations (D. G. Collins) 92
K. Total Gamma-Ray Yield Detector (D. G. Collins) 92
L. 3D Graphics (CONPAR) (J. C. Ferguson) 93
M. Sampling from a Cumulative Probability Distribution (R. G. Schrandt) 93
N. MCNP Testing (J. F. Briesmeister) 96

V. CROSS SECTIONS AND PHYSICS 96

A. Compton Scattering of Photons from Electrons in Thermal (Maxwellian) Motion (J. J. Devaney) 96
B. Mean Energy of Compton Scattered Photons from Electrons in Thermal (Maxwellian) Motion. Heating (J. J. Devaney) 100

REFERENCES 103

RADIATION TRANSPORT

October 1, 1982 - March 31, 1983

by

R. D. O'Dell

ABSTRACT

Research and development progress in radiation transport by the Los Alamos National Laboratory's Group X-6 for the first half of FY 83 is reported. Included are tasks in the areas of Fission Reactor Neutronics, Deterministic Transport Methods, and Monte Carlo Radiation Transport.

I. INTRODUCTION

Research, development, and design analysis performed by Group X-6, Radiation Transport, of the Applied Theoretical Physics Division during the first half of FY 83 are described in this progress report. Included is the unclassified portion of programs in the Group funded by the U.S. Department of Energy (DOE). Our classified work is reported elsewhere. Some of the reported work was performed in direct support of other Laboratory Groups.

This report is organized into four sections: (i) Fission Reactor Neutronics, (ii) Deterministic Transport Methods, (iii) Monte Carlo Radiation Transport, and (iv) Cross Sections and Physics. Technical program management for these areas is provided by William L. Thompson, Group Leader for Group X-6, and by Associate Group Leaders R. Arthur Forster, R. Douglas O'Dell, and Patrick D. Soran.*

*Authors of individual task reports are listed in parentheses after each task title. Authors not in Group X-6 have their affiliation also noted. Readers are encouraged to contact these cognizant technical personnel directly for additional information or further published results.

Effective October 1, 1982, Group T-1, Transport and Reactor Theory, was joined with Group X-6, Radiation Transport. The progress reports previously provided by Group T-1 will no longer be published under the title of Transport and Reactor Theory, but will hereafter be included in the Group X-6 progress report entitled "Radiation Transport." Because of the transition in merging Groups T-1 and X-6 during FY 83, only two progress reports will be issued for FY 83 - each covering a six-month period. Commencing with FY 84, progress reports will be issued quarterly.

II. FISSION REACTOR NEUTRONICS

The Fission Reactor Neutronics effort in Group X-6 is involved in the development and testing of new reactor-oriented deterministic transport codes and methods; in existing code maintenance, improvement, and support; and in selected applications of our codes to civilian nuclear analysis problems.

We report our progress on the existing codes ONEDANT and TWODANT. Included are reports on the general release of ONEDANT to users world wide, on improvements to the ONEDANT/TWODANT input module, and on improvements to both the ONEDANT and TWODANT codes themselves. A report is provided on validation testing of the TWODANT code and on its subsequent release to Argonne National Laboratory (ANL) for trial usage. We also report on the implementation of the ANL diffusion code DIF3D at Los Alamos. Under our new code development effort, we report on progress in the development of the new triangular mesh code TWOHEX.

A. ONEDANT Code Release (F. W. Brinkley, Jr. and D. R. Marr)

The ONEDANT[1] code package for use on CDC-7600 computers was sent to the National Energy Software Center at Argonne and to the Radiation Shielding Information Center (RSIC) at Oak Ridge. A CDC-7600 version was also sent to Jim Morel at Sandia National Laboratories (Albuquerque) and a special version was sent to J. Stepanek at the Swiss Federal Institute for Reactor Research.

An IBM version of ONEDANT was sent to Cy Adams at Argonne National Laboratory (ANL). The code is now operational at ANL in both free-standing form and as part of the ARC system. A small number of changes in the code were required in implementing the code package in the IBM computing environment at ANL.

B. ONEDANT/TWODANT Input Module Improvements (F. W. Brinkley, D. R. Marr, and R. D. O'Dell)

A cross-section check has been added to the generalized input module used by ONEDANT and TWODANT.[2] Now, the run will be aborted if the input total cross section of an isotope is found to be zero. A void cross section (i.e. all cross sections zero) will, however, be accepted. This check applies only to those cases where the cross sections are from cards or card images; it does not apply to ISOTXS or GRUPXS.[3]

Two changes were made to the cross-section processing section of the input module to accommodate the processing of ISOTXS files as commonly specified at ANL. The first change generates the total cross section by summing the partial cross sections found on an ISOTXS. It is used only when the total cross section is not included on the ISOTXS file, a procedure normally used at ANL. The second change ensures that cross sections are balanced before they are passed to the solver module. If the input cross sections are not balanced, the code now modifies them within group scattering cross sections seen by the solver module so that balance is preserved. A warning message is provided for the user when this procedure is used.

The following additional changes have been made to the generalized Input Module:

- According to the standards set by the Committee on Computer Code Coordination,[3] the ISOTXS and GRUPXS files do not contain the 2L+1 factor in the higher order scattering cross sections. Prior to this time, the generalized input module always added the 2L+1 term to the cross sections that it provided to the solver module when the cross sections were from either ISOTXS or GRUPXS. It has now been found that there do exist ISOTXS files in which the 2L+1 term has erroneously been included. In order to properly process these nonstandard files, a new option has been added to the I2LP1 input variable. Setting it to minus one will force an override of the standard treatment allowing the scattering cross sections from nonstandard files to be properly passed on to the Solver Module.

- A bug was found in the GRUPXS cross-section processing. If the file had any isotope with a CHI matrix, the run would abort. Now the CHI matrix is properly skipped and processing continues.

- Additional CHI input is now allowed. Prior to this time, only the zone wide CHI specified in the Solver input (Block V) could be used. Now the file wide chi present on an ISOTXS or GRUPXS file will be used unless it is overridden by the zone wide CHI. Further, if the cross sections are from either ODNINP or XSLIB, a file wide vector CHI may be input in Block III using the CHIVEC= array. Again, this file wide chi can be overridden by the zone wide chi supplied in Block V.

- The geometry module can now write a standard GEODST file for the triangular geometries denoted by IGEOM=9 and NTRIAG either zero or one. These are both parallelogram domains with, respectively, a 120° or a 60° angle at the origin. This option is intended for use with the ANL code DIF3D and with the forthcoming Los Alamos code TWOHEX.

- In the mixing input, isotopes from the library are usually specified with a hollerith name. The name in the mixing input must correspond exactly, character by character, to the name on the library in order to be accepted. Some libraries contain leading blanks in the names; this forces the user to include those blanks in the mixing free field input by using quotes. This nuisance has been eliminated; now, the code strips leading blanks as it reads the names from the library and the quotes are no longer needed.

C. ONEDANT/TWODANT Improvements (D. R. Marr)

The cross-section print in both ONEDANT and TWODANT has been modified to indicate whether the 2L+1 Legendre expansion factor is included in the printed higher-order scattering cross sections. The printed cross sections are now also compatible with the original library form, that is, if the 2L+1 term was included on the original library, it is now included in the print and conversely.

D. TWODANT Code Improvements (D. R. Marr and F. W. Brinkley)

TWODANT has been modified to use the transport cross section from the ISOTXS file, when available. The transport cross section is used only to form the diffusion coefficient for the first diffusion calculation. The subsequent converged transport solution is independent of this transport cross section, but the change allows the first diffusion calculation to be compared with the results from diffusion theory codes.

Another inhomogeneous source option has been added to TWODANT. Users may now input an energy vector (spectrum) together with a single full spatial matrix with the resulting energy-space dependent source being the product of the energy spectrum and the spatial matrix.

The inhomogeneous source calculated capability in TWODANT was tested and validated by comparing several test problem runs with TWODANT-II results.

The input of the ZONES array in two-dimensional problems was changed to make the ZONES array a stringed array, i.e., ZONES (IM;JM). This makes the code consistent in the form of all two-dimensional input arrays.

An additional negative flux fixup test was added to the code at Dr. Alcouffe's suggestion. The test eliminated some convergence problems we had experienced with certain problems.

In the diffusion calculation portion of TWODANT we had previously used bit manipulations. We were quite concerned that such bit manipulations might cause exportability problems. With Dr. Alcouffe's assistance we were able to remove these manipulations with a resulting reduction in computational time.

It was observed that the generation of the source-to-group was relatively time consuming. An IF test was removed with a resultant 5% decrease in running time. In addition, it was noted that the source-to-group calculation involved a large number of SCM-LCM transfers. Recall that on the CDC-7600, a so-called two-level computer, there is a small fast core memory (SCM) and a rapid access large core memory (LCM). On IBM and CRAY computers there is no LCM but only a large fast core. Such computers are called single-level machines. To make such single-level machines appear like the two-level CDC-7600, a portion of fast core is used to simulate LCM. LCM-SCM data transfers are thus simulated by actually performing fast core to fast core transfers. Although such core-core transfers are actually unnecessary, this procedure simplifies the exporting of two-level computer codes to single-level computing environments. On the CRAY single-level machine, core-core transfers are extremely rapid and they essentially cost nothing. On IBM computers, however, core-core transfers can be quite costly. Since such transfers are, in fact, unnecessary on single-level computers we did some selective recoding so that on single-level computers, instead of effecting core-core transfers, we simply change the core pointers. Some 30-50% of our core-core transfers on single-level computers have been eliminated by using this pointer change procedure in portions of the source-to-group calculations.

The periodic dump procedure has been changed so that the user may input the time between dumps. The dumps are only of the scalar fluxes. We also modified the code so that the code shifts the dumps downward so that a maximum of the three most current dumps is in the local file space.

A new iteration monitor has been installed. It provides a print very similar to that from ONEDANT.

For adjoint problems, all printed output now shows the direct group number so that the user no longer needs to invert the group numbers printed in the output as was previously required.

In a major effort, TWODANT is undergoing a thorough internal overhaul. The goals are threefold:

- Eliminate the debris left from the development process.
- Make the code more amenable to future improvements.
- Improve the characteristics of the code that allows it to be used as a test bed for new 2-D discrete-ordinates methods.

Expanding on this last goal, the ONEDANT code system was originally conceived as a very modular one, one in which the flux calculation was isolated from the Input and Edit sections. The flux calculation was done in a section called the solver module. The goal was to be able to replace the Solver module with new Solver modules, using new or different methods, while minimizing changes to the Input and Edit portions of the code. This process was used successfully in the development of TWODANT. The 1-D Solver module of ONEDANT was replaced with a Solver module formed from the TWO-DA code. Now, we would like to extend this philosophy deeper into the 2-D Solver module so that installation of new spatial differencing methods would require minimal changes to areas outside of the innermost flux calculational areas. Very little of this internal overhaul should be apparent to the user.

E. Validation Testing of the Preliminary Production Version of TWODANT

(D. R. McCoy*)

As part of the TWODANT code validation effort, two problems were received from Argonne National Laboratory (ANL) for analysis. TWODANT is our new two-dimensional, time-independent, discrete-ordinates code using diffusion synthetic acceleration. The two problems were (i) an (x,y) geometry ZPPR

*Present address: Group X-5, Los Alamos National Laboratory.

Assembly 11 test problem and (ii) an (r,z) geometry heterogeneous core problem with a great deal of external structure which has been used at ANL to determine shielding requirements and detector responses. The problems were analyzed on the Los Alamos CRAY-I computers. Each of these problems and the results of our analysis are described below.

The ZPPR-11 model problem is a nine energy-group, (x,y) geometry model using a 60x120 spatial mesh. The geometry map of the problem is shown in Fig. 1. Several analyses were performed on this model problem and a summary of results is shown in Table I. The various runs shown in the table are (i) TWODANT S_4P_0 using vectorized line successive overrelaxation (LSOR) for the synthetic diffusion inner iterations and Chebyshev acceleration for the diffusion outer iterations with a very tight convergence criterion of $\varepsilon = 10^{-7}$, (ii) the same as (i) but with a convergence criterion of 10^{-5}, (iii) TWODANT S_4-P_0 with a convergence of 10^{-5} but using our multigrid (MG) method for solving the diffusion inner iterations (instead of LSOR) and with Chebyshev acceleration for the diffusion outer iterations, (iv) TWODANT diffusion calculation only using LSOR on the diffusion inner iterations, $\varepsilon = 10^{-5}$, (v) TWODANT diffusion calculation only using MG on the diffusion inner iterations, $\varepsilon = 10^{-5}$, and (vi) DIF3D[4] using vectorized LSOR on its inner iteration and Chebyshev acceleration on its outer iterations, $\varepsilon = 10^{-5}$.

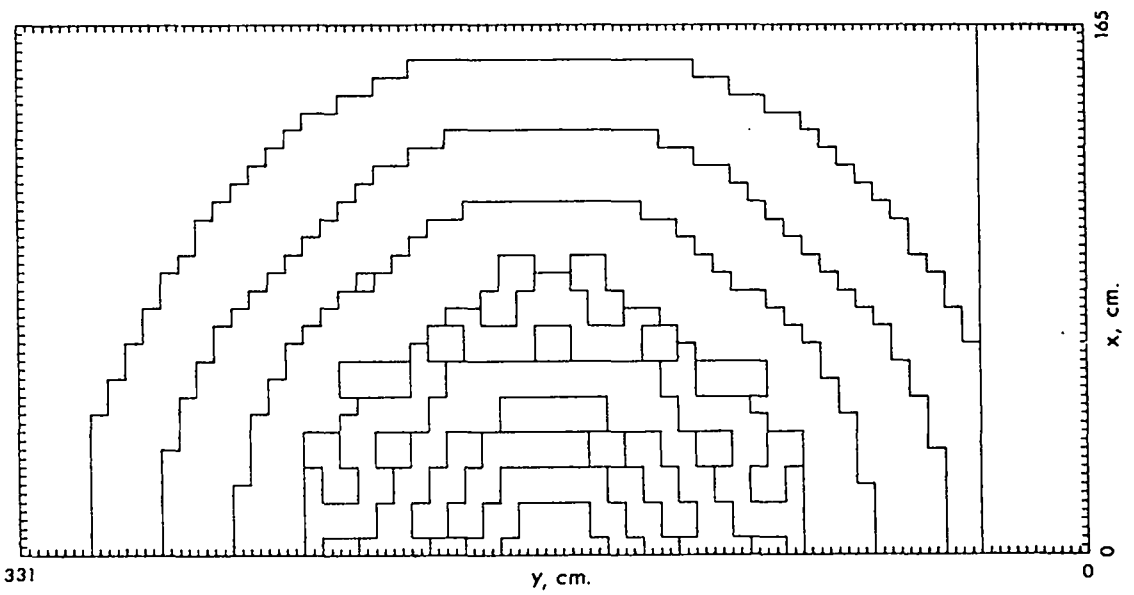

Fig. 1. ZPPR-11 model problem.

TABLE I

SUMMARY OF ZPPR-11 MODEL PROBLEM RESULTS

METHOD	k_{eff}	MAX. POINTWISE FISSION ERROR	NUMBER OF OUTER ITERATIONS		CRAY-I CPU TIME (Sec)
			TRANSPORT	DIFFUSION	
TWODANT[a] (LSOR) $\epsilon=10^{-7}$	0.981359	3.1×10^{-7}	10	161	434
TWODANT[a] (LSOR) $\epsilon=10^{-5}$	0.981359	3.1×10^{-5}	6	39	130
TWODANT[a] (MG) $\epsilon=10^{-5}$	0.981358	6.1×10^{-5}	6	42	112
TWODANT[b] DIFFUSION ONLY (LSOR)	0.970452	9.3×10^{-6}	-	31	53
TWODANT[b] DIFFUSION ONLY (MG)	0.970452	1.1×10^{-5}	-	39	31
DIF3D[c] DIFFUSION	0.976024	8.2×10^{-6}	-	22	46

[a] S_4-P_0

[b] $\epsilon=10^{-5}$

[c] $\epsilon=10^{-5}$, vectorized LSOR

Several observations can be made regarding the results shown in Table I. First, the eigenvalues from TWODANT (diffusion only) and DIF3D differ because the diffusion equation used in TWODANT solves a five-point vertex-differenced diffusion equation while DIF3D uses a five-point cell-centered difference equation. As the mesh spacing is refined, the difference in results from the two methods is reduced. A second observation is that running TWODANT with a very tight convergence, e.g., 10^{-7}, accomplishes little other than consuming much more computer time. The eigenvalues from the 10^{-5} and 10^{-7} are both identical to six significant figures, but the 10^{-7} run took nearly four times

longer than the 10^{-5} run. It is our general observation that because of the convergence controls extant in the preliminary version of TWODANT, any convergence criterion smaller than 10^{-5} constitutes overkill with very little practical improvement in accuracy but with substantial increases in computer run times. Next, we observe that the multigrid diffusion method gives the same results as the LSOR diffusion method. Although not indicated by the results of the ZPPR-11 analysis, the multigrid method can be markedly superior to the LSOR method in many problems, e.g., problems containing void cells. Finally, we note that on the Los Alamos CRAY-I computers, a full S_4-P_0 transport calculation can be effected on the ZPPR-11 problem in about three times the time required for a diffusion calculation. Historically, older two-dimensional transport calculations normally required perhaps 20 to 50 times as much computer time as diffusion calculations.

The successful analysis of the ZPPR Assembly 11 model problem with TWODANT fulfilled one of our DOE physics milestones for FY 1983.

The second ANL test problem is a heterogeneous core model in (r,z) geometry. The core is surrounded by a very large amount of sodium, steel, and structure, so that it is essentially a very deep penetration, shielding-type problem. The geometry map is shown in Fig. 2. The problem used 12 energy groups and a 104x195 spatial mesh. Even though the total number of mesh cells is over 20 000, the problem is still severely undermeshed. A summary of results is shown in Table II. The various runs whose results are shown are (i) TWODANT S_4-P_0 using vectorized LSOR and Chebyshev acceleration on the diffusion inner- and outer-iterations, respectively, with a convergence criterion $\varepsilon = 10^{-4}$, (ii) same as (i) but with multigrid acceleration on the diffusion inner iterations, (iii) TWODANT diffusion only with LSOR on the diffusion inner iterations, $\varepsilon = 10^{-5}$, (iv) same as (iii) but with MG on the diffusion inner iterations, and (iv) DIF3D diffusion with nonvectorized LSOR on the inner iterations, $\varepsilon = 10^{-5}$.

For this core-shielding problem, it is seen that the TWODANT diffusion only calculations ran significantly faster than the DIF3D diffusion calculation presumably due to the lack of vectorization in DIF3D for this problem analysis. The TWODANT MG diffusion only run was significantly faster than the TWODANT LSOR diffusion only calculation indicating the superior performance of the multigrid method over successive overrelaxation for accelerating the

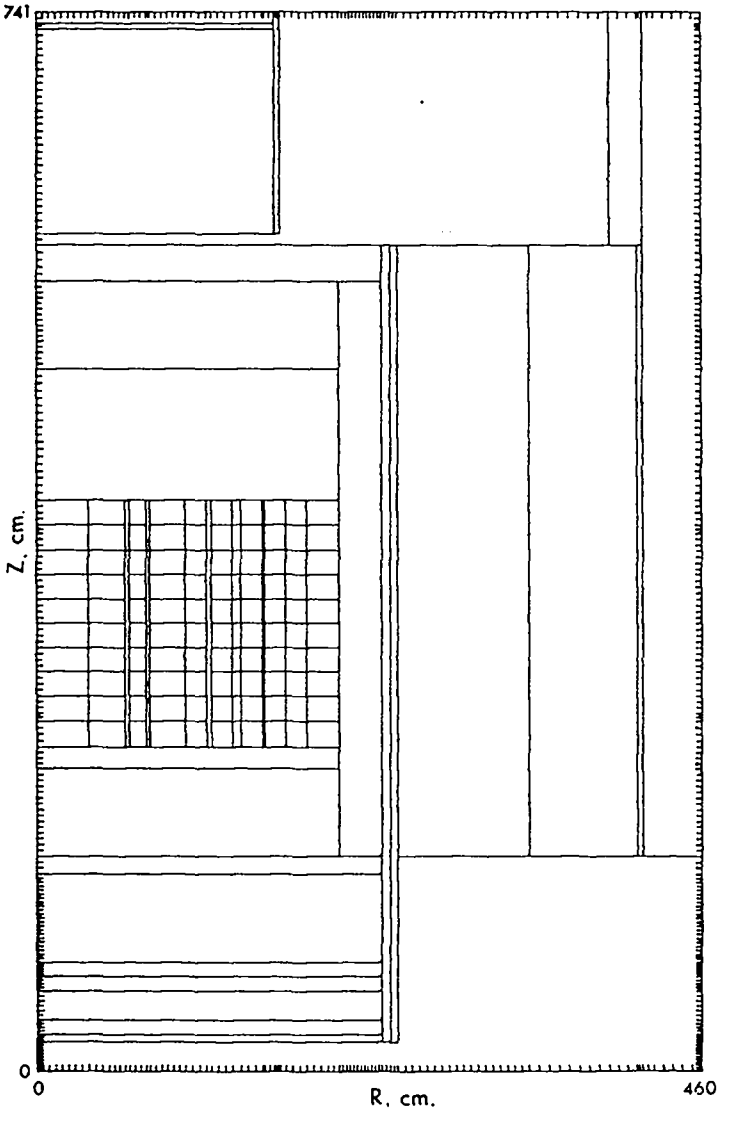

Fig. 2. Heterogeneous core-shielding model problem.

diffusion inner iterations. Just as in the ZPPR-11 analysis, the TWODANT diffusion k_{eff} value differs from the DIF3D diffusion k_{eff} value because of the different differencing schemes in the two codes. That this problem is severely undermeshed was evidenced by the fact that the diffusion analyses yielded negative scalar fluxes in several locations and also by the large difference in k_{eff} (1.8%) between the vertex-differenced and cell-centered-differenced diffusion results. Nevertheless, it was this meshing that was specified and that we used. The two transport calculations, S_4-P_0, using LSOR and MG on the diffusion acceleration inner iterations yielded k_{eff}

TABLE II

SUMMARY OF HETEROGENEOUS CORE - SHIELDING PROBLEM RESULTS

METHOD	k_{eff}	NUMBER OF OUTER ITERATIONS		CRAY-1 CPU TIME (Sec)
		TRANSPORT	DIFFUSION	
TWODANT[a] (LSOR)	1.04965	5	34	740
TWODANT[a] (MG)	1.04966	5	41	552
TWODANT[b] DIFFUSION ONLY (LSOR)	0.99635	-	25	150
TWODANT[b] DIFFUSION ONLY (MG)	0.99635	-	21	48
DIF3D[c] (DIFFUSION)	1.01466	-	21	602

[a] S_4-P_0, $\varepsilon = 10^{-4}$

[b] $\varepsilon = 10^{-5}$

[c] Nonvectorized LSOR, $\varepsilon = 10^{-5}$

values some 4-5% different than diffusion theory. The running time penalty for the MG transport calculation compared with the MG diffusion calculation was roughly a factor of 12 - much higher than the factor of 3 to 4 observed with the ZPPR-11 calculation. This large difference is probably explained by numerical difficulties associated with the coarse meshing used for the heterogeneous core-shielding problem and the manner in which iteration convergence is defined in TWODANT. Using the LSOR version of TWODANT the S_4-P_0 transport calculational time was 5 times that required for a diffusion only calculation. The absolute run times for the LSOR TWODANT, however, were considerably longer than the corresponding times for the MG version of TWODANT. Actually, the fact that the transport calculations held together and were successfully completed is remarkable due to the coarse meshing of the problem. This fact attests to the stability of the diffusion synthetic acceleration method as applied in TWODANT.

In conclusion, then, we have conducted validation tests on two problems provided by ANL using preliminary production versions of TWODANT. The tests showed that the diffusion acceleration employed in TWODANT is an effective method and the transport calculations can be performed with TWODANT with much more acceptable time penalties relative to diffusion calculations. Further, the validation tests have confirmed our feelings that the use of the multigrid method on the diffusion acceleration inner-iterations is more stable and as fast or faster than the use of line successive overrelaxation.

F. Export of TWODANT to Argonne National Laboratory (F. W. Brinkley, Jr.)

At the request of Argonne National Laboratory (ANL), it was agreed to provide them with a preliminary production version of our two-dimensional, time-independent, diffusion synthetic accelerated, discrete-ordinates code TWODANT. It was also agreed that TWODANT would be validated prior to shipping by using the code to calculate two test problems to be provided by ANL. These problems were subsequently received and the test calculations performed successfully with TWODANT. The results of this validation testing are reported in Sec. II.E of this progress report.

As a result of our validation testing, it was decided to drop further development of our regular TWODANT which used a line successive overrelaxation (LSOR) technique on the diffusion inner iteration and, instead, to focus our attention on our version of TWODANT which used the multigrid (MG) method on the diffusion inner iterations. This multigrid version of TWODANT was thus selected for exporting to ANL.

Since the code is used on the CRAY-1 and CDC-7600 computers at Los Alamos, the preparation of TWODANT for use in ANL's IBM Computing environment required that the code be processed to create an IBM-compatible version. Our prior experience with exporting ONEDANT to ANL proved very valuable in converting our CRAY/CDC-7600 version to an IBM version.

Since both ONEDANT and TWODANT use the same Input and Edit Modules and differ only in their Solver Modules, C. H. Adams of ANL requested that both Solver Modules be combined into a single overall ONEDANT/TWODANT code package for ANL. This was done and the package transmitted to Argonne where it was readily compiled with only a few minor changes.

Upon execution of the code package at ANL, however, a subtle but serious problem was uncovered which took several days to uncover and correct. The

problem was traced to the fact that the IBM compiler passes arguments by value if the argument is not thought to be an array. The problem can be illustrated by example.

```
CALL MULTIG (A(LIX))
.
.
.
END
SUBROUTINE MULTIG (IX)
[DIMENSION IX(1)]
.
.
.
CALL MULT (IX)
.
.
.
END
SUBROUTINE MULT (IX)
DIMENSION IX(1)
.
.
.
END
```

In our typical Los Alamos coding, the statement DIMENSION IX(1) enclosed in [ ] in subroutine MULTIG is not required and thus was not present. Without this statement in an IBM environment, however, the following occurs. When subroutine MULTIG is called, the address of A(LIX) is passed to the subroutine as IX. When subroutine MULT is called from MULTIG, IX has not been defined as an array so the IBM Compiler passes the value of IX to MULT instead of the address of IX. Subroutine MULT then tries to use the value of IX as an address which is totally incorrect. All that needed to be done to correct this is add the DIMENSION IX(1) statement indicated in brackets to MULTIG. Several routines in our TWODANT Solver Module had to be corrected in this manner.

Once this problem was corrected, the ONEDANT/TWODANT package executed properly at ANL. The package is now being used as a production test at Argonne.

G. DIF3D Implementation at Los Alamos (F. W. Brinkley, Jr., and D. R. McCoy*)

During this reporting period an improved CRAY version of the Argonne National Laboratory diffusion code DIF3D[4] was received and made operational on our Los Alamos CRAY-1 computers. The implementation also included the introduction of graphics with DIF3D under DISSPLA. Only a few minor problems were encountered in making the code operational, and these were readily corrected.

H. TWOHEX Development (W. F. Walters)

Three test problems have been analyzed using both the DITRI scheme as implemented in the code THREETRAN (hex,z)[5] and the triangular linear characteristic (TLC) scheme as implemented in the code TWOHEX which is still under development. The first two problems are simple one-group problems used to test the accuracy and rate of convergence of the TLC method. The third problem is a four-group problem described in Ref. 6. This problem is used to examine the effect of Chebyshev acceleration on outer iterations.

The first problem is a simple one-energy group problem. The domain is the hexagon shown in Fig. 3. The cross sections are also indicated in this figure.

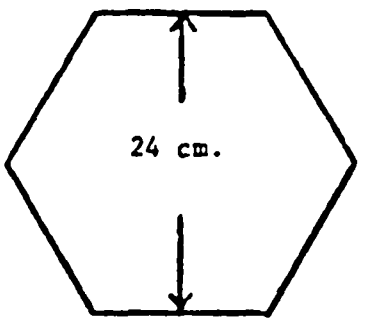

$$\frac{\Sigma_a}{0.1} \quad \frac{\nu\Sigma_f}{0.03} \quad \frac{\Sigma_T}{0.15} \quad \frac{\Sigma_s}{0.14}$$

Fig. 3. Test problem 1.

*Present address: Group X-5, Los Alamos National Laboratory.

The graph in Fig. 4 indicates the manner in which the eigenvalue converges as the size of the triangles in the mesh is reduced. The height of a triangle in the mesh starts at 6 cm and is reduced as indicated. From the graph it is quite clear that the TLC scheme is far superior to the DITRI scheme in terms of accuracy. Table III indicates that the TLC results are converged while the DITRI eigenvalue has not yet converged. Of course, this is a severe high leakage test problem and is simply used to test the methods. The problem is not meant to be characteristic of a reactor core.

Notice that these schemes do not converge to the same result for this problem. This is due to the fact that the THREETRAN (hex,z) code and the TWOHEX code use different quadrature sets. The THREETRAN (hex,z) code uses the 90° rotationally invariant set used by TWOTRAN-II code.[7] The TWOHEX code uses a 60° rotationally invariant Tschebyschev-Legendre set first described by Carlson[8] and used in the DIAMANT2 code.[9] The DITRI result is obtained using the S6 quadrature with 24 directions total. The TLC result is obtained by

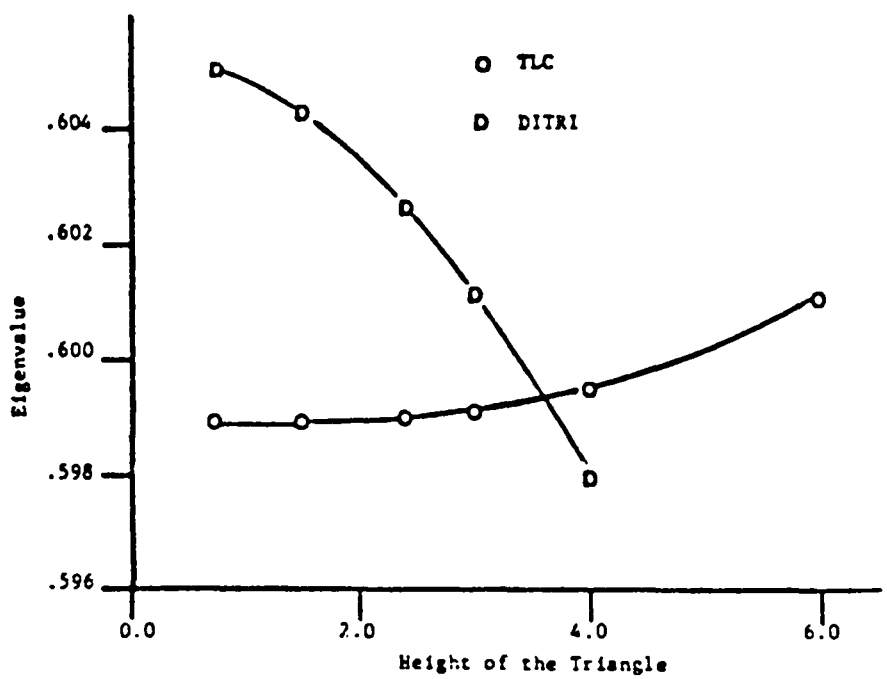

Fig. 4. Eigenvalue as a function of mesh size.

TABLE III

EIGENVALUE COMPARISON

Mesh Size (Height of Triangle) cm	Eigenvalue DITRI S6	Eigenvalue TLC S4 Rectangular
12.00	0.53983	0.62363
6.00	0.58919	0.60111
4.50	0.59796	0.59950
3.00	0.60115	0.59912
2.40	0.60265	0.59900
1.50	0.60424	0.59891
0.75	0.60501	0.59890

using a rectangular S4 set (2 points on each z-direction cosine level). This S4 set also has 24 directions. Additional results indicate that these two sets are converging to the same result as the number of discrete directions is increased.

The second test problem has been used before to test numerical schemes. The geometric configuration for this problem is shown in Fig. 5. Region I is a highly scattering region with a source density of unity and surrounds the almost "black" central region II. The mesh for the second problem is 20 triangles long by 10 triangles high. In region II the side of a triangle is 5 mean free paths. The plot shown in Fig. 6 indicates that the TLC method is much more positive than the DITRI method. No fixup of any kind is used in either of the schemes. The negative fluxes appearing in the TLC plot are so small that they are not apparent in the graph. This plot is along triangle band number 5. This problem was analyzed using the same quadrature set as in the first problem.

The third test problem is problem 1 of Ref. 6. The geometry and material composition is shown in Fig. 7. This problem was run with six triangles per hexagon. The S4 quadrature set with 24 directions was used. It was found that

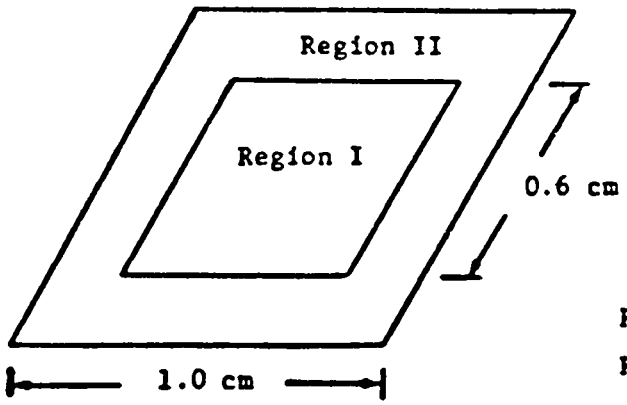

	S	Σ_a	Σ_t	Σ_s
Region I:	0.0	100.0	100.0	0.0
Region II:	1.0	0.05	1.0	0.95

Fig. 5. Test problem 2.

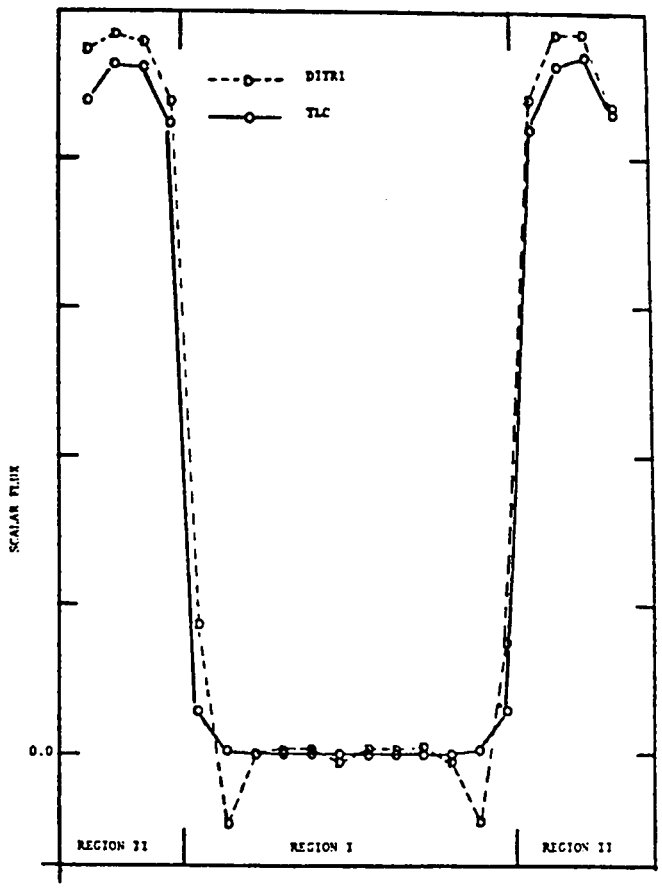

Fig. 6. Cell average scalar flux as a function of position.

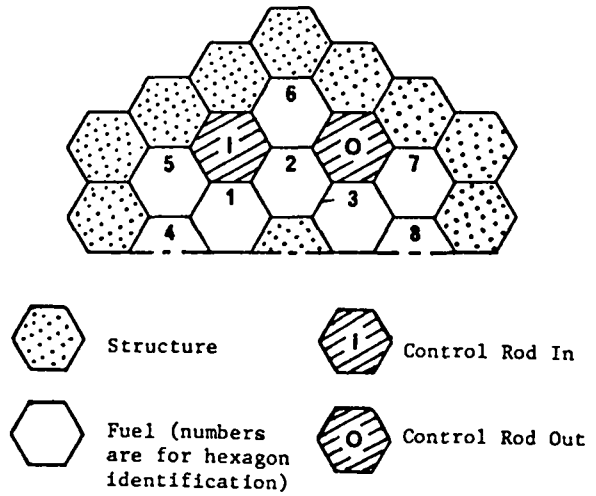

Fig. 7. Two-dimensional problem 3.

the number of outer integrations was reduced from 11 to 9 when three term Chebyshev acceleration method similar to that described in Ref. 4 was used to accelerate the fission source. The theoretical limit for the reduction of outer iterations using this method is reduction by a factor of two. In this problem relatively few outer iterations are required even without acceleration. This happens because the dominance ratio is about 0.7 for this "high leakage" system.

For some of the systems analyzed in Ref. 4 the dominance ratio is closer to unity and the number of outers is reduced by a factor of almost 2. For a full sized LMFBR the dominance ratio will be closer to unity, and it is expected that Chebyshev acceleration of the outer iterations will result in a much larger percentage reduction in the number of outer iterations.

This type of acceleration was used due to the ease with which it could be inserted into the code. No changes were required in the inner "sweeping" routines at all. In the next quarter Chebyshev acceleration will be added for the inner iterations. Again, this acceleration will require no changes in the sweeping routines. It is expected that this additional acceleration will significantly reduce the number of inner iterations.

Additional work this quarter will include testing P1 scattering on the TWOHEX code and adding the one-third core boundary conditions. At present TWOHEX accepts only whole core problems.

III. DETERMINISTIC TRANSPORT METHODS

Our work in Group X-6 on deterministic transport methods involves the development, implementation, and assessment of both analytical and numerical methods and models to aid the advancement of deterministic transport code development.

This reporting period we report on our progress in developing a diffusion synthetic acceleration scheme for the diamond differenced discrete ordinates equation in spherical geometry. This is followed by a report on a linear discontinuous scheme for the general two-dimensional geometry transport equation. Next we report on rapidly converging iterative methods for numerical transport problems. As part of our thermal radiation transport methods development effort, we present reports on modified one-group acceleration of the frequency-dependent diffusion equation, a modal acceleration method for frequency-dependent diffusion equations, the behavior of DSA methods for time dependent transport problems, and new diffusion-synthetic acceleration strategies for frequency-dependent transport equations. Next is a report on calculational results from a test code that solves the thermal radiation transport equation using discrete-ordinates methods. We conclude this section with a report on a sharper version of the Cauchy-Schwarz inequality for real-valued functions.

A. Diffusion Synthetic Acceleration for the Diamond Differenced Discrete Ordinates Equation in Spherical Geometry (R. E. Alcouffe and E. W. Larsen)

The development of the unconditionally stable diffusion-synthetic acceleration (DSA) method for the diamond-differenced discrete ordinates equations has been described fully in one-dimensional slab geometry,[10,11] and also in x,y-geometry.[10] However, the method has never been discussed for curvilinear geometries, where extra considerations involving treatment of the angular redistribution terms occur. Therefore, we shall now describe the DSA method for the one-group, spherical geometry discrete ordinates equation.

We consider a sphere $0 \leq r \leq R$, divided spatially into I concentric shells, $r_{i-1/2} < r < r_{i+1/2}$, with $r_{1/2} = 0$ and $r_{I+1/2} = R$. We also consider any standard, even-order Gauss-Legendre quadrature set on the interval $-1 \leq \mu \leq 1$; the quadrature points are μ_m and the corresponding weights w_m are normalized so that

$$\sum_{m=1}^{N} \mu_m^j w_m = \frac{[1 + (-1)^j]}{j + 1} \quad , \; j = 0,1,2. \tag{1}$$

In addition, we define the angular cell edges $\mu_{m+1/2}$ by

$$\mu_{m+1/2} = -1 + \sum_{n=1}^{m} w_m \quad , \; 0 \leq m \leq N. \tag{2}$$

Then for $1 \leq m \leq N$, the m-th angular cell is $\mu_{m-1/2} < \mu < \mu_{m+1/2}$, and μ_m lies within this cell (but normally not at the center). From Eq. (2) we have

$$w_m = \mu_{m+1/2} - \mu_{m-1/2} \quad , \tag{3a}$$

$$\mu_{1/2} = -1 \quad , \tag{3b}$$

and

$$\mu_{N+1/2} = +1 \quad . \tag{3c}$$

Finally, we define

$$A_{i+1/2} = 4\pi r_{i+1/2}^2 \quad , \tag{4a}$$

$$V_i = \frac{4\pi}{3} \left(r_{i+1/2}^3 - r_{i-1/2}^3\right) \quad , \tag{4b}$$

$$\alpha_{m+1/2,i} = - \left(A_{i+1/2} - A_{i-1/2}\right) \sum_{n=1}^{m} \mu_n w_n \quad , \; 0 \leq m \leq N, \tag{5}$$

and constants τ_m according to two separate definitions:

$$\tau_m = \begin{cases} 0 & \text{(diamond difference)} \\ \dfrac{\mu_m - \frac{1}{2}(\mu_{m+1/2} + \mu_{m-1/2})}{w_m} & \text{(Morel-Montry}^{12}\text{)} \end{cases} . \tag{6}$$

Later we shall discuss the differences between these two definitions. We note that the constants $\alpha_{m+1/2,i}$ satisfy

$$\alpha_{1/2,i} = 0 \quad , \tag{7a}$$

$$\alpha_{N+1/2,i} = 0 \quad , \tag{7b}$$

and are symmetric functions of angle:

$$\mu_{m+1/2} = -\mu_{n+1/2} \rightarrow \alpha_{m+1/2,i} = \alpha_{n+1/2,i} \quad . \tag{7c}$$

The one-group, spherical geometry discrete ordinates equations can now be written as

$$\mu_m \left(A_{i+1/2}\, \psi^{\ell+1/2}_{m,i+1/2} - A_{i-1/2}\, \psi^{\ell+1/2}_{m,i-1/2}\right) + \frac{1}{w_m}\left(\alpha_{m+1/2,i}\, \psi^{\ell+1/2}_{m+1/2,i} - \alpha_{m-1/2,i}\, \psi^{\ell+1/2}_{m-1/2,i}\right) + (\sigma_T V)_i\, \psi^{\ell+1/2}_{mi} = (\sigma_s V)_i\, \phi^{\ell}_{0i} + (VS)_i \quad , \tag{8a}$$

$$\psi^{\ell+1/2}_{mi} = \frac{1}{2}\left(\psi^{\ell+1/2}_{m,i+1/2} + \psi^{\ell+1/2}_{m,i-1/2}\right) \quad , \tag{8b}$$

$$\psi^{\ell+1/2}_{mi} = \frac{1+\tau_m}{2}\, \psi^{\ell+1/2}_{m+1/2,i} + \frac{1-\tau_m}{2}\, \psi^{\ell+1/2}_{m-1/2,i} \quad . \tag{8c}$$

In the analysis here we shall not be concerned with boundary conditions at r=0 or R, or with a starting direction calculation; our primary interest is just in the discretized transport equation described by Eqs. (8). In these equations, ℓ or $\ell+1/2$ denotes an iteration superscript. We assume that ϕ^{ℓ}_{0i} is known, we solve Eqs. (8) for $\psi^{\ell+1/2}_{mi}$, and we wish to construct equations for determining $\phi^{\ell+1/2}_{0i}$.

With the definition

$$\phi_{0i}^{\ell+1/2} = \frac{1}{2} \sum_{m=1}^{N} \phi_{mi}^{\ell+1/2} \, w_m \quad , \tag{9}$$

the standard source-iteration method uses the following prescription:

$$\phi_{0i}^{\ell+1} = \phi_{oi}^{\ell+1/2} \quad . \tag{10}$$

The DSA method does not use Eq. (10); instead, more complicated (but ultimately, more efficient) equations are developed which have the property that the exact solution is computed in one iteration if the angular flux is a linear function of μ. To derive these equations, we operate on Eq. (8a) by the operators

$$\frac{1}{2} \sum_{m=1}^{N} \mu_m^j \, (\cdot) \, w_m \quad , \; j = 0,1, \tag{11}$$

use the definitions

$$\phi_n^{\ell+1/2} = \frac{1}{2} \sum_{m=1}^{N} P_n(\mu_m) \, \phi_m^{\ell+1/2} \, w_m \quad , \; n=0,1,2, \tag{12}$$

and obtain the two equations

$$A_{i+1/2} \, \phi_{1,i+1/2}^{\ell+1/2} - A_{i-1/2} \, \phi_{1,i-1/2}^{\ell+1/2} + (\sigma_T V)_i \, \phi_{0i}^{\ell+1/2} = (\sigma_s V)_i \, \phi_{0i}^{\ell}$$

$$+ (VS)_i \quad , \tag{13}$$

$$\frac{2}{3}\left(A_{i+1/2} \, \phi_{2,i+1/2}^{\ell+1/2} - A_{i-1/2} \, \phi_{2,i-1/2}^{\ell+1/2}\right)$$

$$+ \frac{1}{3} \left(A_{i+1/2} \, \phi_{0,i+1/2}^{\ell+1/2} - A_{i-1/2} \, \phi_{0,i-1/2}^{\ell+1/2}\right) + \frac{1}{2} \sum_{m=1}^{N} \mu_m$$

$$\times \left(\alpha_{m+1/2,i}\ \phi^{\ell+1/2}_{m+1/2,i} - \alpha_{m-1/2,i}\ \phi^{\ell+1/2}_{m-1/2,i}\right) w_m + (\sigma_T V_i)\phi^{\ell+1/2}_{1i} = 0 \quad . \tag{14}$$

Now, using Eq. (7), we have

$$\frac{1}{2}\sum_{m=1}^{N} \mu_m \left(\alpha_{m+1/2,i}\ \phi^{\ell+1/2}_{m+1/2,i} - \alpha_{m-1/2,i}\ \phi^{\ell+1/2}_{m-1/2,i}\right) w_m$$

$$= -\frac{1}{2}\sum_{m=1}^{N-1} \left(\mu_{m+1} - \mu_m\right) \alpha_{m+1/2,i}\ \phi^{\ell+1/2}_{m+1/2,i}\ w_m$$

$$= \left[-\frac{1}{2}\sum_{m=1}^{N-1} \left(\mu_{m+1} - \mu_m\right) \alpha_{m+1/2,i}\ w_m\right] \phi^{\ell+1/2}_{0i}$$

$$+ \frac{1}{2}\sum_{m=1}^{N-1} \left(\mu_{m+1} - \mu_m\right) \alpha_{m+1/2,i} \left(\phi^{\ell+1/2}_{0i} - \phi^{\ell+1/2}_{m+1/2,i}\right) w_m \quad . \tag{15}$$

Also, using Eqs. (1) and (5), we have

$$-\frac{1}{2}\sum_{m=1}^{N-1} \left(\mu_{m+1} - \mu_m\right) \alpha_{m+1/2,i}\ w_m$$

$$= \frac{A_{i+1/2} - A_{i-1/2}}{2} \sum_{m=1}^{N-1}\sum_{n=1}^{m} \left(\mu_{m+1} - \mu_m\right) \mu_n w_n$$

$$= \frac{A_{i+1/2} - A_{i-1/2}}{2} \sum_{n=1}^{N-1}\sum_{m=n}^{N-1} \left(\mu_{m+1} - \mu_m\right) \mu_n w_n$$

$$= \frac{A_{i+1/2} - A_{i-1/2}}{2} \sum_{n=1}^{N-1} \left(\mu_N - \mu_n\right) \mu_n w_n = -\frac{A_{i+1/2} - A_{i-1/2}}{3} \quad . \tag{16}$$

Combining Eqs. (14, (15), and (16), we get

$$\frac{1}{3}\left(A_{i+1/2}\,\phi^{\ell+1/2}_{0,i+1/2} - A_{i-1/2}\,\phi^{\ell+1/2}_{0,i-1/2}\right) - \frac{1}{3}\left(A_{i+1/2} - A_{i-1/2}\right)\phi^{\ell+1/2}_{0i}$$

$$+ (\sigma_T V)_i\,\phi^{\ell+1/2}_{1i} = -\frac{2}{3}\left(A_{i+1/2}\,\phi^{\ell+1/2}_{2,i+1/2} - A_{i-1/2}\,\phi^{\ell+1/2}_{2,i-1/2}\right)$$

$$-\frac{1}{2}\sum_{m=1}^{N-1}(\mu_{m+1} - \mu_m)\,\alpha_{m+1/2,i}$$

$$\times\left(\phi^{\ell+1/2}_{oi} - \phi^{\ell+1/2}_{m+1/2,i}\right) w_m \quad . \tag{17}$$

In addition, operating on Eq. (8b) by the operators in Eq. (11), we obtain

$$\phi^{\ell+1/2}_{ji} = \frac{1}{2}\left(\phi^{\ell+1/2}_{j,i+1/2} + \phi^{\ell+1/2}_{j,i-1/2}\right) \quad . \tag{18}$$

Eqs. (13), (17), and (18) are exactly solved by the solution $\phi^{\ell+1/2}$ of Eq. (8). We define acceleration equations from Eqs. (13), (17), and (18) by

$$A_{i+1/2}\,\phi^{\ell+1}_{1,i+1/2} - A_{i-1/2}\,\phi^{\ell+1}_{1,i-1/2} + (\sigma_R V)_i\,\phi^{\ell+1}_{0i} = (VS)_i \quad , \tag{19a}$$

$$\frac{1}{3}\left(A_{i+1/2}\,\phi^{\ell+1}_{0,i+1/2} - A_{i-1/2}\,\phi^{\ell+1}_{0,i-1/2}\right) - \frac{1}{3}\left(A_{i+1/2} - A_{i-1/2}\right)\phi^{\ell+1}_{0i}$$

$$+ (\sigma_T V)\,\phi^{\ell+1}_{1i} = -\frac{2}{3}\left(A_{i+1/2}\,\phi^{\ell+1/2}_{2,i+1/2} - A_{i-1/2}\,\phi^{\ell+1/2}_{2,i-1/2}\right)$$

$$-\frac{1}{2}\sum_{m=1}^{N-1}(\mu_{m+1} - \mu_m)\,\alpha_{m+1/2,i}\left(\phi^{\ell+1/2}_{0i} - \phi^{\ell+1/2}_{m+1/2,i}\right) w_m \quad , \tag{19b}$$

$$\phi^{\ell+1}_{ji} = \frac{1}{2}\left(\phi^{\ell+1}_{j,i+1/2} + \phi^{\ell+1}_{j,i-1/2}\right) \quad , \; j = 0,1, \tag{19c}$$

where

$$\sigma_R = \sigma_T - \sigma_s \quad . \tag{20}$$

These equations have the following properties:

(i) They agree with Eqs. (13), (17), and (18) upon convergence.

(ii) If the cell edge fluxes are linear in angle in the following senses:

$$\psi^{\ell+1/2}_{m,i+1/2} = \phi^{\ell+1/2}_{0,i+1/2} + 3\mu_m \phi^{\ell+1/2}_{1,i+1/2} \quad , \tag{21a}$$

$$\psi^{\ell+1/2}_{m+1/2,i} = \phi^{\ell+1/2}_{0i} + 3\mu_{m+1/2} \phi^{\ell+1/2}_{1i} \quad , \tag{21b}$$

then the "$\ell+1/2$" terms [on the right side of Eq. (19b)] vanish and Eq. (19) becomes four equations which exactly determine

$$\phi^{\ell+1}_{0,i+1/2}, \ \phi^{\ell+1}_{1,i+1/2}, \ \phi^{\ell+1}_{0i} \ \phi^{\ell+1}_{1i} \quad .$$

To rewrite the acceleration equations in a more computationally useful form, we define

$$f^{\ell+1} = \phi^{\ell+1} - \phi^{\ell+1/2} \tag{22}$$

and subtract Eqs. (13), (17), and (18) from (19a,b,c) to obtain

$$A_{i+1/2} f^{\ell+1}_{1,i+1/2} - A_{i-1/2} f^{\ell+1}_{1,i-1/2} + (\sigma_R V)_i f^{\ell+1}_{0i}$$

$$= (\sigma_s V)_i \left(\phi^{\ell+1/2}_{0i} - \phi^{\ell}_{0i}\right) \quad , \tag{23a}$$

$$\frac{1}{3}\left(A_{i+1/2} f^{\ell+1}_{0,i+1/2} - A_{i-1/2} f^{\ell+1}_{0,i-1/2}\right) - \frac{1}{3}\left(A_{i+1/2} - A_{i-1/2}\right) f^{\ell+1}_{0i}$$

$$+ (\sigma_T V)_i \, f^{\ell+1}_{1i} = 0 \quad , \tag{23b}$$

$$f^{\ell+1}_{ji} = \frac{1}{2}\left(f^{\ell+1}_{j,i+1/2} + f^{\ell+1}_{j,i-1/2}\right) \quad , \ j = 0,1. \tag{23c}$$

Now we reduce these equations to a single (edge-differenced diffusion) equation for $f^{\ell+1}_{0,i+1/2}$. To do this, we first introduce Eqs. (23c) into (23a) and (23b) to eliminate $f^{\ell+1}_{ni}$, and then we manipulate the resulting two equations over two adjacent cells in a straightforward manner; this results in

$$-\frac{1}{3}\frac{A_{i+3/2}}{(\sigma_T V)_{i+1}}\left(f^{\ell+1}_{0,i+3/2}-f^{\ell+1}_{0,i+1/2}\right)+\frac{1}{3}\frac{A_{i-1/2}}{(\sigma_T V)_i}\left(f^{\ell+1}_{0,i+1/2}-f^{\ell+1}_{0,i-1/2}\right)$$

$$+\frac{1}{2}\frac{(\sigma_R V)_{i+1}}{A_{i+3/2}+A_{i+1/2}}\left(f^{\ell+1}_{0,i+3/2}+f^{\ell+1}_{0,i+1/2}\right)+\frac{1}{2}\frac{(\sigma_R V)_i}{A_{i+1/2}+A_{i-1/2}}$$

$$\times\left(f^{\ell+1}_{0,i+1/2}+f^{\ell+1}_{0,i-1/2}\right)=\frac{(\sigma_s V)_{i+1}}{A_{i+3/2}+A_{i+1/2}}\left(\phi^{\ell+1/2}_{0,i+1}-\phi^{\ell}_{0,i+1}\right)$$

$$+\frac{(\sigma_s V)_i}{A_{i+1/2}+A_{i-1/2}}\left(\phi^{\ell+1/2}_{0i}-\phi^{\ell}_{0i}\right)\quad, \tag{24}$$

which is the desired result.

The DSA method now consists of Eqs. (8) [which determine $\phi^{\ell+1/2}$], Eq. (9) [which determines $\phi^{\ell+1/2}_o$], Eq. (24) [which determines $f^{\ell+1}_o$], and Eq. (22), i.e.,

$$\phi^{\ell+1}_{oi}=\phi^{\ell+1/2}_{oi}+f^{\ell+1}_{oi}\quad, \tag{25}$$

which determines $\phi^{\ell+1}$. This iterative method is repeated until convergence. It has been tested over a wide range of problems and it converges very well, leading to an error reduction of about two orders of magnitude for every three iterations, independent of the type of problem and of the mesh size. However, a conceptual difficulty exists, which experimentally appears to have little effect on the stability or convergence rate, but which we now wish to discuss.

The derivation of the DSA equations is based on the concept that if the cell edge fluxes are linear in the sense of Eq. (21), then the exact solution is computed in one iteration. We now wish to discuss the following point: is it <u>possible</u> for the cell edge fluxes to be linear in the sense of Eq. (21)?

The answer is "yes", provided Eqs. (8b,c) and (21a,b) are mutually consistent, and "no" otherwise. From Eq. (8b) we get

$$\phi_{ji}^{\ell+1/2} = \frac{1}{2}\left(\phi_{j,i+1/2}^{\ell+1/2} + \phi_{j,i-1/2}^{\ell+1/2}\right) \quad , \; j = 0,1. \tag{26}$$

Hence, introducing Eq. (21a) into (8b), we find

$$\begin{aligned}\psi_{mi}^{\ell+1/2} &= \frac{1}{2}\left[\phi_{0,i+1/2}^{\ell+1/2} + 3\mu_m\phi_{1,i+1/2}^{\ell+1/2}\right] + \frac{1}{2}\left[\phi_{0,i-1/2}^{\ell+1/2} + 3\mu_m\phi_{1,i-1/2}^{\ell+1/2}\right] \\ &= \phi_{0i}^{\ell+1/2} + 3\mu_m\phi_{1i}^{\ell+1/2} \quad .\end{aligned} \tag{27}$$

Next, we introduce Eq. (21b) into (8c) and use Eq. (6) to obtain

$$\begin{aligned}\psi_{mi}^{\ell+1/2} &= \frac{1+\tau_m}{2}\left[\phi_{0i}^{\ell+1/2} + 3\mu_{m+1/2}\phi_{1i}^{\ell+1/2}\right] \\ &\quad + \frac{1-\tau_m}{2}\left[\phi_{0i}^{\ell+1/2} + 3\mu_{m-1/2}\,\phi_{1i}^{\ell+1/2}\right] \\ &= \phi_{0i}^{\ell+1/2} + 3\left[\begin{array}{ll}\frac{1}{2}\left(\mu_{m+1/2} + \mu_{m-1/2}\right) & \text{(DD)} \\ \mu_m & \text{(Morel-Montry)}\end{array}\right]\phi_{1i}^{\ell+1/2} \quad .\end{aligned} \tag{28}$$

Comparing Eqs. (27) and (28), we see that there is an inconsistency if the diamond difference (DD) definition $\tau_m = 0$ is used, but there is no inconsistency if the Morel-Montry definition is used. [Note that with this latter definition, we have

$$\mu_m = \frac{1+\tau_m}{2}\,\mu_{m+1/2} + \frac{1-\tau_m}{2}\,\mu_{m-1/2} \quad , \tag{29}$$

consistent with Eq. (8c)]. Morel and Montry proposed the weighted-diamond-in-angle approach [Eqs. (6), (8c)] to guarantee that the discrete ordinates equations have the correct diffusion limit, and thus to eliminate the

otherwise-present flux dip at r = 0. With their definition of τ_m, the discrete-ordinates solution can become consistently linear in angle (thus ensuring the correct diffusion limit) and the DSA method can, in principal, converge in one iteration; otherwise, it cannot. For practical problems, the use of the DD definition of τ_m does not appear to damage the overall stability, but it is possible that in extreme cases this could occur, and then the Morel-Montry definition would become a necessity.

B. A Linear Discontinuous Scheme for the Two-Dimensional General Geometry Transport Equation (R. E. Alcouffe)

The linear discontinuous (LD) method for two-dimensional geometries has been developed by many authors elsewhere. In this report we outline a specific method which has been coded with an eye to efficiency and to investigate the interaction with iteration acceleration by the diffusion synthetic method.

To begin, we write the R,Z transport equation for cell (i,j) which has incorporated into it the diamond assumption in the angular direction as:

$$\mu_m \frac{\partial r\psi_m}{\partial r} + (\beta_m - \mu_m)\,\psi_m(r,z) + \eta r \frac{\partial \psi_m}{\partial z} + r\sigma_t \psi_m(r,z) = rS_m(r,z) + \beta_m \psi_{m-1/2}(r,z) \quad , \tag{30}$$

$$m = 1, \ldots, m,$$

for

$$r_{i-1/2} \leq r \leq r_{i+1/2}$$

$$z_{j-1/2} \leq z \leq z_{i+1/2} \quad .$$

The linear discontinuous method assumes the following expansion for the angular flux within the cell i,j,

$$\psi_m(r,z) = \psi_{mij} + \frac{r - \hat{r}_i}{h}\,\psi_{rmij} + \frac{z - \hat{z}_j}{k}\,\psi_{zmij} \quad , \tag{31}$$

$$\psi_{m\pm1/2}(r,z) = \psi_{m\pm1/2ij} + \frac{r - \hat{r}_i}{h}\,\psi_{rm\pm1/2ij} + \frac{z - z_j}{k}\,\psi_{zm\pm1/2ij} \quad ; \tag{32}$$

where h, k are the mesh spacing in the i and j directions, respectively,

$$\hat{r}_j = \frac{2(r^3_{i+1/2} - r^3_{i-1/2})}{3(r^2_{i+1/2} - r^2_{i-1/2})} ,$$

$$z_j = \frac{1}{2}(z_{j+1/2} + z_{j-1/2}) .$$

From the diamond in angle assumption, it is readily shown that,

$$2\psi_{mij} = \psi_{m+1/2ij} + \psi_{m-1/2ij} , \tag{33}$$

$$2\psi_{rmij} = \psi_{rm+1/2ij} + \psi_{rm-1/2ij} , \tag{34}$$

$$2\psi_{zmij} = \psi_{zm+1/2ij} + \psi_{zm-1/2ij} . \tag{35}$$

To develop the requisite equations for the unknowns, we substitute Eqs. (31) and (32) into Eq. (30) and take the first three spatial moments of Eq. (30). This yields the following three equations:

$$\begin{aligned}
&\mu(A_{i+1/2}\,\psi_{i+1/2} - A_{i-1/2}\,\psi_{i-1/2}) + (A_{i+1/2} - A_{i-1/2})(\beta - \mu)(\phi + \delta\phi_r) \\
&\quad + \eta B(\phi_{j+1/2} - \phi_{j-1/2}) + \sigma_t V\psi \\
&\quad = VS + (A_{i+1/2} - A_{i-1/2})\,\beta(\psi_{m-1/2} + \delta\phi_{rm-1/2})
\end{aligned} \tag{36}$$

$$\begin{aligned}
&\mu\left[(r_{i+1/2} - \hat{r})\,A_{i+1/2}\psi_{i+1/2} + (\hat{r} - r_{i-1/2})\,A_{i-1/2}\psi_{i-1/2}\right] \\
&\quad + (\beta - \mu)(A_{i+1/2} - A_{i-1/2})\,h\delta(\phi - \frac{\hat{r}}{h}\,\phi_r) \\
&\quad - \mu V\psi + \eta\,\frac{W'}{k}\,(\phi_{rj+1/2} - \phi_{rj-1/2}) \\
&\quad + \sigma_t W\psi_r \\
&\quad = WS_r + \beta(A_{i+1/2} - A_{i-1/2})\,(h\delta)(\psi_{m-1/2} - \frac{\hat{r}}{h}\,\psi_{rm-1/2}) ,
\end{aligned} \tag{37}$$

$$\mu(A_{i+1/2}\psi_{zi+1/2} - A_{i-1/2}\psi_{zi-1/2}) + (A_{i+1/2} - A_{i-1/2})(\beta - \mu)\ \phi\ -12\eta B\phi)$$

$$+ \eta B(\phi_{j+1/2} + \phi_{j-1/2}) + \sigma_t V\psi_z$$

$$= S_z V + \beta(A_{i+1/2} - A_{i-1/2})\ \psi_{zm-1/2} \quad , \tag{38}$$

where all but the cell edge subscripts have been suppressed. The coefficients for X,Y, R,Z and R-θ geometry are shown in Table IV. In the above we have three equations in 7 unknowns (the outgoing or downstream boundary fluxes, ψ_r, ψ_z, and their slopes on the outgoing boundaries). The essence of this linear discontinuous scheme is the following approximations for the unknown slopes,

$$\psi_{rmij} = \frac{h}{r_{i\pm1/2} - \hat{r}}\ (\psi_{mi\pm1/2j} - \psi_{mij}) \quad , \text{ for } \mu \lessgtr 0 \quad ; \tag{39}$$

TABLE IV

EXPRESSIONS FOR THE VARIOUS COEFFICIENTS IN EQUATIONS (36)-(38) AS A FUNCTION OF GEOMETRY

Coefficient	X,Y	R,Z	R,θ
$A_{i+1/2j}$	k	$2\pi r_{i+1/2}k$	$2\pi r_{i+1/2}\Delta\theta$
V_{ij}	hk	$\pi(r^2_{i+1/2} - r^2_{i-1/2})k$	$\pi(r^2_{i+1/2} - r^2_{i-1/2})\ \Delta\theta$
B_i	k	$\pi(r^2_{i+1/2} - r^2_{i-1/2})$	h
δ_i	0	$-\frac{h}{6(r_{i+1/2} + r_{i-1/2})}$	$-\frac{h}{6(r_{i+1/2} + r_{i-1/2})}$
W_{ij}	$\frac{1}{12}h^2k$	$\frac{kB}{h}\ \frac{r^2_{i+1/2} + r^2_{i-1/2}}{2} - \hat{r}^2_i$	$\frac{\Delta\theta_j B}{h}\ \frac{r^2_{i+1/2} + r^2_{i-1/2}}{2} - \hat{r}^2_i$
$\hat{r}_i$	$\frac{1}{2}(r_{i+1/2} + r_{i-1/2})$	$\frac{2(r^2_{i+1/2} - r^2_{i-1/2})}{3(r^2_{i+1/2} - r^2_{i-1/2})}$	$\frac{2(r^3_{i+1/2} - r^3_{i-1/2})}{3(r^2_{i+1/2} - r^2_{i-1/2})}$
Z_j	$\frac{1}{2}(z_{j+1/2} + z_{j-1/2})$	$\frac{1}{2}(z_{j+1/2} + z_{j-1/2})$	$\frac{1}{2}(\Delta\theta_{j+1/2} + \Delta\theta_{j-1/2})$
W'	W	W	$\Delta\theta_j\ (\frac{1}{12}\frac{\hat{r}h^2}{\bar{r}_i})$

$$\psi_{zmij} = \pm\ 2\ (\psi_{mij\pm1/2} - \psi_{mij}) \quad , \quad \text{for} \quad \eta \gtrless 0 \quad ; \tag{40}$$

$$\psi_{zmi\pm1/2j} = \psi_{zmij} \quad , \tag{41}$$

$$\psi_{rmij\pm1/2} = \psi_{rmij} \quad . \tag{42}$$

It has also been established that in Eq. (36), very little loss of accuracy is obtained when δ is set to zero. Thus, our set of equations, for $\mu < 0$ and $\eta < 0$ is the following:

$$\begin{aligned}
&- |\mu|\ (A_{i+1/2}\psi_{i+1/2} - A_{i-1/2}\psi_{i-1/2}) + (A_{i+1/2} - A_{i-1/2}(\beta + |\mu|)\ \psi \\
&- |\eta|\ B(\psi_{j+1/2} - \psi_{j+1/2}) + \sigma_t V\psi = VS + \beta(A_{i+1/2} - A_{i-1/2})\ \psi_{m-1/2}
\end{aligned} \tag{43}$$

$$\begin{aligned}
&- |\mu|[(r_{i+1/2} - \hat{r})\ A_{i+1/2}\psi_{i+1/2} - (\hat{r} - r_{i-1/2})\ A_{i-1/2}\psi_{i-1/2}] \\
&+ \left[\ |\mu|V + (\beta + |\mu|)(A_{1+1/2} - A_{i-1/2})h\delta\right]\psi \\
&- (\beta + |\mu|)(A_{i+1/2} - A_{i-1/2})(\delta\hat{r})\left(\frac{h}{\hat{r} - r_{i-1/2}}\right)\ (\psi - \psi_{i-1/2}) \\
&- |\eta|\ \frac{W}{k}\left[\psi_{rj+1/2} - \frac{h}{\hat{r} - r_{i-1/2}}\ (\psi - \psi_{i-1/2})\right] \\
&+ \sigma_t W\left(\frac{h}{\hat{r} - r_{i-1/2}}\right)(\psi - \psi_{i-1/2}) = WS_r \\
&+ \beta(A_{i+1/2} - A_{i-1/2})(h\delta)\ \psi_{m-1/2} - \frac{\hat{r}}{h}\ \psi_{rm-1/2})
\end{aligned} \tag{44}$$

$$\begin{aligned}
&- |\mu|\ [A_{i+1/2}\psi_{zi+1/2} - 2A_{i-1/2}\ (\psi - \psi_{j-1/2})] + 2(A_{i+1/2} - A_{i-1/2}) \\
&\times (\beta + |\mu|)(\psi\ \ \psi_{j-1/2}) + 12|\eta|\ B\psi - 6|\eta|\left[B[\psi_{j+1/2} + 2(\psi - \psi_{j-1/2})]\right] \\
&+ 2\sigma_t V(\psi - \psi_{j-1/2}) = S_z V + \beta(A_{i+1/2} - A_{i-1/2})\ \psi_{zm-1/2} \quad .
\end{aligned} \tag{45}$$

Equations (43-45) then give the relationship among the basic unknowns ψ, $\psi_{j-1/2}$ and $\psi_{i-1/2}$ for the incoming-downward directions in terms of the known $\psi_{i+1/2}$, $\psi_{j+1/2}$, $\psi_{m-1/2}$, $\psi_{rm-1/2}$, and $\psi_{zm-1/2}$.

The next ingredient in the method as we have implemented it is to define the source moments S_{rij} and S_{zij}. The strictly correct method is to store the flux moments in a multigroup problem (with isotropic scattering) as:

$$S^g_{rij} = \sum_{g'=1}^{g} \sigma_{sog' \to g} \, \phi_{rg'ij} \quad , \tag{46}$$

$$S^g_{zij} = \sum_{g'=1}^{g} \sigma_{sog' \to g} \, \phi_{zg'ij} \quad , \tag{47}$$

where

$$\phi_{rgij} = \sum_{m=1}^{m} w_m \psi_{rgmij} \quad , \tag{48a}$$

$$\phi_{zgij} = \sum_{m=1}^{m} w_m \psi_{zgmij} \quad . \tag{48b}$$

This implies that the storage required is two more flux arrays per group which for many realistic problems is a large penalty associated with the linear discontinuous method. We have an alternative in that we are accelerating the iterative procedure with the diffusion synthetic method. Thus, we have available the corrected diffusion flux at the mesh vertices. From this we may compute estimates of the slopes for the source. That is, if

$f_{i+1/2j+1/2} \equiv$ the corrected diffusion flux,

an estimate of the scalar flux slopes is given by

$$\hat{\phi}^{\ell+1}_{rgij} \simeq 2\phi^{\ell+1/2}_{gij}\left(\frac{f_{i+1/2j+1/2} + f_{i+1/2j-1/2} - f_{i-1/2j+1/2} - f_{i-1/2j-1/2}}{f_{i+1/2j+1/2} + f_{i+1/2j-1/2} + f_{i-1/2j+1/2} + f_{i-1/2j-1/2}}\right)^{\ell+1}, \tag{49}$$

$$\hat{\phi}^{\ell+1}_{zgij} \simeq 2\phi^{\ell+1/2}_{gij}\left(\frac{f_{i+1/2j+1/2} + f_{i-1/2j+1/2} - f_{i+1/2j-1/2} - f_{i-1/2j-1/2}}{f_{i+1/2j+1/2} + f_{i+1/2j-1/2} + f_{i-1/2j+1/2} + f_{i-1/2j-1/2}}\right)^{\ell+1} \tag{50}$$

where ℓ is an iteration index. These are estimates of the flux moments from which the source moments are computed but which are computed as needed.

The last ingredient is the positivity of the source. That is, we desire the source representation to be positive and we adjust the slopes to accomplish this. The source expansion may be written as,

$$S(r,z) = S_{ij} + \frac{r - \hat{r}_i}{h} S_{rij} + \frac{z - z_i}{k} S_{zij} \quad . \tag{51}$$

The source is nonnegative if

$$S_{ij} \geq \frac{1}{2}\left(2\,\frac{r_{i+1/2} - \hat{r}_i}{h}\,|S_{rij}| + |S_{zij}|\right) \quad \text{for} \quad S_{rij} < 0 \quad ,$$

or

$$S_{ij} \geq \frac{1}{2}\left(2\,\frac{\hat{r}_i - r_{i-1/2}}{h}\,|S_{rij}| + |S_{zik}|\right) \quad \text{for} \quad S_{rij} > 0 \quad .$$

Thus, assuming $S_{ij} \geq 0$, we can guarantee a positive source of adjusting the slope so that

$$S(r,z) = S_{ij} + a_{ij}\left(\frac{r - \hat{r}_i}{h} S_{rij} + \frac{z - z_i}{k} S_{zij}\right) \tag{52}$$

where

$$a_{ij} = \min\left(1 \, , \frac{2S_{ij}}{2\frac{r_{i+1/2} - \hat{r}}{h}\left|S_{rij}\right| + \left|S_{zij}\right|}\right) \text{ for } \quad S_{rij} < 0$$

$$a_{ij} = \min\left(1, \frac{2S_{ij}}{2\frac{\hat{r} - r_{i-1/2}}{h}\left|S_{rij}\right| + \left|S_{zij}\right|}\right) \text{ for } \quad S_{rij} > 0 \; .$$

With this method coded into the TWODANT code, we have run some preliminary test problems to assess the performance of the method. The test problem selected here is a two-region, two-group, R,Z problem with dimensions 5 x 5 cm. The left and bottom boundaries are reflective and a uniform source is in the left hand, bottom, 1 x 1 cm region. The two group cross sections are:

$$\sigma_{t1} = 1.5 \quad , \quad \sigma_{s1} = 1.0 \quad , \quad \sigma_{s1\to 2} = 0.5 \quad ;$$

$$\sigma_{t2} = 1.0 \quad , \quad \sigma_{s2} = 0.5 \quad .$$

The calculated leakage from the system for each group is given in Table V as a function of spatial mesh size; the coarsest mesh is 1 x 1 cm. A diamond-differenced calculation of this problem is also displayed for comparison. We

TABLE V

A COMPARISON OF THE LINEAR DISCONTINUOUS METHOD WITH THE DIAMOND METHOD ON A MODEL PROBLEM

Spatial mesh size	Leakage Error as a function of group and method			
	Diamond		Linear Discontinuous	
	group 1	group 2	group 1	group 2
1	-43.9%	-32.8%	-11.5%	5.50%
1/2	-18.6%	-9.5%	-2.0%	1.32%
1/4	-4.2%	-2.4%	-0.4%	0.26%
1/8	-0.9%	-0.5%	-0.06%	0.08%
1/16	0.006863	0.033698	0.006881	0.033763

see that in this problem the performance of LD is indeed better than diamond differencing. The convergence rate of the solution with mesh size is between $O(h^2)$ and $O(h^3)$ and hence is not as good as expected. That is, we expect $O(h^3)$ in the integral parameters for LD.

The timing studies done thus far show that on the CRAY-1, LD is about 1.5-2 times slower than diamond with fixup. What remains to be done is to test this method on fission-eigenvalue problems in order to assess the impact of the spatial moment approximations (Eqs. (49), (50)).

C. Rapidly Converging Iterative Methods for Numerical Transport Problems

(E. W. Larsen)

We have taken a close look at two previously-proposed iterative methods for solving numerical transport problems, the first a nonlinear method due to Gol'din,[13] the second a linear method due to Lewis and Miller.[14] These methods have certain features which we have recently observed numerically (or, in some cases, are apparent analytically):

(i) Both methods are based on equations which are derived from and equivalent to the exact linear transport equation.

(ii) Numerical solutions generated by both methods are observed to converge extremely rapidly, with an error reduction of approximately two orders of magnitude for every three iterations, for any reasonable discretization of space, angle, and energy.

(iii) These numerical solutions possess the diffusion limit.

(iv) These numerical solutions are generally not equal to the numerically-generated standard discrete ordinates solutions computed on the same mesh.

In the following, we describe these methods and outline the above results in more detail.

First we shall outline Gol'din's (or equivalently, the Variable Eddington Factor[15]) method. We consider the transport equation

$$\mu \frac{\partial \psi}{\partial x}(x,\mu) + \sigma_T \psi(x,\mu) = \frac{\sigma_s}{2} \int_{-1}^{1} \psi(x,\mu')d\mu' + Q \quad . \tag{53}$$

Defining

$$\phi_n(x) = \frac{1}{2} \int_{-1}^{1} \mu^n \phi(x,\mu) d\mu \quad , \; n = 0,1,2, \tag{54}$$

and taking the zero-th and first angular moments of Eq. (53), we obtain

$$\frac{d\phi_1}{dx} + (\sigma_T - \sigma_s)\, \phi_0 = Q \quad , \tag{55}$$

$$\frac{d\phi_2}{dx} + \sigma_T \phi_1 = 0 \quad . \tag{56}$$

Eliminating ϕ_1 between these equations, we obtain

$$- \frac{d}{dx} \frac{1}{\sigma_T} \frac{d}{dx} \phi_2(x) + (\sigma_T - \sigma_s)\phi_0(x) = Q(x) \quad . \tag{57}$$

Gol'din's method, based on Eqs. (53), (54), and (57), is now described by:

$$\mu \frac{\partial \phi^{\ell+1/2}}{\partial x} + \sigma_T \phi^{\ell+1/2} = \sigma_s \phi_0^{\ell} + Q \quad , \tag{58}$$

$$- \frac{d}{dx} \frac{1}{\sigma_T} \frac{d}{dx} \frac{\phi_2^{\ell+1/2}}{\phi_0^{\ell+1/2}} \phi_0^{\ell+1} + (\sigma_T - \sigma_s)\, \phi_0^{\ell+1} = Q \quad . \tag{59}$$

We have tested this method numerically, for various discretizations constrained only by the requirement that each iterative solution be positive, so that $\phi_0^{\ell+1/2} > 0$ in Eq. (59). For each discretization the method generates solutions which converge very rapidly, with an error reduction of three orders of magnitude for every two iterations, and for spatial meshes up to 10^3 mean free paths across. We observed no degradation of stability for the thicker spatial meshes. We also observed that while $\phi_0^{\ell+1/2}$ and $\phi_0^{\ell+1}$ converge very rapidly, they do not converge to identical limits. In other words, for the numerically computed values on any mesh,

$$\lim_{\ell\to\infty} \phi_0^{\ell+1/2} = \hat{\phi}_0 \quad , \tag{60a}$$

$$\lim_{\ell\to\infty} \phi_0^{\ell} = \tilde{\phi}_0 \quad , \tag{60b}$$

and

$$\hat{\phi}_0 \neq \tilde{\phi}_0 \quad . \tag{60c}$$

In addition, if Φ_0 denotes the converged discrete ordinates solution, then in general Φ_0, $\hat{\phi}_0$, and $\tilde{\phi}_0$ are all distinct. Of course, the extent of this phenomenon is problem- and mesh-dependent; as the independent-variable mesh becomes increasingly fine, the three solutions all merge together to the solution of the exact transport equation.

Finally, we observed that numerical solutions obtained by Gol'din's method possess the diffusion limit. To explain this precisely, let us consider the following rescaling of the cross sections and source in Eq. (53):

$$\begin{aligned} &\sigma_T \to \frac{\sigma_T}{\varepsilon} \quad , \\ &\sigma_s \to \frac{\sigma_T}{\varepsilon} + \varepsilon\,(\sigma_s - \sigma_T) \quad , \qquad 0 < \varepsilon \leq 1 \\ &Q \to \varepsilon Q \quad . \end{aligned} \tag{61}$$

We note that for $\varepsilon = 1$, the original cross sections and source are obtained. Eq. (61) imply

$$\begin{aligned} &\frac{1}{\sigma_T} \to \frac{\varepsilon}{\sigma_T} \quad , \\ &\sigma_T - \sigma_s \to \varepsilon\,(\sigma_T - \sigma_s) \quad , \\ &Q \to \varepsilon\, Q \quad . \end{aligned} \tag{62}$$

Therefore, in the diffusion approximation to Eq. (53),

$$-\frac{d}{dx}\frac{1}{3\sigma_T}\frac{d}{dx}\phi(x) + (\sigma_T - \sigma_s)\phi(x) = Q(x) \quad , \tag{63}$$

if the substitutions (61) are made, the identical equation is recovered! In other words, Eq. (63) is invariant under the change of scale described by Eq. (61). On the other hand, the transport equation is not invariant under this change of scale. In particular, as $\varepsilon \to o$, we have $\sigma_T \to \infty$, $\sigma_s \to \infty$, $\left|\sigma_T - \sigma_s\right| \to 0$, and $Q \to 0$, and it can be shown that in this limit, the transport solution converges to the diffusion solution. [The method in Sec. 2 of Ref. 16 gives this result very easily.]

Based on the above observations, we now make a definition. We say that a numerical solution of the transport equation (53), with a fixed spatial and angular mesh, has the diffusion limit if the following condition is met: under the change of scale of cross sections described by Eq. (61), the numerical solution of Eq. (53) converges, as $\varepsilon \to 0$, to the solution of a discretized version of the diffusion equation (63). [This is a stronger definition of diffusion limit than that used in Ref. 16.]

To show that the analytic equations (58) and (59) possess this limit is easy; introducing Eq. (61) into (58) and (59) and keeping only the leading order terms in ε, we obtain

$$\phi^{\ell+1/2} = \phi_0^{\ell} \quad , \tag{64}$$

$$-\frac{d}{dx}\frac{1}{\sigma_T}\frac{d}{dx}\left(\frac{\phi_2^{\ell+1/2}}{\phi_0^{\ell+1/2}}\right)\phi_0^{\ell+1/2} + (\sigma_T - \sigma_s)\,\phi_0^{\ell+1} = Q \quad . \tag{65}$$

Eq. (64) implies that $\phi^{\ell+1/2}$ is isotropic (independent of angle). Therefore, using Eq. (54), we have

$$\frac{\phi_2^{\ell+1/2}}{\phi_0^{\ell+1/2}} = \frac{1}{3} \quad , \tag{66}$$

and so Eq. (65) reduces to the standard diffusion equation (63). Thus, ϕ_0^{ℓ} satisfies this equation, and by Eq. (64),

$$\phi_0^{\ell+1/2} = \phi_0^{\ell} \quad . \tag{67}$$

To summarize, as $\varepsilon \to 0$, the transport and diffusion scalar fluxes agree ($\hat{\phi}_0 = \tilde{\phi}_0$), and both satisfy Eq. (63). This same reasoning can be applied to any reasonable discretizations of Eqs. (58) and (59). In fact, we have tested this concept numerically for values of ε as small as 10^{-3}, and the numerical solutions follow precisely the same pattern as the analytic solutions; as $\varepsilon \to 0$, the transport and diffusion scalar fluxes agree, and both satisfy (the discretized version of Eq. (63).

The second method we wish to discuss, due to Lewis and Miller, is derived from Eq. (53) as follows. Defining

$$\bar{\phi}_n(x) = \frac{1}{2} \int_{-1}^{1} P_n(\mu)\psi(x,\mu)d\mu \tag{68}$$

(where $P_n(\mu)$ is the n-th Legendre polynomial) and taking the zero-th and first angular moments of Eq. (53), we get

$$\frac{d\bar{\phi}_1}{dx} + (\sigma_T - \sigma_s)\,\bar{\phi}_0 = Q \quad , \tag{69}$$

$$\frac{2}{3}\frac{d\bar{\phi}_2}{dx} + \frac{1}{3}\frac{d\bar{\phi}_0}{dx} + \sigma_T\bar{\phi}_1 = 0 \quad . \tag{70}$$

Eliminating $\bar{\phi}_1$ between Eqs. (69) and (70), we obtain

$$-\frac{d}{dx}\frac{1}{3\sigma_T}\frac{d}{dx}\bar{\phi}_0 + (\sigma_T - \sigma_s)\,\bar{\phi}_0 = Q + \frac{d}{dx}\frac{2}{3\sigma_T}\frac{d}{dx}\bar{\phi}_2 \quad . \tag{71}$$

The Miller-Lewis method, based on Eqs. (53), (68), and (71), is described as follows:

$$\mu \frac{\partial \psi^{\ell+1/2}}{\partial x} + \sigma_T \psi^{\ell+1/2} = \sigma_s \phi_0^{\ell} + Q \quad , \tag{72}$$

$$- \frac{d}{dx} \frac{1}{3\sigma_T} \frac{d}{dx} \phi_0^{\ell+1} + (\sigma_T - \sigma_s) \phi_0^{\ell+1} = Q + \frac{d}{dx} \frac{2}{3\sigma_T} \frac{d}{dx} \bar{\phi}_2^{\ell+1/2} \quad . \tag{73}$$

We have tested this method numerically, for various discretizations (which now are not constrained by positivity). Overall, the behavior of this method is identical to that of Gol'din's method. The argument that the Lewis-Miller method has the diffusion limit proceeds as follows: introducing Eq. (61) into (72) and (73), we obtain (to leading order in ε) Eq. (64) and (73). By Eq. (64), $\psi^{\ell+1/2}$ is isotropic, implying $\bar{\phi}_2^{\ell+1/2} = 0$, and hence $\phi_0^{\ell+1}$ satisfies the correct diffusion equation. Moreover, Eq. (64) implies that

$$\phi_0^{\ell+1/2} = \phi_0^{\ell} \quad , \tag{74}$$

and so the transport and diffusion scalar fluxes agree.

The Lewis-Miller method has the computational disadvantage that in its discretized form, one cannot guarantee a positive solution, whereas Gol'din's method (at least 1-D geometries) can be discretized to guarantee a positive solution. On the other hand, the Lewis-Miller method is linear and can be Fourier-analyzed (doing this proves the method's stability and effectiveness), whereas Gol'din's method is nonlinear, and thus perhaps somewhat less reliable.

To conclude, either of these methods (or a variant) seems attractive for obtaining rapidly convergent numerical solutions of transport problems in situations where the standard diffusion-synthetic method will not work, (i.e., Lagrangian meshes, or a two-dimensional non-diamond differencing scheme). The main difficulty is that neither of these schemes produces the standard discrete ordinates solutions, and therefore numerical studies will have to be performed to determine the accuracy of the solutions obtained. It is possible that in some respects these solutions are more accurate than the discrete ordinates result, but in other respects they are worse. The extent of these differences,

as well as the ultimate use of the final method of choice, will jointly have to be taken into account. We plan to pursue these questions, as well as the problem of modifying Gol'din's method in two dimensions so as to guarantee a positive solution.

D. Modified One-Group Acceleration of the Frequency-Dependent Diffusion Equation (E. W. Larsen)

Previously[17] we described a method for accelerating the convergence of a frequency dependent (multigroup) diffusion equation by a one-group diffusion equation. This method is defined by

$$-\frac{\partial}{\partial x}\frac{1}{3\sigma}\frac{\partial}{\partial x}\phi^{\ell+1/2} + \sigma\phi^{\ell+1/2} = \chi\phi_0^{\ell}(x) + Q(x,\nu) \quad , \tag{75}$$

$$\phi_0^{\ell+1/2}(x) = \int_0^{\infty} \sigma\phi^{\ell+1/2}\, d\nu \quad , \tag{76}$$

$$-\left(\int_0^{\infty} \frac{\partial}{\partial x}\frac{1}{3\sigma}\frac{\partial}{\partial x}\frac{\chi}{\sigma}\, d\nu\right) F_0^{\ell+1}(x) = \phi_0^{\ell+1/2} - \phi_0^{\ell} \quad , \tag{77}$$

$$\phi_0^{\ell+1}(x) = \phi_0^{\ell+1/2}(x) + F_0^{\ell+1}(x) \quad . \tag{78}$$

Here we have $\phi = \phi(x,\nu)$, $\sigma = \sigma(x,\nu)$, $\chi = \chi(x,\nu)$, and

$$\int_0^{\infty} \chi(x,\nu)\, d\nu = 1 \quad . \tag{79}$$

For the cross sections

$$\sigma(\nu) = \beta\frac{1 - e^{-\alpha\nu}}{\nu^3} \quad , \tag{80}$$

$$\chi(\nu) = \alpha e^{-\alpha\nu} \quad , \tag{81}$$

the infinite medium spectral radius of the above method is computed by a Fourier analysis to be 0.867, for any choice of the constants α and β.

A modified (and improved) version of this method is described as follows:

$$-\frac{\partial}{\partial x}\frac{1}{3\sigma}\frac{\partial}{\partial x}\phi^{\ell+1/3} + \sigma\phi^{\ell+1/3} = \chi\,\phi_0^{\ell} + Q \quad , \tag{82}$$

$$\phi_0^{\ell+1/3} = \int_0^{\infty} \sigma\phi^{\ell+1/3}\, d\nu \quad , \tag{83}$$

$$-\frac{\partial}{\partial x}\frac{1}{3\sigma}\frac{\partial}{\partial x}\phi^{\ell+2/3} + \sigma\phi^{\ell+2/3} = \chi\,\phi_0^{\ell+1/3} + Q \quad , \tag{84}$$

$$\phi_0^{\ell+2/3} = \int_0^{\infty} \sigma\phi^{\ell+2/3}\, d\nu \quad , \tag{85}$$

$$-\left(\int_0^{\infty} \frac{\partial}{\partial x}\frac{1}{3\sigma}\frac{\partial}{\partial x}\frac{\chi}{\sigma}\, d\nu\right) F_0^{\ell+1} = -\rho\left(\phi_0^{\ell+2/3} - \phi_0^{\ell+1/3}\right) + (1+\rho)\left(\phi_0^{\ell+1/3} - \phi_o^{\ell}\right) \quad , \tag{86}$$

$$\phi_0^{\ell+1} = \phi_0^{\ell+1/2} + F_0^{\ell+1} \quad . \tag{87}$$

The infinite medium eigenvalue ω of this method is given by

$$\omega = \gamma^2 \frac{1-\gamma}{\lambda^2 \int_0^{\infty} \frac{\chi}{3\sigma^2}\, d\nu}\,(\rho + 1 - \rho\gamma) \quad , \tag{88}$$

where

$$\gamma = \int_0^{\infty} \frac{3\sigma^2\chi}{\lambda^2+3\sigma^2}\, d\nu \tag{89}$$

and λ is the Fourier Transform parameter. (See Ref. 17 for details.) However, for the cross sections given by Eqs. (80) and (81), the above formulas reduce to

$$\omega = \gamma^2 - \frac{1 - \gamma}{z^2\theta} (\rho + 1 - \rho\gamma) \quad , \tag{90}$$

where

$$\theta = \int_0^\infty \left(\frac{t^3}{1 - e^{-t}} \right)^2 \frac{e^{-t}}{3} \, dt \quad , \tag{91}$$

$$\gamma(z) = \int_0^\infty \frac{3t^3(1 - e^{-t})\, e^{-t} \, dt}{z^2 t^6 + 3(1 - e^{-t})^2} \quad , \tag{92}$$

$$z = \frac{\lambda}{\alpha^3 \beta} \quad . \tag{93}$$

Thus, ω is a function only of ρ and $z = \lambda/\alpha^3\beta$, and for any given ρ the spectral radius is

$$\text{spr} = \sup_z \left| \omega \right| \quad .$$

Numerically, we observe that the choice $\rho = 218.0$ leads to the minimum value

$$\text{spr} \simeq 0.3 \quad .$$

Since $\sqrt{0.3} \simeq 0.55$, we have that for this new method, the error reduction per multigroup diffusion calculation is about 0.55, whereas for the earlier method [Eqs. (75)-(78)] it is only 0.867. Thus, this modification of the method (75)-(78) appears to be much more efficient. However, in general problems including time dependence, the factor ρ must be computed, and we do not yet know how efficiently this can be done. We plan to pursue this topic in the near future.

E. A Modal Acceleration Method for Frequency-Dependent Diffusion Equations

(E. W. Larsen)

The frequency-dependent (multigroup) diffusion equation

$$-\frac{\partial}{\partial x}\frac{1}{3\sigma(x,\nu)}\phi(x,\nu)+\sigma(x,\nu)\,\phi(x,\nu)$$

$$=\chi(x,\nu)\int_0^\infty \sigma(x,\nu')\,\phi(x,\nu')\,d\nu'+S(x,\nu)\quad, \tag{94a}$$

with

$$\int_0^\infty \chi(x,\nu)\,d\nu=1\quad, \tag{94b}$$

can be solved by the following acceleration method:[17]

$$\frac{\partial}{\partial x}\frac{1}{3\sigma}\frac{\partial}{\partial x}\phi^{\ell+1/2}+\sigma\phi^{\ell+1/2}=\chi\phi_0^{\ell}(x)+S\quad, \tag{95a}$$

$$\phi_0^{\ell+1/2}(x)=\int_0^\infty \sigma\phi^{\ell+1/2}\,d\nu\quad, \tag{95b}$$

$$-\left(\int_0^\infty \frac{\partial}{\partial x}\frac{1}{3\sigma}\frac{\partial}{\partial x}\frac{\chi}{\sigma}\,dx\right)F^{\ell+1}(x)=\phi_0^{\ell+1/2}(x)-\phi_0^{\ell}(x)\quad, \tag{95c}$$

$$\phi_0^{\ell+1}(x)=\phi_0^{\ell+1/2}(x)+F^{\ell+1}(x)\quad. \tag{95d}$$

For the cross sections

$$\chi(\nu)=\alpha e^{-\alpha\nu}\quad, \tag{96a}$$

$$\sigma(\nu)=\beta\frac{1-e^{-\alpha\nu}}{\nu^3}\quad, \tag{96b}$$

the spectral radius of the above method is 0.867, for all choices of the constants α and β. (See Ref. 17.)

Equations (95) are derived by examining the stability of the unaccelerated method [Eqs. (95a,b,d) with $F^{\ell+1}$ set equal to zero]. The eigenfunctions are

$$f_\lambda(x,\nu) = \frac{3\sigma\chi}{\lambda^2 + 3\sigma^2} e^{i\lambda x} \quad , \tag{97}$$

and the most slowly converging mode corresponds to $\lambda = 0$:

$$f_0 = \frac{\chi}{\sigma} \quad .$$

Equation (95c) is derived by requiring that if the frequency variation of the solution ϕ can be described solely by this $\lambda = 0$ eigenfunction, then ϕ should be computed in one iteration. Here we describe a method which generalizes this idea; it requires that given a fixed number (n) of functions, or "modes" (the first of which is χ/σ, but the rest of which are arbitrary), the solution should be computed exactly in one iteration if its frequency variation at each point can be described solely as a linear combination of these n modes.

To derive this method, we retain Eqs. (95a,b) but discard Eqs. (95c,d). We begin by introducing n-1 functions $P_j(x,\nu)$, $2 \leq j \leq n$. These functions are arbitrary but fixed. Next we define the functions γ_j, $1 \leq j \leq n$, by

$$\gamma_1(x,\nu) = 1 \quad , \tag{98a}$$

$$\gamma_2(x,\nu) = b_2(x)\ [1 + a_{21}(x)\ P_1(x,\nu)] \quad , \tag{98b}$$

$$\gamma_3(x,\nu) = b_3(x)\ [1 + a_{31}(x)\ P_1(x,\nu) + a_{32}(x)\ P_2(x,\nu)] \quad , \tag{98c}$$

etc., where $b_j(x)$ and $a_{ij}(x)$ are uniquely determined by the conditions

$$\int_0^\infty \chi(x,\nu)\ \gamma_p(x,\nu)\ \gamma_q(x,\nu)\ d\nu = \delta_{pq} \quad , \ 1 \leq p,q \leq n \quad . \tag{99}$$

Thus, the functions $\gamma_j(x,\nu)$ are determined explicitly in terms of, and are an orthonormalization of, the functions $P_j(x,\nu)$.

Now we express the solution of Eq. (95a) as

$$\phi^{\ell+1/2}(x,\nu) = \frac{\chi(x,\nu)}{\sigma(x,\nu)} \sum_{j=1}^{n} \gamma_j(x,\nu)\, \Phi_j^{\ell+1/2}(x) + R^{\ell+1/2}(x,\nu) \quad , \tag{100}$$

where

$$\Phi_k^{\ell+1/2}(x) = \int_0^\infty \sigma(x,\nu)\, \gamma_k(x,\nu)\, \phi^{\ell+1/2}(x,\nu)\, d\nu \tag{101}$$

and $R^{\ell+1/2}(x,\nu)$ is a "remainder" which, by Eqs. (99)-(101), satisfies

$$\int_0^\infty \sigma(x,\nu)\, \gamma_j(x,\nu)\, R^{\ell+1/2}(x,\nu)\, d\nu = 0 \quad , \qquad j=1, \ldots, n \quad .$$

We remark that if $\phi^{\ell+1/2}$ can be expressed solely as a linear combination of the n functions $\chi\gamma_j/\sigma$, then $R^{\ell+1/2} = 0$.

We now write Eq. (95a) as

$$-\frac{\partial}{\partial x}\frac{1}{3\sigma}\frac{\partial}{\partial x}\phi^{\ell+1/2} + \sigma\phi^{\ell+1/2} = \chi\, \gamma_1 \Phi_1^{\ell}(x) + S \quad .$$

We multiply this equation by γ_k, integrate over ν, and use Eqs. (99) and (101) to get

$$-\int_0^\infty \gamma_k \frac{\partial}{\partial x}\frac{1}{3\sigma}\frac{\partial}{\partial x}\phi^{\ell+1/2}\, d\nu + \Phi_k^{\ell+1/2}(x) = \delta_{k1}\Phi_1^{\ell}(x) + \int_0^\infty \gamma_k\, S\, d\nu \quad . \tag{102}$$

Next we introduce the expansion (100) into Eq. (102):

$$-\sum_{j=1}^{n}\left(\int_0^\infty \gamma_k \frac{\partial}{\partial x}\frac{1}{3\sigma}\frac{\partial}{\partial x}\frac{\chi}{\sigma}\gamma_j\, d\nu\right)\Phi_j^{\ell+1/2}(x) + \Phi_k^{\ell+1/2}(x)$$

$$= \delta_{kl}\, \Phi_l^{\ell}(x) + \int_0^{\infty} \gamma_k\, S\, d\nu + \int_0^{\infty} \gamma_k \frac{\partial}{\partial x} \frac{1}{3\sigma} \frac{\partial}{\partial x}\, R^{\ell+1/2}\, d\nu \quad . \tag{103}$$

This equation is automatically satisfied by the solution of Eq. (95a). We now define a system of n acceleration equations for the n unknowns $\Phi_k^{\ell+1}(x)$, $1 \leq k \leq n$, as

$$-\sum_{j=1}^{n}\left(\int_0^{\infty} \gamma_k \frac{\partial}{\partial x} \frac{1}{3\sigma} \frac{\partial}{\partial x} \frac{\chi}{\sigma} \gamma_j\, d\nu\right) \phi_j^{\ell+1} + (1 - \delta_{kl})\, \Phi_l^{\ell+1}$$

$$= \int_0^{\infty} \gamma_k\, S\, d\nu + \int_0^{\infty} \gamma_k \frac{\partial}{\partial x} \frac{1}{3\sigma} \frac{\partial}{\partial x}\, R^{\ell+1/2}\, d\nu \quad . \tag{104}$$

Defining

$$F_k^{\ell+1}(x) = \Phi_j^{\ell+1}(x) - \Phi_j^{\ell+1/2}(x) \quad ,$$

and subtracting Eq. (103) from Eq. (104), we obtain the result

$$-\sum_{j=1}^{n} \int_0^{\infty} \gamma_k \frac{\partial}{\partial x} \frac{1}{3\sigma} \frac{\partial}{\partial x} \frac{\chi}{\sigma}\, \gamma_j\, d\nu\; F_j^{\ell+1}(x) + (1 - \delta_{kl})\, F_k^{\ell+1}(x)$$

$$= \delta_{kl}\, \Phi_l^{\ell+1/2}(x) - \Phi_l^{\ell}(x) \qquad , \qquad 1 \leq k \leq n \quad . \tag{105}$$

This procedure reduces to that of Eqs. (95) for the case n=1. Moreover, if there exist functions $\Phi_j(x)$ such that for every spatial point

$$\phi(x,\nu) = \sum_{j=1}^{n} \frac{\chi \gamma_j}{\sigma}\, \Phi_j(x) \quad , \tag{106}$$

then ϕ is obtained in one iteration.

However, we have not yet specified the functions P_j in Eqs. (98), and thus the functions γ_j are not fully determined. Also, we do not know in general whether the system (105) is ill-posed (or well-posed) for determining the functions $F_k^{\ell+1}$, or whether special functions P_j have to be determined to make this system well-posed. Finally, we do not know in general whether taking n large in Eqs. (105) leads to an acceleration method with better convergence properties than that obtained by taking n small.

Thus, in the following, we shall consider the cases n=1 and n=2 in detail. For the moment, we assume that Eqs. (105) can be (and are) solved to determine $F_1^{\ell+1}(x)$, and we focus on the stability question for the acceleration method (95a), (95b), (105), and (106).

Following the Fourier stability analysis outlined in Ref. 17, we obtain the following. If we define

$$\rho_{jk} = \int_0^\infty \frac{\chi P_1^j}{\sigma^k}\, d\nu \quad , \tag{107}$$

$$\omega_0 = \int_0^\infty \frac{3\sigma^2\chi}{\lambda^2 + 3\sigma^2}\, d\nu \quad , \tag{108}$$

then ω_0 is the unaccelerated eigenvalue (λ is the Fourier transform parameter satisfying $-\infty < \lambda < \infty$). ω_1, the eigenvalue for the n=1 acceleration method, is defined by

$$\omega_1 = \omega_0 - \frac{3(1-\omega_0)}{\lambda^2 \rho_{02}} \quad , \tag{109}$$

and ω_2, the eigenvalue for the n=2 acceleration method, is defined by

$$\omega_2 = \omega_0 - \frac{3(1-\omega_0)}{\lambda^2 (\rho_{02} - \kappa)} \quad , \tag{110}$$

where

$$\kappa = \frac{\lambda^2(\rho_{10}\rho_{02} - \rho_{12})^2}{3(\rho_{20} - \rho_{10}^2) + \lambda^2(\rho_{10}^2\,\rho_{02} - 2\rho_{10}\rho_{12} + \rho_{22})} \quad . \tag{111}$$

At this point we shall assume

$$0 = \rho_{10} = \int_0^\infty \chi P_1 \, d\nu \quad , \tag{112a}$$

$$0 \neq \rho_{12} = \int_0^\infty \frac{\chi\rho_1}{\sigma^2} \, d\nu \quad . \tag{112b}$$

[By Eq. (98b), we can add a constant function (i.e., independent of ν) to P_1 without affecting the form of γ_2, and this constant can be chosen so that Eq. (112a) is satisfied. Thus, without loss of generality, Eq. (112a) is satisfied. However, we must simply assume that Eq. (112b) is satisfied (which it clearly is, in general).] Thus, Eq. (111) reduces to

$$\kappa = \frac{\lambda^2\rho_{12}^2}{3\rho_{20} + \lambda^2\rho_{22}} > 0 \quad . \tag{113}$$

Now we shall prove analytically that for all choices of χ and σ, any $\chi \neq 0$, and any function $P(\nu)$ satisfying Eqs. (112),

$$0 < \omega_2 < \omega_1 < \omega_0 < 1 \quad . \tag{114}$$

Then, defining the spectral radii

$$\mathrm{spr}_n = \sup_\lambda \left|\omega_n\right| \quad , \tag{115}$$

we obtain from (21)

$$\mathrm{spr}_2 \leq \mathrm{spr}_1 \leq \mathrm{spr}_0 \leq 1 \quad . \tag{116}$$

Thus (unless equality holds) the n=2 method is stable and converges more rapidly than the n=1 method, which in turn is stable and converges more rapidly than the n=0 (unaccelerated) method.

To begin, we note from Eqs. (94b) and (109) that

$$0 < \omega_0 < 1 \quad , \qquad \lambda \neq 0 \quad . \tag{117a}$$

This result and Eq. (109) implies

$$\omega_1 < \omega_0 \quad , \qquad \lambda \neq 0 \quad . \tag{117b}$$

Next, by Eqs. (110) and (113),

$$\omega_2 < \omega_1 \quad , \qquad \lambda \neq 0 \quad . \tag{117c}$$

To proceed, we use the inequality[18]

$$\omega_0 > \frac{1}{1 + \frac{\lambda^2}{3}(\rho_{02} - \kappa)} \quad . \tag{118}$$

Using the Cauchy-Schwarz inequality,[18] we obtain

$$\rho_{12}^2 = \left(\int_0^\infty \frac{\chi P_1}{\sigma^2} \, d\nu \right)^2 = \left(\int_0^\infty \frac{\chi^{1/2}}{\sigma} \frac{\chi^{1/2} P_1}{\sigma} \, d\nu \right)^2$$

$$\leq \left(\int_0^\infty \frac{\chi}{\sigma^2} \, d\nu \right) \left(\int_0^\infty \frac{\chi P_1^2}{\sigma^2} \, d\nu \right) = \rho_{02}\rho_{22} \quad ,$$

and hence, by Eq. (113),

$$\kappa < \frac{\rho_{12}^2}{\rho_{22}} < \rho_{02} \quad .$$

Thus the denominator on the right side of Eq. (118) is positive, and so we can easily rearrange this inequality to obtain

$$\omega_0 \frac{\lambda^2}{3} (\rho_{02} - \kappa) > 1 - \omega_0$$

or

$$\omega_0 > \frac{3(1 - \omega_0)}{\lambda^2(\rho_{02} - \kappa)} \quad .$$

This result and Eq. (110) imply

$$0 < \omega_2 \quad . \tag{119}$$

Combining the inequalities (117) and (119), we obtain the desired string of inequalities (114).

We have numerically computed spr_n [Eq. (115)] for σ and χ given by Eqs. (96) with $\alpha = \beta = 1$ and (for $n = 2$) various choices of $P(\nu)$. We find

$$spr_0 = 1.0 \quad ,$$

$$spr_1 = 0.867 \quad , \qquad (N = 16)$$

and

$P_1(\nu)$	spr_2	N
ν^2	0.81	11.0
ν	0.75	8.0
$\nu^{1/2}$	0.69	6.2
$\nu^{1/3}$	0.67	5.7
$\nu^{1/4}$	0.65	5.3
χ^2	0.79	9.8
χ	0.73	7.3
$\chi^{1/2}$	0.63	5.0
$\chi^{2/5}$	0.59	4.4
$\chi^{1/3}$	0.61	4.7
$f^*(\nu)$	0.53	3.6

Here N, the number of iterations required to converge the answer by one order of magnitude, is explicitly defined by

$$spr^N = 0.1 \quad ,$$

and the function f^*, defined by

$$f^*(\nu) = \frac{3\sigma\chi}{\left[\frac{0.131}{\alpha^3\beta}\right]^2 + 3\sigma^2} \quad ,$$

arises from Eq. (97) with an optimal choice of λ (which was determined numerically). Thus, for all of the considered choices of P_1, we have

$$spr_2 < spr_1 < spr_0 = 1 \quad ,$$

which is consistent with the theoretical result (116).

It remains to discuss possible procedures for solving the system of Eq. (105). For n = 1 this system reduces to a single diffusion equation, which needs no further discussion. For n = 2, the system can be written

$$- L_{00} F_0(x) - L_{01} F_1(x) = Q(x) \quad , \tag{120a}$$

$$- L_{10} F_0(x) - L_{11} F_1(x) + F_1(x) = 0 \quad , \tag{120b}$$

where

$$Q(x) = \Phi_1^{\ell+1/2}(x) - \Phi_1^{\ell}(x) \quad ,$$

$$L_{ij} = \int_0^\infty \gamma_i \frac{\partial}{\partial x} \frac{1}{3\sigma} \frac{\partial}{\partial x} \frac{\chi}{\sigma} \gamma_j \, d\nu \quad ,$$

and for simplicity we have deleted the iteration superscripts $\ell+1$. Let us define

$$\theta_{ij}(x) = \int_0^\infty \gamma_i \frac{\chi}{3\sigma^2} \gamma_j \, d\nu \quad ;$$

then, for a homogeneous medium,

$$L_{ij} = \theta_{ij} \frac{d^2}{dx^2} \quad . \tag{121}$$

Now let us write F_0 and F_1 in the form

$$F_0 = \theta_{01} U_0 + \theta_{11} U_1 \tag{122a}$$

$$F_1 = - \theta_{00} U_0 - \theta_{01} U_1 \tag{122b}$$

where $U_0(x)$ and $U_1(x)$ are to be determined. Introducing Eqs. (122) into Eqs. (120) and rearranging, we obtain

$$- (L_{00}\theta_{11} - L_{01}\theta_{01})\, U_1 = Q + (L_{00}\theta_{01} - L_{01}\theta_{00}) - U_0 \quad , \tag{123a}$$

$$- (L_{11}\theta_{00} - L_{10}\theta_{01})\, U_0 + \theta_{00}U_0 + \theta_{01}U_1 = (L_{11}\theta_{01} - L_{10}\theta_{11})\, U_1 \quad . \tag{123b}$$

For a homogeneous medium, Eq. (121) holds and Eqs. (123) reduce to

$$- (\theta_{00}\theta_{11} - \theta_{01}^2)\, \frac{d^2}{dx^2}\, U_1 = Q \quad , \tag{124a}$$

$$- (\theta_{00}\theta_{11} - \theta_{01}^2)\, \frac{d^2}{dx^2}\, U_0 + \theta_{00}U_0 + \theta_{01}U_0 = 0 \quad . \tag{124b}$$

This is a triangular system which can be solved without having to iterate between the two equations, and this suggests the following iteration scheme for Eq. (123): introduce initial choices for U_0 and U_1 on the right side of Eqs. (123) and solve for the improved values of U_0 and U_1 on the left side. Then insert these improved values into the right side and repeat the procedure as often as required. Only one such iteration is required if the system is homogeneous. Moreover,

$$\theta_{01}^2 = \left(\int_0^\infty \frac{\chi}{3\sigma^2}\, \gamma_1\, d\nu \right)^2 = \left[\int_0^\infty \left(\frac{\chi}{3\sigma^2} \right)^{1/2} \left(\frac{\chi}{3\sigma^2}\, \gamma_1^2 \right)^{1/2} \right] d\nu \Bigg)^2$$

$$< \left(\int_0^\infty \frac{\chi}{3\sigma^2}\, d\nu \right) \left(\int_0^\infty \frac{\chi \gamma_1^2}{3\sigma^2}\, d\nu \right) = \theta_{00}\theta_{11} \quad ,$$

and hence the diffusion coefficients in Eqs. (124) [and (123)] have the correct sign. [Also, Eqs. (122) can be inverted and solved for U_1 and U_0.]

To summarize, this model method appears to be advantageous in accelerating the convergence of iterative solutions of the frequency-dependent diffusion Eq. (94). However, testing will be required to determine whether the extra calculations which need to be done will be significantly outweighed by the savings obtained from having to perform fewer multigroup diffusion calculations.

F. Behavior of DSA Methods for Time-Dependent Transport Problems with Unaccelerated Diffusion Iterations (E. W. Larsen)

At each time step in the fully implicit method for solving time-dependent radiation transport problems, one must solve the equation

$$\mu \frac{\partial}{\partial x} \psi + (\sigma+\tau)\, \psi(x,\nu,\mu) - \frac{\chi}{2} \int_0^\infty \int_{-1}^{1} \sigma\psi \, d\mu' \, d\nu' = Q \quad , \tag{125}$$

where

$$\int_0^\infty \chi(x,\nu) \, d\nu = 1 \quad , \tag{126}$$

$$\tau = \frac{1}{c\Delta t} \quad , \tag{127}$$

and Q depends on information obtained from the previous time step. The acceleration method

$$\mu \frac{\partial}{\partial x} \psi^{\ell+1/2} + (\sigma+\tau)\, \psi^{\ell+1/2}(x,\nu,\mu) = \chi\Psi^{\ell}(x) + Q \quad , \tag{128a}$$

$$\Psi^{\ell+1/2}(x) = \frac{1}{2} \int_0^\infty \int_{-1}^{1} \sigma\psi^{\ell+1/2} \, d\mu' d\nu' \quad , \tag{128b}$$

$$- \frac{\partial}{\partial x} \frac{1}{3(\sigma+\tau)} \frac{\partial}{\partial x} f^{\ell+1} + (\sigma+\tau)\, f^{\ell+1} - \chi \int_0^\infty \sigma f^{\ell+1}(x,\nu') \, d\nu'$$

$$= \chi \, (\Psi^{\ell+1/2} - \Psi^{\ell}) \quad , \tag{128c}$$

$$\Psi^{\ell+1}(x) = \Psi^{\ell+1/2}(x) + \int_0^\infty \sigma f^{\ell+1}(x,\nu') \, d\nu' \quad , \tag{128d}$$

can be used to obtain the solution, but the diffusion Eq. (128c) must itself be iterated to obtain a solution. Here we shall describe properties of the above acceleration method obtained by iterating Eq. (128c) directly (i.e., without acceleration) a finite number of time. (This number is denoted by n.) In particular, we wish to determine how the spectral radius of the resulting acceleration method depends upon τ and n.

The acceleration method is described as follows:

$$\mu \frac{\partial \phi^{\ell+1/2}}{\partial x} + (\sigma+\tau)\, \phi^{\ell+1/2}(x,\nu,\mu) = \chi \Psi^{\ell}(x) + Q \quad , \tag{129a}$$

$$\Psi^{\ell+1/2}(x) = \frac{1}{2} \int_0^{\infty} \int_{-1}^{1} \sigma \phi^{\ell+1/2} d\mu' d\nu' \quad , \tag{129b}$$

$$F^{\ell+1,0}(x) = 0 \quad , \tag{129c}$$

$$\left.\begin{aligned} - \frac{\partial}{\partial x} \frac{1}{3(\sigma+\tau)} \frac{\partial}{\partial x} f^{\ell+1,m+1} + (\sigma+\tau)\, f^{\ell+1,m+1}(x,\nu) \\ = \chi\, F^{\ell+1,m}(x) + \Psi^{\ell+1/2}(x) - \Psi^{\ell}(x) \quad , \end{aligned}\right\} \quad 0 \le m \le n-1 \tag{129d}$$

$$F^{\ell+1,m+1}(x) = \int_0^{\infty} \sigma f^{\ell+1,m+1}(x,\nu)\, d\nu \quad , \tag{129e}$$

$$\Psi^{\ell+1}(x) = \Psi^{\ell+1/2}(x) + F^{\ell,m}(x) \quad . \tag{129f}$$

The results of the stability analysis are as follows. Setting

$$\Psi^{(\ell)}(x) = \omega_n^{\ell}\, e^{i\lambda x} \quad , \qquad Q = 0 \quad ,$$

then ω is the eigenvalue, given by the following equations:

$$\rho = \int_0^\infty \frac{\sigma\chi}{\lambda} \tan^{-1} \frac{\lambda}{\sigma + \tau} \, d\nu \quad , \tag{130a}$$

$$\gamma = \int_0^\infty \frac{3\sigma(\sigma+\tau)}{\lambda^2 + 3(\sigma+\tau)^2} \chi \, d\nu \quad , \tag{130b}$$

$$\omega_n = \rho - \frac{1 - \rho}{1 - \gamma} \gamma(1 - \gamma^n) \quad . \tag{130c}$$

For the special choice of cross sections

$$\chi = \alpha e^{-\alpha\nu} \quad , \tag{131a}$$

$$\sigma = \beta \frac{1 - e^{-\alpha\nu}}{\nu^3} \quad , \tag{131b}$$

we find numerically that for all values of α and β, the maximum value of ω_n occurs for $\lambda = 0$ provided ω_n is not much smaller than 0.2. Thus,

$$\max_{0 \leq \lambda < \infty} \omega_n(\lambda) = \omega_n(0) \quad \text{if } \omega_n(0) \geq 0.2 \quad . \tag{132}$$

For $\lambda = 0$, we obtain from Eqs. (130)

$$\rho = \gamma = \int_0^\infty \frac{\sigma\chi}{\sigma + \tau} \, d\nu \tag{133a}$$

and

$$\omega_n(0) = \rho^n \quad . \tag{133b}$$

For small τ, Eq. (133a) can be expanded to give

$$\rho = \int_0^\infty \left(1 - \frac{\tau}{\sigma} + \frac{\tau}{\sigma^2} \cdots \right) \chi \, d\nu$$

$$= 1 - \tau\theta + O(\tau^2) \quad ,$$

$$= \frac{1}{1 + \tau\theta} + O(\tau^2) \quad , \tag{134}$$

where, using Eqs. (131),

$$\theta = \int_0^\infty \frac{\chi}{\sigma} \, d\nu \simeq \frac{6.494}{\alpha^3\beta} \quad . \tag{135}$$

Combining Eqs. (127), (132)-(135), and defining r_n as the largest value of ω_n (the spectral radius), we get

$$r_n \simeq \frac{1}{\left(1 + \dfrac{6.494}{c\Delta t\alpha^3\beta}\right)^n} \quad , \tag{136}$$

provided the resulting value of r_n is greater than 0.2. Equation (136) shows that, as expected, r_n increases to 1 as Δt increases to ∞, and that for fixed Δt, r_n is a decreasing function of n. However, for large Δt, r_n is a very slowly decreasing function.

Let us now ask a different question: for large Δt, what value of n is needed to produce a given spectral radius for the full method? If this desired spectral radius is $r_n = 1/4$, then we must solve

$$4 = \left(1 + \frac{6.494}{\alpha^3\beta c\Delta t}\right)^n \quad .$$

Hence,

$$n = \frac{\ell n 4}{\ell n\left(1 + \dfrac{6.494}{\alpha^3 \beta c \Delta t}\right)} \simeq \frac{1.386}{\left(\dfrac{6.494}{\alpha^3 \beta c \Delta t}\right)}$$

$$n \simeq 0.213\ \alpha^3 \beta c \Delta t \quad . \tag{137}$$

This is our main result, and is valid for large values of $\alpha^3 \beta c \Delta t$, say larger than 10. It shows that for large values of Δt, proportionately large values of n are required to maintain a constant value of the spectral radius. In other words, as Δt increases, the number n of diffusion iterations must increase according to Eq. (137) so that the total number of iterations of the full method (129) [i.e., the total number of transport iterations] is held constant.

G. New Diffusion-Synthetic Acceleration Strategies for Frequency-Dependent Transport Equations (E. W. Larsen)

In a previous quarterly report,[17] we discussed several diffusion-synthetic acceleration methods for the frequency-dependent (or "multigroup") transport equation

$$\mu \frac{\partial}{\partial x} \psi(x,\nu,\mu) + \sigma(x,\nu)\ \psi(x,\nu,\mu)$$

$$= \chi(x,\nu) \int_0^\infty \int_{-1}^{1} \sigma(x,\nu')\ \psi(x,\nu',\mu')\ d\mu' d\nu' + Q(x,\nu) \tag{138}$$

with the constraint

$$\int_0^\infty \chi(x,\mu)\ d\nu = 1 \quad . \tag{139}$$

The procedure for accelerating the iteration of Eq. (138) by a one-group diffusion equation is:

$$\mu \frac{\partial \phi^{\ell+1/2}}{\partial x} + \sigma\phi^{\ell+1/2}(x,\nu,\mu) = \chi\Psi^{\ell}(x) + Q \quad , \tag{140a}$$

$$\Psi^{\ell+1/2}(x) = \frac{1}{2}\int_0^{\infty}\int_0^{\infty} \sigma\phi^{\ell+1/2}\, d\mu' d\nu' \quad , \tag{140b}$$

$$-\left(\int_0^{\infty} \frac{\partial}{\partial x}\frac{1}{3\sigma}\frac{\partial}{\partial x}\frac{\chi}{\sigma}\, d\nu\right) F^{\ell+1}(x) = \Psi^{\ell+1/2}(x) - \Psi^{\ell}(x) \quad , \tag{140c}$$

$$\Psi^{\ell+1}(x) = \Psi^{\ell+1/2}(x) + F^{\ell+1}(x) \quad . \tag{140d}$$

The procedure for accelerating the iterative solution of Eq. (138) by a frequency-dependent (or multigroup) diffusion equation is:

$$\mu \frac{\partial \phi^{\ell+1/2}}{\partial x} + \sigma\phi^{\ell+1/2}(x,\nu,\mu) = \chi\Psi^{\ell}(x) + Q \quad , \tag{141a}$$

$$\Psi^{\ell+1/2}(x) = \frac{1}{2}\int_0^{\infty}\int_{-1}^{1} \sigma\phi^{\ell+1/2}\, d\mu' d\nu' \quad , \tag{141b}$$

$$- \frac{\partial}{\partial x}\frac{1}{3\sigma}\frac{\partial}{\partial x} f^{\ell+1} + \sigma f^{\ell+1}(x,\nu) - \chi\int_0^{\infty} \sigma f^{\ell+1}\, d\nu'$$

$$= \chi\left[\Psi^{\ell+1/2}(x) - \Psi^{\ell}(x)\right] \quad , \tag{141c}$$

$$\Psi^{\ell+1}(x) = \Psi^{\ell+1/2}(x) + \int_0^{\infty} \sigma f^{\ell+1}\, d\nu' \quad . \tag{141d}$$

For the special choice of cross sections

$$\sigma(\nu) = \beta \frac{1 - e^{-\alpha\nu}}{\nu^3} \quad , \tag{142a}$$

$$\chi(\nu) = \alpha e^{-\alpha\nu} \quad , \tag{142b}$$

the spectral radii of the two acceleration methods are respectively 0.888 and 0.164, for all choices of the constants α and β. [The spectral radius of the latter method is erroneously reported as 0.082 in Ref. 17.] In practice, the one-group diffusion acceleration method probably converges too slowly to be of practical use. The multigroup diffusion acceleration method has acceptable convergence properties, but one must generally perform a considerable amount of iterating to get the multigroup diffusion equation (141c) converged. Thus, to solve this multigroup diffusion equation, written as

$$-\frac{\partial}{\partial x}\frac{1}{3\sigma(x,\nu)}\frac{\partial}{\partial x} f(x,\nu) + f(x,\nu) - \chi(x,\nu)\int_0^\infty \sigma(x,\nu')\, f(x,\nu')\, d\nu' = S(x,\nu) \quad ,$$

we proposed[17] the following one-group diffusion acceleration method:

$$-\frac{\partial}{\partial x}\frac{1}{3\sigma}\frac{\partial}{\partial x} f^{\ell+1/2} + \sigma f^{\ell+1/2}(x,\nu) = \chi F^{\ell}(x) + S \quad , \tag{143a}$$

$$F^{\ell+1/2}(x) = \int_0^\infty \sigma f^{\ell+1/2}\, d\nu' \quad , \tag{143b}$$

$$-\left(\int_0^\infty \frac{\partial}{\partial x}\frac{1}{3\sigma}\frac{\partial}{\partial x}\frac{\chi}{\sigma}\, d\nu\right) G^{\ell+1}(x) = F^{\ell+1/2}(x) - F^{\ell}(x) \quad , \tag{143c}$$

$$F^{\ell+1}(x) = F^{\ell+1/2}(x) + G^{\ell+1}(x) \quad . \tag{143d}$$

With the cross sections given by Eq. (142), this method has the spectral radius 0.867.

Here we describe a "family" of acceleration methods for the transport equation that combine the methods (140), (141), and (143). Conceptually, these methods each consist of four parts, the third of which is repeated n times, where n is an arbitrary nonnegative integer. For n=0, the method reduces to the one-group acceleration method described by Eq. (140). For n=∞, the method becomes the multigroup acceleration method described by Eq. (141). For finite positive n, we obtain new acceleration methods that have convergence properties intermediate between those of the n=0 and n=∞ methods, and which tend monotonically toward the n=∞ properties as n increases. The methods are described as follows.

$$\mu \frac{\partial \phi^{\ell+1/2}}{\partial x} + \sigma\phi^{\ell+1/2}(x,\nu,\mu) = \chi\Psi^{\ell}(x) + Q \quad , \qquad (144a)$$

$$\Psi^{\ell+1/2}(x) = \frac{1}{2}\int_0^{\infty}\int_{-1}^{1} \sigma\phi^{\ell+1/2}\, d\mu' d\nu' \quad , \qquad (144b)$$

A

$$-\int_0^{\infty} \frac{\partial}{\partial x}\frac{1}{3\sigma}\frac{\partial}{\partial x}\frac{\chi}{\sigma}\, d\nu' \quad F^{\ell,0}(x) = \Psi^{\ell+1/2}(x) - \Psi^{\ell}(x) \quad . \qquad (145)$$

B

For $n \geq 1$ and $0 \leq m \leq n-1$,

$$-\frac{\partial}{\partial x}\frac{1}{3\sigma}\frac{\partial}{\partial x} f^{\ell,m+1/2} + \sigma f^{\ell,m+1/2}(x,\nu) = \chi\, F^{\ell,m}(x) + \Psi^{\ell+1/2}(x) - \Psi^{\ell}(x) \quad , \qquad (146a)$$

$$F^{\ell,m+1/2}(x) = \int_0^{\infty} \sigma f^{\ell,m+1/2}\, d\nu' \quad , \qquad (146b)$$

$$-\left(\int_0^{\infty} \frac{\partial}{\partial x}\frac{1}{3\sigma}\frac{\partial}{\partial x}\frac{\chi}{\sigma}\, d\nu\right) \quad G^{\ell,m+1}(x) = F^{\ell,m+1/2}(x) - F^{\ell,m}(x) \quad , \qquad (146c)$$

C

$$F^{\ell,m+1}(x) = F^{\ell,m+1/2}(x) + G^{\ell,m+1}(x) \quad , \tag{146d}$$

$$\left.\begin{aligned} \Psi^{\ell+1}(x) &= \Psi^{\ell+1/2}(x) + F^{\ell,n}(x) \quad . \end{aligned}\right\} \text{D} \tag{147}$$

Step A describes the transport sweep, which is the first step for all transport acceleration methods. Step B is patterned after the one-group diffusion acceleration of the transport equation [Eqs. (140)]. Step C is patterned after the one-group diffusion acceleration of the multigroup diffusion equation [Eqs. (143)]. Step D is patterned after the final step in both the one-group and the multigroup diffusion acceleration of the transport equation [Eqs. (140d) and (141d)].

For n=0, step C is omitted and the above method reduces to the one-group diffusion acceleration method described by Eqs. (140). For n=∞, the diffusion equation (146a,b) is fully converged, and the above method becomes the full multigroup diffusion acceleration method described by Eqs. (141). For each positive, finite value of n, we have a new acceleration method for which the multigroup diffusion equation is not fully converged.

The stability analysis proceeds exactly as before, and for uniform cross sections we obtain ω (the eigenvalue of the full method) versus λ (the Fourier Transform parameter) defined by the following equations:

$$\rho = \int_0^\infty \chi \frac{\sigma}{\lambda} \tan^{-1} \frac{\lambda}{\sigma} \, d\nu \quad , \tag{148a}$$

$$r_0 = \frac{\rho - 1}{\lambda^2 \int_0^\infty \frac{\chi}{3\sigma^2} \, d\nu} \quad . \tag{148b}$$

For $n \geq 1$ and $0 \leq m \leq n - 1$,

$$r_{m+1} = (r_m + \rho - 1) \left[\int_0^\infty \frac{3\sigma^2 \chi}{\lambda^2 + 3\sigma^2} \, d\nu - \frac{\int_0^\infty \frac{\chi}{\lambda^2 + 3\sigma^2} \, d\nu}{\int_0^\infty \frac{\chi}{3\sigma^2} \, d\nu} \right] + r_0 \quad ; \tag{148c}$$

$$\omega_n = \rho + r_n \quad . \tag{148d}$$

In Eqs. (148), ρ is the unaccelerated eigenvalue, ω_0 is the eigenvalue for the one-group diffusion-acceleration method described by Eqs. (140), and for $n \geq 1$, ω_n is the eigenvalue for the acceleration method with step C repeated n times. For the cross sections given by Eq. (142), we have plotted ρ and ω_n versus $\lambda/\alpha^3\beta$ for $n = 0, 1, 2, 3, 4, 5,$ and ∞ in Fig. 8. As can be seen, the method for each choice of n is stable, and as n increases, the eigenvalues uniformly decrease. The spectral radii for $n = 0, 1, \ldots, 10$ are listed in Table VI together with M, the number of full iterations of the method (144)-(147) required to reduce the transport error by a factor of 10.

In principle, for any given problem, one can now select the value of n which minimizes the computing cost. For small values of n the cost of doing the multigroup diffusion iterations [step C] is low, but spr is high and so the cost of doing the transport iterations [step A] is high. For large values of n the spr is low and the cost of doing the transport iterations is low, but the cost of doing the multigroup diffusion iterations is high. Thus, the total cost will be minimized for some finite value of n (possible even n=0).

TABLE VI

THE SPECTRAL RADIUS AND M VERSUS N

n	spr	M
0	0.888	19.4
1	0.791	9.8
2	0.707	6.6
3	0.635	5.1
4	0.572	4.1
5	0.517	3.5
6	0.470	3.0
7	0.429	2.7
8	0.393	2.5
9	0.362	2.3
10	0.336	2.1

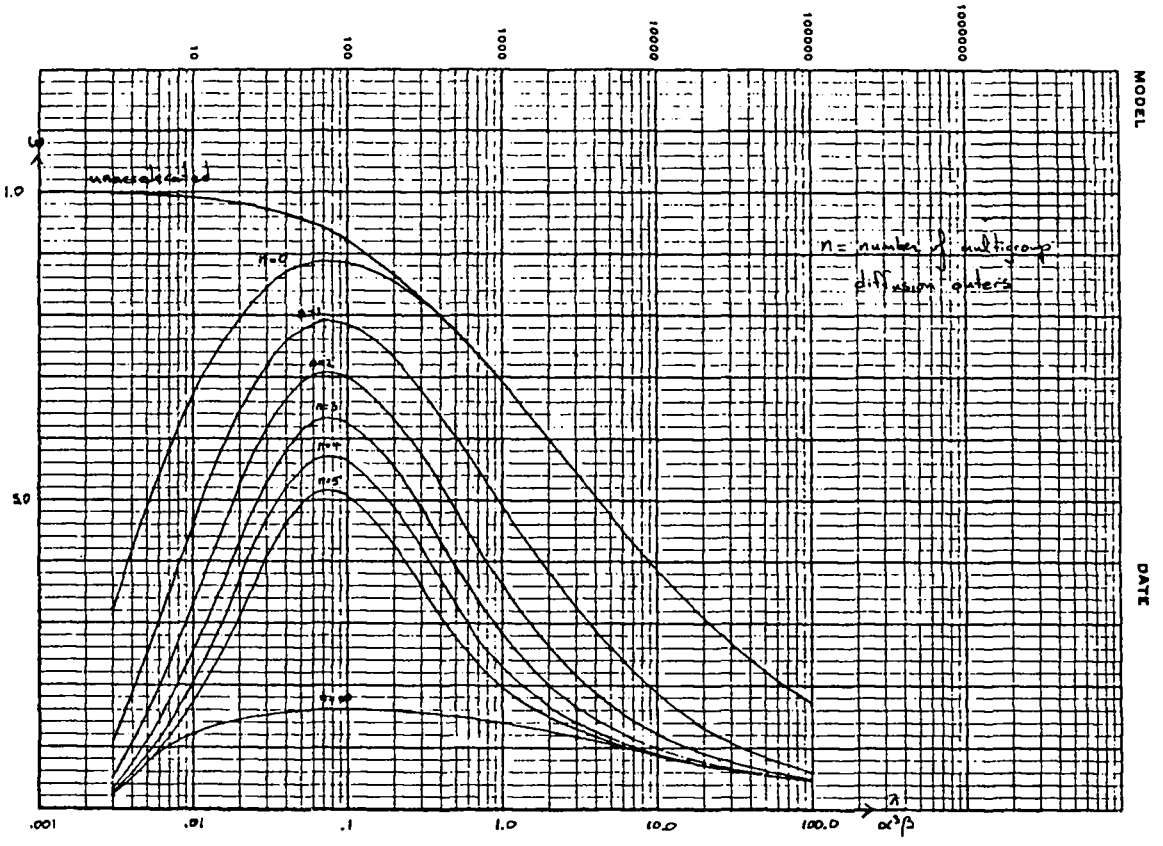

Fig. 8. ω versus $\lambda/\alpha^3\beta$.

Our analysis answers two questions which have been asked about the multigroup diffusion acceleration method (141). First: what happens to stability if the diffusion equation (141c) is not fully converged? In the context of the undiscretized equations, the method is stable, but its overall convergence properties improve as the multigroup equation is better converged. (However, we have not shown what happens when the one-group equations themselves have to be iterated upon and are not fully converged. Second: is it possible, without loss of stability or efficiency, to perform relatively few iterations on the multigroup diffusion equation (141c) in the early stages of the entire iteration process and then more fully converge this equation in the final stages? The answer is no. Stability will not be affected, but efficiency will almost certainly be hurt by such a strategy, as is shown by the results in Table VI.

H. Thermal Radiation Transport (B. A. Clark)

In previous quarterly reports, we have reported our progress in solving the thermal radiation transport equation using discrete-ordinates methods. During this quarter we have run three sample problems to verify the accuracy of our current methods.

The first problem is a 4 cm slab of material with opacity described by the analytic model

$$\sigma(\nu,\theta) = \frac{27}{(h\nu)^3}\left(1 - e^{-h\nu/\theta}\right) \quad , \tag{149}$$

where $\theta = kT$ is the material temperature in keV. The results of this problem have been reported previously.[19,20,21] The Rosseland mean optical depth of the problem varies from 5×10^9 mfp (1 eV isothermal slab) to 0.5 mfp (1 keV isothermal slab); thus, we refer to this as a thin slab problem. The discrete-ordinates solution of this problem is in excellent agreement with previous transport solutions.

However, the thin slab problem does not test the accuracy of following a radiation thermal wave through the material. For this reason, the "thick slab problem" was run; it consists of a 20 cm slab of material described by Eq. (149) driven by a 1 keV black body boundary source. The Rosseland mean optical depth varies from 2.5×10^{10} mfp at 1 eV to 2.5 mfp at 1 keV. Ten spatial zones are utilized and S_4 discrete-ordinates quadrature is adequate. The results of this problem showed significant advantages over the multigroup diffusion theory solution. Multigroup diffusion, without variable Eddington factors or flux limiters, allowed radiation to propagate through the slab faster than the speed of light. The discrete-ordinates transport solution did not suffer from this problem.

The third test problem is a modification of the thin wall problem; in the region 2 cm $< z <$ 2.5 cm, the constant in the analytic opacity (Eq. (149)) is replaced by 1000. This thick "wall" region has a Rosseland mean optical depth that varies from 10^{10} mfp at 1 eV to 2.3 mfp at 1 keV. The wall is treated using two mesh cells. Comparisons of solutions using discrete-ordinates and Implicit Monte Carlo (IMC) are in agreement for this problem. The timing of the

penetration of the thermal wave through the wall agreed to within 10%. Spatial temperature distributions, chosen at various times, also agreed with IMC solutions.

The discrete-ordinates method provides accurate solutions to these difficult problems using the simplest positive spatial difference scheme, diamond-difference with set-to-zero fixup. The results indicate that this difference scheme is adequate for one-dimensional problems. These solutions also illustrate the performance of the nonlinear DSA scheme developed for time-dependent thermal radiation transport calculations.

The wall problem also brought forward some unexpected results. The number of transport iterations required for convergence of the thermal source is expected to be a smooth function of time step; also, the total number of transport iterations per time step should remain less than 5-7. This expected behavior was observed in the calculations before the thermal wave hit the wall. After the wave hit the wall, the number of iterations per time step became "noisy" and some time steps required as many as 50 iterations. This unexpected behavior is, as yet, unexplained. Some potential causes for the noise have been identified and are being examined. We are confident that these problems can be explained in the near future.

Our future work will include examination of the noise in the iteration strategy. Also, a 1-group acceleration method will be employed to accelerate the convergence of the iterative multigroup DSA calculation. Further refinements in the opacity/transport iteration process will be studied to reduce the number of opacity calculations, a first step toward adding tabular equation-of-state and multigroup opacity capabilities.

I. A Sharper Version of the Cauchy-Schwarz Inequality for Real-Valued Functions (E. W. Larsen)

The standard Cauchy-Schwarz inequality[22,23] for real-valued functions can be stated as follows. Let

$$\langle \bullet \rangle = \int_a^b (\bullet)\, dx \quad ,$$

and let f and g be real-valued functions of x such that $\langle f^2 \rangle$ and $\langle g^2 \rangle$ exist. Then $\langle fg \rangle$ exists and

$$0 \leq \langle f^2 \rangle \langle g^2 \rangle - \langle fg \rangle^2 \quad , \tag{150}$$

with equality holding if and only if f and g are linearly dependent.

A simple proof of (150) is as follows. We define the functional

$$F(\lambda) = \langle (f - \lambda g)^2 \rangle \quad , \tag{151}$$

which is quadratic in λ and attains a minimum value of zero if and only if f and g are linearly dependent. The value of λ at which F assumes its minimum, λ^*, is determined by

$$0 = F'(\lambda^*) = -2 \langle (f - \lambda g) g \rangle \tag{152}$$

and is

$$\lambda^* = \frac{\langle fg \rangle}{\langle g^2 \rangle} \quad . \tag{153}$$

Introducing this result into the inequality

$$0 \leq F(\lambda^*) \tag{154}$$

and rearranging, we obtain the inequality (150). Also, equality holds in (150) if and only if equality holds in (154), which holds if and only if f and g are linearly dependent.

We shall now derive the following sharper version of the inequality (150): Let f, g, and h be any real-valued functions such that $\langle f^2 \rangle$, $\langle g^2 \rangle$, and $\langle h^2 \rangle$ exist with $\langle h^2 \rangle \neq 0$. Then

$$\frac{\langle (f\langle gh \rangle - g \langle fh \rangle)^2 \rangle}{\langle h^2 \rangle} \leq \langle f^2 \rangle \langle g^2 \rangle - \langle fg \rangle^2 \quad , \tag{155}$$

with equality holding if and only if f, g, and h are linearly dependent. The derivation of this inequality is based on a simple generalization of the procedure (151)-(154).

To begin, one can easily show that if g and h are linearly dependent, then (155) explicitly becomes an equality. Thus, from this point on we assume that g and h are linearly independent. We define the functional

$$F(\lambda,\rho) = \langle (f - \lambda g - \rho h)^2 \rangle \quad ,$$

which is quadratic in λ and ρ and attains a minimum value of zero if and only if f, g, and h are linearly dependent. The values of λ and ρ at which F assumes its minimum, λ^* and ρ^*, are determined by

$$0 = F_\lambda(\lambda^*,\rho^*) = -2(\langle fg \rangle - \lambda^* \langle g^2 \rangle - \rho^* \langle gh \rangle)$$

$$0 = F_\rho(\lambda^*,\rho^*) = -2(\langle fh \rangle - \lambda^* \langle gh \rangle - \rho^* \langle h^2 \rangle) \quad ,$$

and are given explicitly by

$$\lambda^* = \frac{\langle fg \rangle \langle h^2 \rangle - \langle fh \rangle \langle gh \rangle}{\langle g^2 \rangle \langle h^2 \rangle - \langle gh \rangle^2} \quad , \tag{156a}$$

$$\rho^* = \frac{\langle fh \rangle \langle g^2 \rangle - \langle fg \rangle \langle gh \rangle}{\langle g^2 \rangle \langle h^2 \rangle - \langle gh \rangle^2} \quad . \tag{156b}$$

(We note that λ^* and ρ^* uniquely exist because g and h are assumed linearly independent.) Now we explicitly introduce Eqs. (156) into the inequality

$$0 < F(\lambda^*,\rho^*) \tag{157}$$

and after considerable algebraic manipulation, obtain

$$0 \leq \frac{\langle f^2\rangle\langle g^2\rangle\langle h^2\rangle - \langle f^2\rangle\langle gh\rangle^2 - \langle g^2\rangle\langle fh\rangle^2 - \langle h^2\rangle\langle fg\rangle^2 + 2\langle fg\rangle\langle gh\rangle\langle hf\rangle}{\langle g^2\rangle\langle h^2\rangle - \langle gh\rangle^2} \quad .$$

The denominator in this inequality is positive, and hence the numerator must be nonnegative. This implies

$$\langle h^2\rangle[\langle f^2\rangle\langle g^2\rangle - \langle fg\rangle^2] \geq \langle f\rangle^2\langle gh\rangle^2 - 2\langle fg\rangle\langle gh\rangle\langle hf\rangle$$

$$+ \langle g^2\rangle\langle fh\rangle^2 = \langle(f\langle gh\rangle - g\langle fh\rangle)^2\rangle \quad ,$$

which immediately gives (155). Also, equality holds in (155) if and only if equality holds in (157), which holds if and only if f, g, and h are linearly dependent.

To illustrate the ability of (155) to produce sharper results than (150), let us take $a = 0$, $b = \infty$,

$$f = \left[\chi\left(1 + \frac{\lambda^2}{3\sigma^2}\right)\right]^{1/2}$$

$$g = \left[\frac{\chi}{1 + \lambda^2/3\sigma^2}\right]^{1/2}$$

$$h = P_1\left[\chi\left(1 + \frac{\lambda^2}{3\sigma^2}\right)\right]^{1/2} \quad ,$$

where $\chi(x)$ is a nonnegative function satisfying

$$1 = \int_0^\infty \chi \, dx \quad ,$$

$\sigma(x)$ is a nonnegative function satisfying

$$\int_0^\infty \frac{\chi}{\sigma^2} \, dx < \infty \quad ,$$

$P_1(x)$ is any function satisfying

$$0 = \int_0^\infty P_1 \chi \, dx \quad , \tag{158a}$$

$$\rho_{ij} \equiv \int_0^\infty \frac{\chi P_1^i}{\sigma^j} \, dx < \infty \qquad , \qquad 0 \leq i,j \leq 2 \quad , \tag{158b}$$

$$0 \neq \rho_{12} \quad , \tag{158c}$$

and λ can assume any real value. We then have

$$\langle f^2 \rangle = 1 + \frac{\lambda^2}{3} \rho_{02} \quad , \tag{159a}$$

$$\langle g^2 \rangle = \int_0^\infty \frac{3\sigma^2 \chi}{3\sigma^2 + \lambda^2} \, dx \equiv \omega_0(\lambda) \quad , \tag{159b}$$

$$\langle fg \rangle = 1 \quad , \tag{159c}$$

$$\langle gh \rangle = 0 \quad , \tag{160a}$$

$$\langle fh \rangle = \frac{\lambda^2}{3} \rho_{12} \, , \tag{160b}$$

$$\langle h^2 \rangle = \rho_{20} + \frac{\lambda^2}{3} \rho_{22} \, . \tag{160c}$$

Introducing Eqs. (159) into the standard Cauchy-Schwarz inequality (150) and rearranging , we obtain

$$\omega_0(\lambda) \geq \frac{1}{1 + \frac{\lambda^2}{3}\rho_{02}} \quad . \tag{161}$$

However, introducing Eqs. (159) and (160) into the new inequality (155) and rearranging, we obtain

$$\omega_0(\lambda) > \frac{1}{1 + \frac{\lambda^2}{3}\left[\rho_{02} - \frac{\lambda^2\rho_{12}^2}{3\rho_{20} + \lambda^2\rho_{22}}\right]} \quad , \tag{162}$$

which provides a sharper estimate than that of Eq. (161) for any function P_1 satisfying Eqs. (158).

IV. MONTE CARLO RADIATION TRANSPORT

Group X-6 has a significant effort devoted to the development, implementation, assessment, and application of Monte Carlo methods and codes for radiation transport calculations.

During the reporting period, we present our progress on the MCNP, Version 3 Monte Carlo code, on portability techniques used in the code, and on implementation of MCNP, Version 3 in numerous computing environments. These reports are followed by a discussion of a new surface source capability in MCNP. Next come reports on the generalization of MCNP standard sources, on a new biasing technique, and on a new weight-window generator for MCNP. As part of our coupled electron/photon transport work, we report on calculations for two electron-gamma converters performed with our CYLTRAN computer code. Next are two reports pertaining to our multigroup Monte Carlo code MCMG. These are followed by a brief report on the application of MCNP to a total gamma ray yield detector. Progress on 3-D graphics is also reported. The section concludes with a description of a method of sampling from a cumulative probability distribution and a brief report on further MCNP testing.

A. MCNP Version 3 (T. N. K. Godfrey)

MCNP is a general-purpose, continuous-energy, generalized-geometry, time-dependent, coupled neutron-photon Monte Carlo transport code.[24] It has been widely accepted and is heavily used both within and outside Los Alamos National

Laboratory. The code continues to be actively improved and enhanced by members of Group X-6.

The portable version of MCNP, Version 3, has started a period of trial use at Los Alamos and by volunteers among RSIC's correspondents. Version 3 has been developed over the last two years in parallel with the sequence of Los Alamos production versions of MCNP. Version 3 presently has all the features of the current production version, which is Version 2D. Now that Fortran 77 compilers and libraries are available on all widely-used scientific computer systems, including ours at Los Alamos, it is time for Version 3 to go into production. When the period of trial use is complete, Version 3 will replace Version 2D at Los Alamos and will be distributed to other installations by RSIC.

B. Portability Techniques used in MCNP Version 3 (T. N. K. Godfrey)

The potential users of MCNP outside Los Alamos have a wide variety of computers, operating systems, and utility software. We would like to be able to provide MCNP to anyone who has access to any fairly common computing system. Our success in making a single MCNP program (with a few isolated system-dependent sections) run on LTSS and CTSS in production at Los Alamos and at the NMFECC, and the recent availability of a standard programming language adequate for large-scale scientific and engineering computing, FORTRAN 77,[25] led us to believe that we could provide and maintain a single MCNP program for use on all common computing systems. Using this approach, we have successfully run the FORTRAN 77 version of MCNP, Version 3, on a CRAY-1 with CTSS, on CDC machines with LTSS or NOS and with LCM, ECS or neither, on a VAX-780 with VMS, on an IBM 3033, and on a PRIME-750. We are satified that our approach is a good one and are presently polishing up MCNP Version 3 for distribution through the Radiation Shielding Information Center (RSIC) at Oak Ridge.

The most important portability technique in MCNP Version 3 is the use of FORTRAN 77. With FORTRAN 77 most of the difficulties with character representation, internal conversion between character data and numeric data, file opening and closing, structure of binary files, and nonuniform interpretation of control statements are avoided. The generic intrinsic functions make it easy to use double precision type on 32-bit machines and real type on 60 or 64-bit machines. The PARAMETER statement for defining constants of all types greatly simplifies the creation of system-dependent sections of code where they are required. In addition, FORTRAN 77 is a good convenient programming language,

without the narrow limitations that made the previous standard, FORTRAN 66,[26] difficult to use for large programs. The only significant limitation of FORTRAN 77 for MCNP is the absence of a way to allocate storage dynamically. Storage is dynamically allocated in MCNP only during the setup phase of a problem. This limited dynamic allocation of storage can be done within FORTRAN 77, albeit clumsily, by means of statement functions or by offsets in subscripts. The latter method is illegal (subscript expression value exceeds upper dimension bound) but works on all the systems we have tried.

System-dependent sections of code are necessary to provide features that are outside the scope of the programming language. Some important examples are overlays or segments, graphics, execute line message, field-length control, and double precision type on 32-bit machines. The system-dependent sections are defined by *IF,DEF,name,range or *IF,DEF,name and *ENDIF directives and are evoked by a *DEFINE,name,...,name directive. These directives are interpeted by a pre-processor which can be HISTORIAN or UPDATE, at least one of which is available most places, or by PRPR in MCNP's own preprocessor. PRPR which is only 107 lines long, is written in pure FORTRAN 77, and works everywhere.

At present we provide system-dependent features such as the time and terminal interrupts only if it can be done by calling, from FORTRAN, subroutines provided by the system vendor or, in some cases, by the local installation. We may someday consider writing assembly language subroutines to provide these features in cases where the necessary system calls exist but there are no FORTRAN-callable subroutines that can make the system calls. We use comdecks in MCNP to shorten the code, to make maintenance easier, and to isolate and concentrate some of the system-dependent material. A good example is the comdeck ZC, which is called in most of the subroutines of MCNP. It contains thirty system-independent named constants and seven system-dependent constants that handle peculiarities ranging from the effect of double precision on dynamically allocated storage to the effect of automatic vectorization on the strategy used for storing tally scores. The comdecks are defined by *COMDEC,name directives and are called by *CALL,name directives, which are interpreted by HISTORIAN, UPDATE or PRPR.

Another strategy used to isolate system-dependent code is to concentrate it in a few subroutines. The subroutines GRAFIX has twelve ENTRYs providing elementary graphics operations such as "move to a specified point" or "skip to the next frame." Each ENTRY section of GRAFIX has alternative code for calling

subroutines from CGS, PLOT10, or DISSPLA. The subroutines that call the GRAFIX ENTRYs are free from the clutter of the alternative coding and, even more important, are free from the nonstandard Fortran required by many of the calls to the graphics systems. If any of the graphics systems are made standard-conforming, only the one subroutine GRAFIX in MCNP will need to be changed.

In spite of good efforts to create and distribute a standard library of mathematical subroutines, it is not yet practical to assume that it will be available everywhere. Fortunately MCNP does not use very many mathematical subroutines. Those that are used were taken from the Los Alamos mathematics library, were converted to FORTRAN 77 and to MCNP programming style (which shortened them a great deal), and were incorporated into MCNP as the last 600 lines of the program.

Some limitations of some systems are accommodated without providing alternative sections of code. For example, the IBM compiler complains if double-precision quantities do not fall on even word boundaries. Correct code is generated in that case, but to avoid the annoyance of all the warning messages from the compiler and to avoid the reduced computing speed that could result on some IBM systems, we have put all of the integer variables and arrays in each common block at the end of the block.

The cross-section libraries that we provide with MCNP have to be as portable as MCNP is. So we provide them as formatted files of 80-character records. Such files are about twice as large as corresponding unformatted files and are much slower to read. So we provide with MCNP a small conversion code to translate the formatted files into direct access unformatted files. This code can also be used to put the cross-section tables into files in any arbitrary arrangement. An installation where only one kind of MCNP problem is run can put just the tables for the nuclides they regularly use in their main cross-section file, thus saving public file space if it is scarce. MCNP is able to read both formatted and unformatted cross-section files. Note that although the formatted cross-section files are both standard-conforming and portable, the unformatted files are standard-conforming but not portable. This is because the FORTRAN 77 standard specifies how files are to be written and read but says nothing about how they are to exist in the actual hardware storage medium. Each system does files its own way. The only reason the formatted files are portable is that there are a few ways of putting 80-column

card images on 9-track 1/2" magnetic tape such that just about any installation can manage to read them somehow.

A Monte Carlo program has to have a generator of pseudo-random numbers. It is highly desirable to have the generator produce the same sequence of pseudo-random numbers on all systems. The generator in MCNP does this. It implements the commonly-used algorithm, X' = A*X (mod M) with M=2**48. A and X are each a pair of 24-bit integers carried in real (double-precision in 32-bit machines) variables. The multiplication is done by a programmed double-precision multiply. This gets around the lack of a low-order multiply on most computers. The whole thing is done in five executable FORTRAN 77 statements.

C. MCNP Version 3 Implementation (J. T. West)

MCNP Version 3 has now been implemented on CDC 7600, CRAY, VAX 780, PRIME 750, IBM 3033, Cyber 176, and Cyber 825 computer. Version 3 is written in the new FORTRAN 77 Standard for probability. The new FORTRAN 77 compilers currently in existence contain many minor bugs, but in general perform satisfactorily. A serious problem exists in the IBM and CDC systems that will require correction. IBM's FORTRAN 77 compiler has problems reading and writing character type arrays, where the array limits are specified only in "Dimension" statements. This problem makes it impossible to generate and use as MCNP RUNTPE on IBM. CDC has a problem performing character comparisons on character type variables stored in LCM. The problem is in a CDC system library routine called "DCC=". A local fix exists at Los Alamos and is required on CDC machine using LCM and the CDC FTN5 compiler. Implementation on the VAX was accomplished with all features available on LTSS and CTSS, including the interrupt capability. CRAY implementation has been successful on both CTSS and COS.

The type 1, card image cross-section format, has proved very portable. Conversion to binary has been accomplished on all systems using the auxiliary program MAKXSF. The concept of a cross-section directory pointing to either disk files or peripherial storage devices has proven and will prove in the future to be very versatile and flexible in implementing cross-section files on different computer hardware.

MCNP Version 3 graphics is operational using the Los Alamos Common Graphic System, CGS, the Tektronics PLOT10 software, and the ISSCO DISSPLA graphics systems. The Los Alamos CGS software has been installed and implemented on several systems not having either PLOT10 or DISSPLA, including the Defense

Nuclear Agency's Cyber 176 for the Naval Weapons Evaluation Facility, NWEF. CGS is not proprietary to Los Alamos and is available to the general public.

D. MCNP, A New Surface Source Capability (J. T. West)

Frequently in running radiation transport problems it is desirable to break up a problem into parts and concentrate effort on a part of a geometry system rather than trying to compute the complete system. This approach is effective when:

1. the parts of a geometry system can be decoupled, either due to distance or size, and,
2. when albedo effects are properly treated at the coupling boundary.

This procedure is effective in studying small geometric perturbations that have a negligible effect on the larger system. For these applications, the smaller or secondary system is decoupled from the larger system. Changes in the smaller system therefore do not affect radiation transport in the larger system. An advantage to being able to conduct parametric studies on the smaller system without rerunning the complete larger geometry system is to be able to obtain better Monte Carlo statistics in considerably shorter computer runs. This technique allows more design information to be obtained with less demands on computer and manpower resources. Running coupled calculations is a common practice in many radiation transport applications. The two most commonly used coupled links are coupling S_N to S_N and coupling S_N to Monte Carlo.

X-6 has developed a general Monte Carlo to Monte Carlo coupling technique for use in MCNP. The method utilized in MCNP preserves both the particle current and the statistics of the particle distribution on a surface source. Several methods are in common use for surface source coupling. Most techniques in the past used either discrete distribution tables, or functions (such as Legendre Polynomials) to preserve the phase space distribution of particles on the surface. These approaches to surface source sampling may preserve the flux and possibly the current on a surface, but directly wash out the statistical information of the particles which generated the surface source.

In order to preserve exactly the statistical information of the particle distribution on a surface source, it is necessary to correlate particle tracks with the individual histories, which generated the track. The relative error computed for tallies in MCNP is:

$$\left[\frac{\sum_{i=1}^{N} X_i^2}{\left(\sum_{i=1}^{N} X_i\right)^2} - \frac{1}{N}\right]^{1/2} = \text{Relative Error} , \tag{163}$$

where X_i represents the tally contribution from the ith particle history. Actually X_i is

$$X_i = \sum_{j=1}^{M_i} Y_{i,j} , \tag{164}$$

where $Y_{i,j}$ is the tally contribution from the jth particle track born from the ith history and M_i is the number of tracks for the ith history. Several processes exist for generating secondary particles from a parent particle. For example, secondary particle generation or particle splitting. MCNP computes statistics based on individual particle histories, as opposed to calculating statistics for a batch of particles, and then calculating errors based on variances between batch averages. The MCNP approach allows computation of statistics during the run, and may be terminated cleanly at the end of any history.

Surface sources in MCNP are generated by saving all relevant particle phase space information at a boundary on a file. A surface source file is a boundary crossing file. It is clear that,

$$\sum_{i=1}^{N} \sum_{j=1}^{M_i} Y_{i,j} = \sum_{i=1}^{N} X_i \tag{165a}$$

and that

$$\sum_{i=1}^{N}\sum_{j=1}^{M_i}(Y_{i,j})^2 \neq \sum_{i=1}^{N}(X_i)^2 \qquad (165b)$$

while it is true

$$\sum_{i=1}^{N}\sum_{j=1}^{M_i}(Y_{i,j})^2 = \sum_{i=1}^{N}(X_1)^2 \quad . \qquad (165c)$$

The MCNP surface source, by correlating particle tracks with their respective histories preserves both the sum of particle contributions on a surface and the sum of squares of the history contributions, thereby preserving the flux, the current, and the statistical distribution of particles on a surface source.

By allowing splitting and Russian roulette on a surface source, the number of particles tracked from a surface source may be independent from the number of particles used to generate the surface source in the initial calculation. The absolute variance of a surface source will be modified, if all particle tracks on the surface are not tracked.

The new MCNP surface source has the following features:

1. The surface source may be composed of an arbitrary number of surfaces; all or selected surfaces may be sampled.
2. All surface types are available for use as a surface source.
3. Biased sampling by energy is allowed. This is convenient where tally results are being computed, which are more sensitive to a given energy range. It is then possible to sample from a biased distribution more efficiently then the true distribution on the surface source.
4. Surfaces may be segmented to allow partial sampling from a given area of interest.
5. Surface sources may be repeated and arbitrarily positioned, an arbitrary number of times, and sampled from a biased distribution of repetitions.

6. Uncollided (i.e. from the surface) point detector estimates may be made from a surface source using discrete tables defining the angular emission probability on the surface.

Point detector estimates made from a surface source, presently, do not compute the correct detector variance where the angular emission distribution is not known exactly. Much effort has gone into benchmarking and understanding uncollided point detector estimates from a surface. A peripherial program, FRED, computes as many as four sets of six dimensional tables for describing the angular distribution of particles on the surface.

Two sets of tables are computed for neutrons on a surface, and two sets are computed for gammas on a surface. One set of tables describes the angular distributions for particles on a surface source which suffered no collisions in reaching the surface source. Another set of tables describes the angular distribution of particles which suffered a collision before reaching the surface source.

The reason for two tables is that the angular distribution of uncollided particles on a surface can be drastically different from the angular distribution of collided particles on a surface source. Therefore, the angular distribution tables for collided and uncollided particles on a surface must be kept separately.

An extreme case is a point source in a sphere, or a line source in a cylinder. The uncollided particle angular distribution from such a hypothetical source is a true delta function valid only in a monodirectional beam emitted from the surface. If the sphere or cylinder contained a scattering medium, the collided particle angular distribution on the surface would be completely different, such as a cosine of the angle of emission raised to some power.

The peripherial program, FRED, bins each set of tables in six domains of phase space. They are time, energy, two space domains, polar angle of emission, and azimuthial angle of emission. Tables are generated in a single FRED run for each surface in a surface source file. At present a method has been developed and implemented in FRED to compute relative errors for each bin. Plans are to eventually be able to complete correctly the errors on direct point detector estimates from a surface source. The problem may be understood as:

$$T_{i,j}(\vec{R}, \vec{\Omega}, E, t) = \frac{P_{i,j}(R, \Omega, R, t)\, e^{-\Sigma\gamma_{i,j}}}{r_{i,j}^2} \quad , \tag{166}$$

where

$T_{i,j}(\vec{R}, \vec{\Omega}, E, t)$ - is the tally contribution to a point detector from the j^{th} track of the i^{th} history at space position $\vec{R}$, emitted in direction $\vec{\Omega}$ with energy E at time t.

$P_{i,j}(\vec{R}, \vec{\Omega}, E, t)$ - is the probability density function for particle emission from a surface source at location $\vec{R}$ with direction $\vec{\Omega}$, energy E, and time t.

$r_{i,j}$ - distance from location $\vec{R}$ to the point detector of interest.

$\gamma_{i,g}$ - number of mean free paths from $\vec{R}$ to the point detector.

$P_{i,j}(\vec{R}, \vec{\Omega}, E, t)$ is not a precisely known quantity when making direct estimates to a point detector from a particle bin emitted from a surface source. The probability of emission is computed from a statistical distribution of particles on a surface. The probability, $P_{i,j}(R, \vec{\Omega}, \vec{E}, t)$, has a relative error associated with it which implies that each individual tally $r_{i,j}(\vec{R}, \vec{\Omega}, E, t)$ has a relative error. The sum of the individual tallies then becomes the sum of partial estimates, each containing relative errors. The problem is to compute the error on the sum of the individual estimates.

The probability density function $P_{i,j}(\vec{R}, \vec{\Omega}, E, t)$ is a function of azimuthial angle of emission, polar angle of emission, two space domains, energy, and time. As a discretely binned density function for six domains of phase space, there exists six hierarchial probability density functions and six hierarchial cumulative distribution functions. Since each density table is normalized, an individual bin element in each table is a fraction, where the numerator has an error associated with it, the denominator has an error associated with it, and a covariance error exists due to the addition of the numerator in the denominator. To illustrate consider

$$P_{i,j}(\phi, \mu, x, y, E, t) = \frac{Q_{i,j}(\phi, \mu, x, y, E, t)}{Q'_{i,j}(\mu, x, y, E, t)} \quad , \tag{167a}$$

where

$$Q'_{i,j}(\mu, x, y, E, t) = \sum_{\phi} Q_{i,j}(\phi, \mu, x, y, z, t) \quad . \tag{167b}$$

$Q_{i,j}(\phi, \mu, x, y, E, t)$ is the weight found in some bin defined about some azimuthial angle of emission ϕ, about some polar angle of emission μ, about some space domain x, about some space domain y, about some energy E, about some time t. $Q'_{i,j}$ represents $Q_{i,j}$ summed over all ϕ . Both $Q_{i,j}$ and $Q'_{i,j}$ are not absolute quantities, but are statistical quantities. The problem is to compute the relative error of $P_{i,j}$. This may be accomplished by computing the relative error of $Q_{i,j}$, the relative error of $Q'_{i,j}$, and the covariance relative error of $Q_{i,j}$'s contribution to the error in $Q'_{i,j}$. This approach has been implemented in FRED, so that tables of angular emission probability density tables are computed and their respective tables on relative errors on the angular emission probability tables.

In the future further development of the direct point detector contribution from surface sources will include calculation of the error due to statistical fluctuation on a surface source.

Surface source development has occurred in X-6 through the efforts of Ed Snow, Art Forster, Dick Prael, and mainly Jim West. Ed Snow has successfully blended the surface source patch in MCNP, so that its file organization and input requirement follow standard MCNP guidelines. Art Forster contributed to the conceptual development of the surface source and contributed to its verification by developing simple analytic models of angular distribution on simple surface geometries. Dick Prael contributed to the conceptual development of the surface source method and to the understanding of error analysis involving the surface source. Jim West contributed to the conceptual development of the surface source, the initial programming of the surface source patch, the benchmarking and verification of its initial operation.

E. Generalization of MCNP Standard Sources (R. G. Schrandt)

The existing standard sources of MCNP have been modified to allow more flexibility and some generalization. Dependency between source variables can be defined. Up to fifty source distributions are allowed and can be associated with any of these variables.

In particular, particles can now start uniform in volume in more than one cell. The probabilities are computed from the cell volumes. Multiple energy spectra are allowed and can be selected as a function of cell.

For energy-angle depending, either one can be defined to be the independent variable. This variable is then sampled from a tabular distribution. The index of the bin selected then points to a set of spectra for the dependent variable. A spectra from this set is selected and the dependent variable is then sampled from this distribution. These spectra are in the SI, SP, SB format[24] of MCNP which allows any or all of them to be biased. A frequency table can be printed for each distribution.

This modification is in a friendly user version and is not as yet part of the standard MCNP. An X-6 memo of November 16, 1982, describes it in more detail and gives some examples.

F. A New Biasing Technique for MCNP (T. E. Booth)

During this reporting period, I have tested a new biasing technique based on preferentially choosing random numbers so as to enhance those random number sequences that have been most successful in previous histories. Before reading further, be advised that this "biased random number technique" appears to have failed for the moment. However, there is still hope for this technique, in my opinion.

My personal goal for MCNP is to relieve the user of all concern about variance reduction; the user should set up his problem and MCNP should figure out what to do about "appropriate" variance reduction parameters. Although I do not always obtain my goals, there is truly some reason to believe that this one is obtainable, albeit perhaps not easily.

It is well known (for linear Monte Carlo) that zero-variance solutions of Monte Carlo transport problems are possible if the adjoint solution is known exactly; however, then the problem is already solved. As a practical matter, low variance solutions are possible with an approximate adjoint. The weight

low variance solutions are possible with an approximate adjoint. The weight window/importance generator has had major (although not universal) success in using an adjoint solution estimated during the previous Monte Carlo run. Factors of two to twenty improvement over the "best" user's run are common for the generator. The user still must partition up the phase-space in an "appropriate" way because the generator estimates importance in the user-specified phase-space cells.

The importance generator works by keeping records of the average score generated by a particle entering a phase-space cell. The generator essentially answers the question "what particle trajectories generate the highest scores?" The particle trajectories are determined by the random number sequence; so, suppose instead, one asks "what random number sequences generate the highest scores?" Suppose that a random number sequence ($\vec{r} = r_1, r_2, r_3, \ldots$) generates a high score, one probably wishes to sample more random number sequences in the "neighborhood" of $\vec{r}$. Thus, instead of keeping records of what cells are most important, a generator could keep records of what random number sequences are important. This relieves the user from specifying cells.

Another way of considering the idea is to think of the Monte Carlo problem as a function that assigns a score (or tally) $T(\vec{r})$ to each random number sequence $\vec{r}$. Traditional biasing schemes work by changing T so that the random number sequence is the argument of a new function $T_1(\vec{r})$, and $\vec{r}$ specifies an entirely different particle trajectory. What I propose to do is to always have $\vec{r}$ specify a given particle trajectory but alter the probability of choosing $\vec{r}$; that is, I propose to do the biasing in the random number space rather than the physical space. The mean can be preserved by multiplying the tally by the true density $p_t(\vec{r})$ divided by the density $p(\vec{r})$ actually used. Thus, the tally associated with $\vec{r}$ would be $[p_t(\vec{r})/p(\vec{r})]T(\vec{r})$.

Thus far, this approach has failed.

G. A New Weight Window Generator for MCNP (T. E. Booth)

An effective space-angle weight window generator was developed and debugged through versions 2B, 2C, and 2D. The method and some calculational results are described in Ref. 27. Another problem that the space-angle generator has solved is the infamous "Tophat" problem. This problem is shown in Fig. 9. The material is concrete, but the density (g/cc) in regions A, B, C, and D is 20, 10, 0.5, and 2, respectively. The horizontal lines are planes,

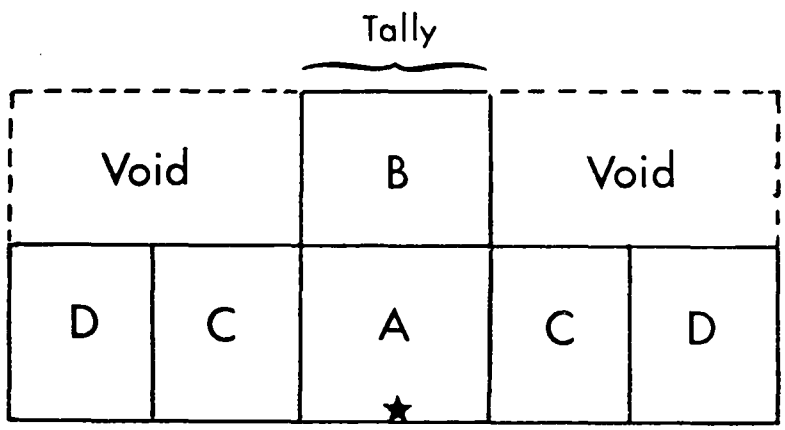

Fig. 9. The "Tophat" Problem.

and the vertical lines are cylinders so that A and B form a central cylinder with C and D being rings. The source is 14-MeV point isotropic neutrons and is ever so slightly just inside region A. The radii of the cylinders are 5, 10, and 15 cm; a plane at 8 cm bounds the top of the regions A, B, and C; a plane at 16 cm bounds the top of region B and the void above regions C and D. The object is to calculate the total current (integrated over everything) leaking through the segmented plane above region B.

The average mean free paths in regions A, B, C, and D are about 0.8, 1.5, 33, and 8 cm, respectively. As part of the problem, there is absolutely no variance reduction except for splitting and Russian roulette; even obvious (obvious you think) source direction biasing is not used. Capture is analog, and the energy cutoff is 1 MeV. Although not shown in the drawing, there is a horizontal plane every centimeter used for splitting.

The "best" and most reliable calculational results obtained in 1980 are shown in Table VII. These were obtained using a CDC-7600 computer. Note the jumps in the figure of merit; the error even at 3-4% statistics is unreliable. Now compare Table VIII and note how well behaved the error is. Table VIII is the result of the same space-angle weight window and space-angle generator described in the Tokyo paper and calculated on a CRAY-1 computer. Although much

TABLE VII

"BEST" TOPHAT RESULTS OF 1980
(Weight Window, energy independent)

NPS	MEAN x 10^{-5}	ERROR	FIGURE OF MERIT
10000	3.17	.133	110
20000	3.59	.099	96
30000	3.91	.077	104
40000	3.92	.066	106
50000	4.08	.073	70
60000	3.96	.066	71
70000	4.09	.061	70
80000	4.07	.056	72
90000	4.09	.052	74
100000	4.10	.049	76
110000	4.09	.047	76
120000	4.11	.045	75
130000	4.05	.043	77
140000	4.05	.041	78
150000	4.05	.041	73
160000	4.06	.040	72
170000	4.12	.039	72
180000	4.17	.037	72
190000	4.16	.037	69
200000	4.10	.037	69
210000	4.13	.036	66
220000	4.14	.035	67
230000	4.23	.046	38
240000	4.24	.044	39
250000	4.23	.043	40

TABLE VIII

1983 TOPHAT RESULTS

NPS	MEAN	ERROR	FOM
32000	5.04912E-05	0.0441	114
64000	5.07058E-05	0.0329	102
96000	4.96510E-05	0.0267	104
128000	4.82126E-05	0.0232	104
160000	4.77104E-05	0.0206	106
192000	4.80046E-05	0.0187	107
224000	4.79021E-05	0.0173	107
256000	4.79770E-05	0.0162	108
288000	4.80059E-05	0.0152	108
320000	4.76699E-05	0.0144	108
352000	4.81356E-05	0.0138	108
384000	4.78260E-05	0.0132	108
416000	4.80842E-05	0.0126	109
425519	4.80287E-05	0.0124	109

7600 equivalent FOM = $\frac{109}{1.8}$ = 61.

refinement is required, this technique shows great promise for highly angle-dependent problems.

H. Cyltran Calculations for Two Electron-Gamma Converters (H. G. Hughes and J. M. Mack)

At the request of R. F. Hoeberling (NSP/WAC), who has an interest in pulsed radiography, we have investigated the energy and angular distribution of photons produced when electrons impinge on a tungsten target. The calculations were carried out using CYLTRAN,[28] a general purpose Monte Carlo code for the solution of coupled electron/photon transport problems in cylindrical geometry. The physical situation that we modeled is shown in Figure 10. The incident electrons are uniformly distributed in the cosine of the angle relative to

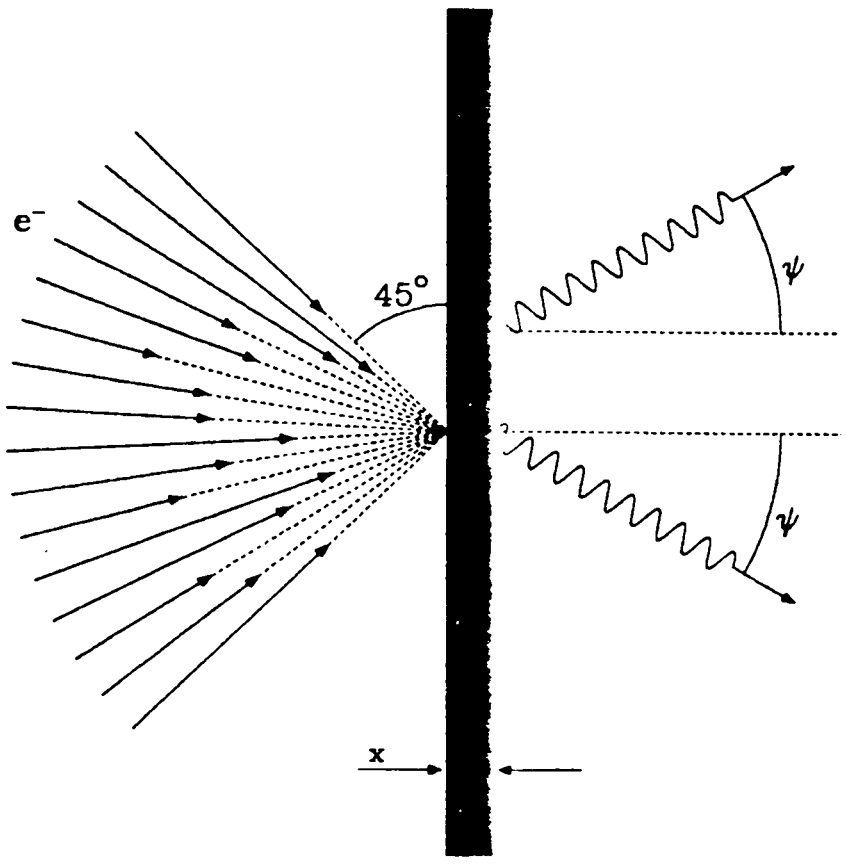

Fig. 10. Model Geometry for the CYLTRAN Calculation.

the normal, but are confined to a cone with a half-angle of 45 degrees. Two problems were studied, namely an incident electron energy of 1.1 MeV with a target thickness of 0.02746 cm, and an incident electron energy of 5 MeV with a target thickness of 0.11399 cm. The transmitted photons were tallied in 10-degree angular bins and in energy bins with lower limits of 0.9, 0.8, and 0.5 times the incident energy. The target was essentially treated as a semi-infinite slab, and no spatial information about the emerging photons is available.

The results for the 1.1-MeV problem are summarized in Tables IX and X, which give respectively the transmitted photon energy per steradian, and the number of transmitted photons per steradian, in the three energy groups of interest. (The totals given at the bottom of each table are integral quantities, and are no longer per steradian.) The corresponding quantities for the 5 MeV problem are given in Tables XI and XII. All of the numbers in these tables are normalized to one incident electron. The customary association of a one-sigma error with each number has been omitted here, since through a combination of variance reduction techniques and brute force, all of these numbers have been driven to a precision of one percent or better. It should be emphasized that this refers only to the precision of the Monte Carlo calculations. Comparison between these calculations and actual experiments can be cruder than this, because of uncertainties in the cross sections, differences between the model and the experiment, and other factors.

I. MCMG Update (D. G. Collins and W. M. Taylor)

The MCMG patch to version 1B of MCNP has been updated to version 2C of MCNP. MCMG Version 2C is a multi-energy group version of the continuous energy MCNP Version 2C code. The main advantages for maintaining a multigroup version of MCNP are: 1) Solution of adjoint equation are possible with MCMG and 2) multigroup cross-sections sets prepared for Los Alamos discrete-ordinate codes can be utilized in MCMG.

The updated version of MCMG is currently being tested through comparisons with problems run with MCNP, ONEDANT, and TWODANT. A test problem designed to compute the photon fluxes transmitted through and reflected from a 10 centimeter iron slab was run to produce results to compare with an MCNP calculation. The source consisted of a 5-cm-thick slab of 1 MeV, isotropic photons adjacent to the iron slab. A 22-group photon cross-section set obtained from Doug O'Dell was used in the MCMG calculation. The comparison between MCNP and MCMG results is shown in Fig. 11.

TABLE IX

TRANSMITTED PHOTON ENERGIES AS A FUNCTION OF ANGLE (MeV/STERADIAN, NORMALIZED TO ONE INCIDENT ELECTRON) INCIDENT ELECTRON ENERGY = 1.1 MeV

Angular Bin (Degrees)	Photons Above 0.55 MeV	Photons Above 0.88 MeV	Photons Above 0.99 MeV
0 to 10	1.08e-03	2.17e-04	7.37e-05
10 to 20	1.05e-03	2.09e-04	7.05e-05
20 to 30	9.93e-04	1.93e-04	6.40e-05
30 to 40	8.99e-04	1.70e-04	5.49e-05
40 to 50	7.86e-04	1.43e-04	4.43e-05
50 to 60	6.79e-04	1.16e-04	3.39e-05
60 to 70	5.77e-04	9.16e-05	2.47e-05
70 to 80	4.71e-04	7.00e-05	1.73e-05
80 to 90	2.67e-04	3.91e-05	8.95e-06
Total Energy	4.00e-03	6.98e-04	2.09e-04

TABLE X

TRANSMITTED PHOTON NUMBERS AS A FUNCTION OF ANGLE (NUMBER/STERADIAN, NORMALIZED TO ONE INCIDENT ELECTRON) INCIDENT ELECTRON ENERGY = 1.1 MeV

Angular Bin (Degrees)	Photons Above 0.55 MeV	Photons Above 0.88 MeV	Photons Above 0.99 MeV
0 to 10	1.50e-03	2.25e-04	7.14e-05
10 to 20	1.46e-03	2.17e-04	6.83e-05
20 to 30	1.38e-03	2.01e-04	6.21e-05
30 to 40	1.26e-03	1.77e-04	5.32e-05
40 to 50	1.10e-03	1.49e-04	4.30e-05
50 to 60	9.57e-04	1.21e-04	3.29e-05
60 to 70	8.19e-04	9.61e-05	2.40e-05
70 to 80	6.71e-04	7.35e-05	1.69e-05
80 to 90	3.79e-04	4.11e-05	8.71e-06
Total Number	5.64e-03	7.29e-04	2.02e-04

TABLE XI

TRANSMITTED PHOTON ENERGIES AS A FUNCTION OF ANGLE (MeV/STERADIAN, NORMALIZED TO ONE INCIDENT ELECTRON) INCIDENT ELECTRON ENERGY = 5.0 MeV

Angular Bin (Degrees)	Photons Above 2.5 MeV	Photons Above 4.0 MeV	Photons Above 4.5 MeV
0 to 10	3.19e-02	5.65e-03	1.65e-03
10 to 20	3.06e-02	5.41e-03	1.59e-03
20 to 30	2.82e-02	4.92e-03	1.45e-03
30 to 40	2.44e-02	4.11e-03	1.18e-03
40 to 50	1.89e-02	2.94e-03	7.92e-04
50 to 60	1.36e-02	1.84e-03	4.30e-04
60 to 70	9.80e-03	1.13e-03	2.18e-04
70 to 80	6.75e-03	6.54e-04	1.05e-04
80 to 90	2.78e-03	2.27e-04	3.02e-05
Total Energy	8.68e-02	1.29e-02	3.38e-03

TABLE XII

TRANSMITTED PHOTON NUMBERS AS A FUNCTION OF ANGLE (NUMBER/STERADIAN, NORMALIZED TO ONE INCIDENT ELECTRON) INCIDENT ELECTRON ENERGY = 5.0 MeV

Angular Bin (Degrees)	Photons Above 2.5 MeV	Photons Above 4.0 MeV	Photons Above 4.5 MeV
0 to 10	9.82e-03	1.30e-03	3.53e-04
10 to 20	9.43e-03	1.25e-03	3.40e-04
20 to 30	8.71e-03	1.13e-03	3.08e-04
30 to 40	7.55e-03	9.48e-04	2.53e-04
40 to 50	5.87e-03	6.79e-04	1.69e-04
50 to 60	4.28e-03	4.27e-04	9.19e-05
60 to 70	3.11e-03	2.62e-04	4.68e-05
70 to 80	2.16e-03	1.53e-04	2.25e-05
80 to 90	8.98e-04	5.33e-05	6.51e-06
Total Number	2.71e-02	2.99e-03	7.22e-04

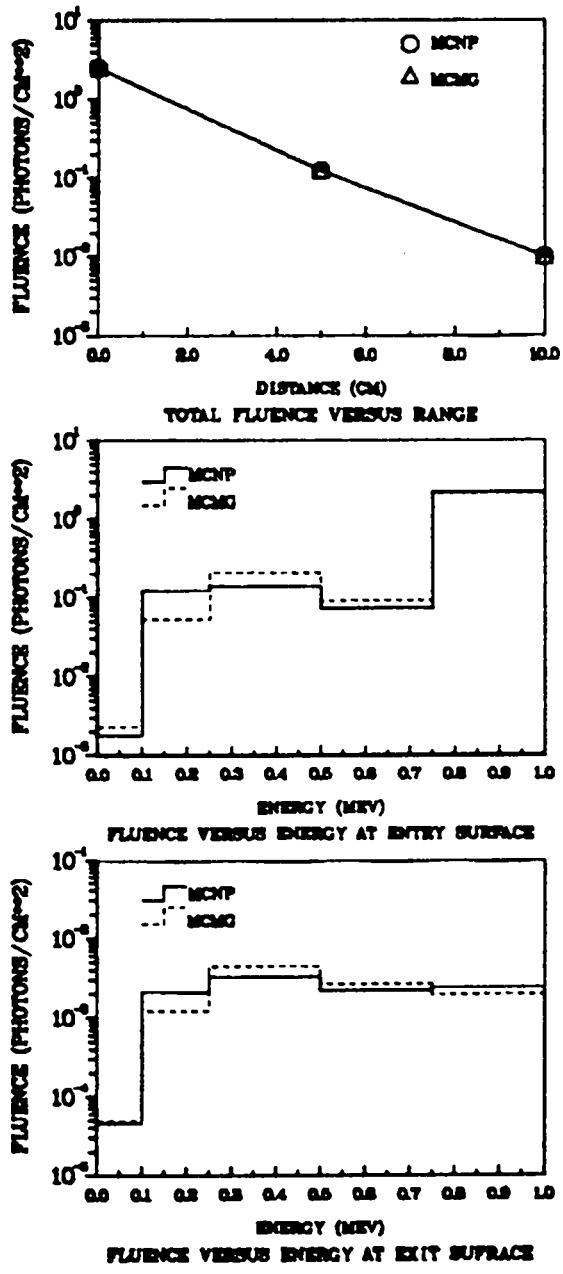

Fig. 11. MCMG-MCNP Comparison on Iron Slab Problem.

The upper plot shows the comparisons of total photon fluence at the entry surface, mid-way and exit surface of the iron slab. The two lower plots show the energy dependences of the fluences at the entry and exit surfaces of the iron slab. Since all source photons were 1-MeV photons, the 0.75 to 1.0 MeV

energy group shown in the center plot contains the uncollided fluence entering the slab while the lower energy groups contain only those fluences reflected back out of the iron slab.

Discussion of additional test problems being run with the MCMG program are included within the classified portion of the progress report.

Thus far, all test problems run with MCMG have utilized equiprobable step cosine bins for defining the scattering angle distribution. Both neutron and gamma-ray problems have been run, but no coupled problems have been run thus far.

J. MCMG Utilization and Adjoint Calculations (D. G. Collins)

Bill Taylor has updated the MCMG (Multigroup Monte Carlo) patch to version 2D of MCNP. At the same time the patch was reduced in size by removing much of the cross-section processing routines from the patch and incorporating those routines into a separate program named CRSRD.

As Mr. Taylor has been updating MCMG, I have been using the new version of the program to insure this version tracks problems that I had run with earlier versions of the code. I also have conducted an extensive review of the MCMG code in an effort to understand the methods employed to bias the sampling of the upscattered energy groups in adjoint calculations and to determine the cell and energy dependent importances.

MCMG currently allows the user to make a forward calculation to generate cell and energy dependent importances for an adjoint calculation, but does not provide for using adjoint fluxes to develop importances for a forward calculation. We plan to add this capability to MCMG.

Comparison between MCMG and ONEDANT and TWODANT are being continued. Since the same set of multigroup cross sections may be used in all three codes, these comparisons reveal the differences that one may expect between Monte Carlo and discrete ordinance calculations and help to determine which of the two methods is the more suitable for a particular type problem.

K. Total Gamma-Ray Yield Detector (D. G. Collins)

Several MCNP calculations have been made to aid in the design of a total gamma-ray yield detector. The design criteria has been to determine the optimum shape of a water filled chamber which will absorb a high percentage of

the energy within a collimated beam of gamma rays incident to the chamber. An additional criteria is to make the chamber as small as possible. Calculations of the gamma-ray energy leaking from spherical chambers and cylindrical chambers with hemispherical domes on either end have been made for collimated sources incident to the chambers. Monoenergetic gamma-ray sources of .5, 1., 2., 5., and 10 MeV and a fission gamma-ray source have been considered in the calculations.

L. 3D Graphics (CONPAR) (J. C. Ferguson)

MOVIE[29] is a utility which can produce quality 3D computer graphic displays, in either line drawing or shaded surface modes. It is available worldwide (a product of Brigham Young University), inexpensive (≈ $300), and efficiently maintained and improved by B.Y.U. It thus provides us with a product which is not only very useful, but codes based on it are transportable.

In order to significantly extend the applicability of the MOVIE program, CONPAR serves the purpose of transforming a set of constrained mathematical surfaces into the necessary polygonal geometry required by MOVIE. Surface segments are internally represented by parametric equations while constraint surfaces are defined implicitly. If a surface is to be used both for plotting as well as for a constraint, then it must have a dual representation.[30]

Applications to the MCNP program are quickly recognized since quadric and torii surfaces have dual representations. CONPAR is still in development. However, it has already been used on several MCNP geometry plotting tasks (see Figs. 12, 13, 14).

M. Sampling from a Cumulative Probability Distribution (R. G. Schrandt)

In Reference 31 a method of sampling from a cumulative probability distribution (cpd) is given. The algorithm was applied to the sampling of long energy-angle scattering functions in Reference 32.

The usual scheme of sampling a cpd of length ℓ uses a binary search. This can take some time if ℓ is large. This new method pre-calculates ℓ-1 conditional cdf $Q_j, j = 1 \text{ --- } \ell$, together with a pair of minimum and maximum indices $I_{1,j}$ and $I_{2,j}$. These indices can take on all values from 1 to ℓ. A random number ξ is chosen, and $j = 1 + \xi\,(\ell-1)$. The sampled index of the distribution is either $I_{1,j}$ if $\xi > Q_j$ or $I_{2,j}$ if $\xi \leq Q_j$.

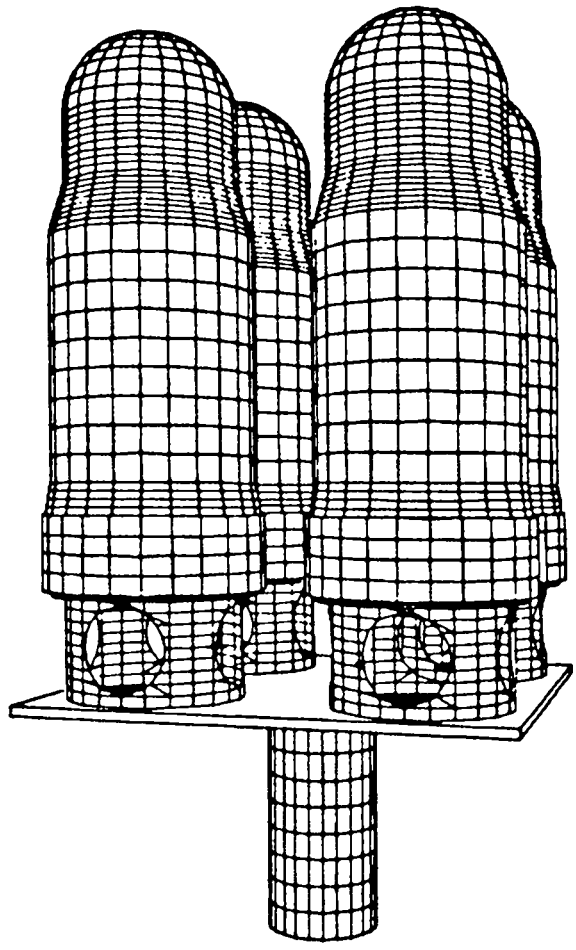

Fig. 12. Sample MCNP Geometry Plot using CONPAR.

The method is obviously directed toward vectorized sampling. It was decided to try the method in a scalar mode with the new standard sources of MCNP.

In one typical problem there were 10 source distributions of different lengths from 14 to 152. The longest distribution was only sampled 5% of the time, but there was one of length 101 that was sampled 36% of the time. There were about 1.3 collisions per particle started. It ran about 2.4% faster with this method compared to the binary search. A second but more artificial problem was run sampling a single source distribution of length 1000 in a void geometry. This ran about 7% faster with this scheme.

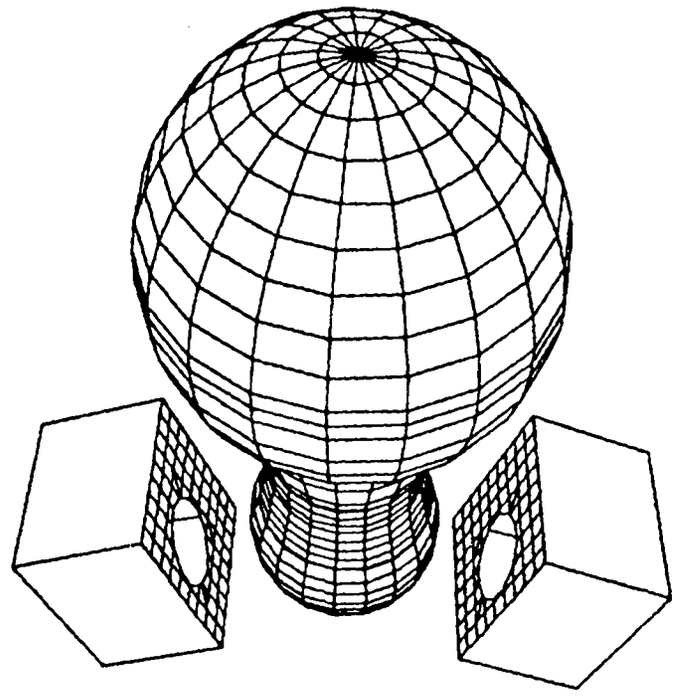

Fig. 13. Sample MCNP Geometry Plot using CONPAR.

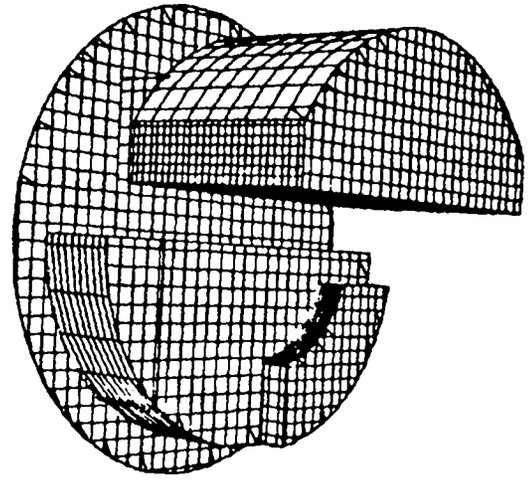

Fig. 14. Sample MCNP Geometry Plot using CONPAR.

One disadvantage to this method is the amount of storage required. For a distribution of length ℓ, $3(\ell-1)$ words are needed, although the indices could possibly be doubly stored.

A typical source distribution in MCNP would probably be of length less than 100. The savings in time in the scalar mode would be marginal, especially since very little time is typically spent anyway in MCNP in the source subroutine. A more practical application for this or some other such scheme might be in the total cross-section selection.

N. MCNP Testing (J. F. Briesmeister)

Version 2D of MCNP was tested and various new features were tried. Later Version 3 was tested against 2D using a wide variety of real problem input files. Certain sections of the manual were rewritten for clarity or to incorporate changes. A flow diagram of MCNP Version 2D and Version 3 was begun. A memo was written to W. L. Thompson detailing the setup and calculation of a beryllium problem he had requested. Experiments were performed by Basu et al.[33] to measure the neutron multiplication in beryllium produced by 14-MeV neutrons to check basic nuclear data. Using Version 2D of MCNP, our results (1.90) matched quite closely the calculated results (2.03) presented in the technical note, but did not agree with the experimental results (1.58) presented in the note for the 12-cm thickness case.

V. CROSS SECTIONS AND PHYSICS

A portion of our effort in Group X-6 is devoted to the acquisition, validating, and creating libraries of cross section for use in our deterministic and probabilistic codes. We also devote effort to supporting research and evaluation of physics models for radiation transport problems of interest.

In this report we present a discussion of Compton scattering of photons from electrons in thermal (Maxwellian) motion. We also report on the mean energy of Compton scattered photon from electron in thermal (Maxwellian) motion and the resultant electron heating.

A. Compton Scattering of Photons from Electrons in Thermal (Maxwellian) Motion (J. J. Devaney)

We have critically reviewed the exact Compton differential scattering of a photon from electrons distributed according to a relativistic Maxwell velocity distribution for possible use in transport codes.[24] Our study is based on the

form derived by Wienke using field theoretic methods.[34-40] If K' is the initial electron energy, m the electron rest mass energy, r_o the classical electron radius, T the temperature in energy units, ν' the initial photon energy, ν the final photon energy, θ the photon scattering angle, α' the angle between initial photon and electron momenta, α the angle between final photon and initial electron momenta, and ϕ the angle between the sides θ and α' in the spherical triangle θ,α',α, then the law of cosines gives

$$\cos\alpha = \cos\alpha' \cos\theta + \sin\alpha' \sin\theta \cos\phi \tag{168}$$

and we use the exact scattering expressions in the forms:

$$\kappa = \left(1 + (K'/m)\right) \tag{169}$$

$$\kappa_1 = \kappa - \sqrt{\kappa^2-1}\cos\alpha' \tag{170}$$

$$\kappa_2 = \kappa - \sqrt{\kappa^2-1}\cos\alpha \tag{171}$$

$$\mu = \cos\theta \tag{172}$$

$$K = \frac{(1-\mu)^2}{\kappa_1^2\kappa_2^2} - \frac{2(1-\mu)}{\kappa_1\kappa_2} + \frac{\nu'\kappa_1}{\nu\kappa_2} + \frac{\nu\kappa_2}{\nu'\kappa_1} \tag{173}$$

with relativistic Maxwellian (normalized)

$$f(K') \equiv \left[4\pi m^2 T K_2(m/T)\right]^{-1} e^{-(m+K')/T} \quad , \tag{174}$$

where K_2 is the modified Bessel function of the second kind and order. Our differential photon scattering cross section into solid angle $d\Omega$ is then:

$$\frac{d\sigma}{d\Omega} = \frac{r_o^2}{2}\int dK' \cdot (K' + m) \cdot \sqrt{K'^2 + 2mK'} \cdot f(K') \cdot \frac{1}{\kappa\kappa_1} \cdot \left(\frac{\nu}{\nu'}\right)^2$$

$$\times K \cdot d\cos\alpha' \cdot d\phi \tag{175}$$

The Compton energy relation becomes:

$$\kappa_1 m\nu' = \nu\nu'(1-\mu) + \kappa_2 m\nu \quad . \tag{176}$$

These last two relations reduce in the limit T→o to the standard Klein-Nishina formula and the Compton energy relations, respectively:[41]

$$\frac{d\sigma}{d\Omega} = \frac{r_o^2}{2}\left(\frac{\nu}{\nu'}\right)^2\left[\frac{\nu'}{\nu} + \frac{\nu}{\nu'} + \mu^2 - 1\right] \tag{177}$$

$$m\nu' = \nu\nu'(1-\mu) + \nu m \quad . \tag{178}$$

We have verified the derivation of the above exact formulas,[42,43] Eqs. (168)-(176) and have checked them numerically over the ranges $1 \leq T \leq 100$ keV, $1 \leq \nu' \leq 1000$ keV, and $0 \leq \theta \leq 180°$.

In addition we have critically reviewed the Wienke-Lathrop Isotropic Approximation[44] and its development. We verified its plausibility derivation and numerically checked its accuracy against the exact theory. Although for worst combination of parameters in our range of interest, to wit $\nu' = 1$ keV, $T = 100$ keV, and $\theta = 180°$, the error can be as high as -28%, we find the approximation to be simple, only one integration, and reasonably accurate (≈5-8% mid-range). The form of the approximation used by us was

$$\frac{d\sigma}{d\theta} = r_o^2 \cdot \frac{\sin\theta}{\kappa^2} \int_o^{\pi} d\phi \left(\frac{\nu}{\nu'}\right)^2 \left[\frac{(1-\mu)^2}{(\kappa\kappa_2)^2} - \frac{2(1-\mu)}{\kappa\kappa_2} + \frac{\nu'\kappa}{\nu\kappa_2} + \frac{\nu\kappa_2}{\nu'\kappa}\right] \quad . \tag{179}$$

Actually the ϕ-integration has been performed by us, but the result is complicated and is the small difference of large quantities so that numerical integration of Eq. (179) is both simpler and for smaller computers, more accurate.

In Eq. (179), κ is now:

$$\kappa = \sqrt{1 + \frac{3T}{m}\left[1 + 20\left(\frac{T}{8m}\right) + 120\left(\frac{T}{8m}\right)^2 - 960\left(\frac{T}{8m}\right)^3 + 4320\left(\frac{T}{8m}\right)^4 + \ldots\right]} \tag{180}$$

and κ_2 is:

$$\kappa_2 = \kappa - \sqrt{\kappa^2-1} \cdot (\sin\theta \cos\phi) \tag{181}$$

with Compton energy relation:

$$\kappa\, m\nu' = \nu\nu'(1-\mu) + \kappa_2 m\nu \quad . \tag{182}$$

Eqs. (179) and (182) also reduce in the limit T→0 to the Klein-Nishina and Compton energy equations, Eqs. (177) and (178), respectively.

We studied also the Wienke-Lathrop one-parameter Fitted Approximation, but found it of only slightly less complication than the Isotropic Approximation and considerably less accurate. However, its merit is the substitution of a table or a graph for an integration, and that may be of value to some. Moreover, additional parameters may be used in the approximation to improve accuracy.

By numerical verification we determined that the Cooper-Cummings[45] total cross-section approximation is simple and accurate (error $\leq$1%). It is given as a ratio of the T≠0 to T=0 Compton total cross sections, σ_c:[45]

$$\sigma_c(\nu',T) = \sigma_c(\nu',T=0) \cdot \left[1 - \frac{\nu' T}{47703 + 637.69\nu'} \right] . \tag{183}$$

The Compton total cross sections for T=0 may be found in Heitler.[41] They are, for $\gamma \equiv \nu'/m$:

For γ small, it is best to use:

$$\sigma_c \simeq \frac{8\pi r_o^2}{3} \left(1-2\gamma + \frac{26}{5}\gamma^2\right) \tag{184}$$

because smaller computers may fail to compute logarithms accurately in the exact expression:

$$\sigma_c\ (T=0) = 2\pi r_o^2 \left\{ \frac{(1+\gamma)}{3}\left[\frac{2\gamma(1+\gamma)}{1+2\gamma} - \ell n(1+2\gamma)\right] + \frac{1}{2\gamma}\,\ell n\ (1+2\gamma) \right.$$

$$\left. - \frac{(1+3\gamma)}{(1+2\gamma)^2} \right\} . \qquad (185)$$

The Thomson scattering cross section is of course $8\pi r_o^{2/3}$. Other total cross-section approximations investigated turned out to be considerably less accurate.

We recommend the ordinary Klein-Nishina Formula for most problems up to an electron temperature of 10 keV. The formula is already in the Monte Carlo Code MCNP and other Los Alamos codes. One may then expect accuracies of better than 1.5% in the total Compton cross section (maximum ν' = 1000 keV) and about 5% or better in the differential cross section. For higher accuracies or for special results, such as for example photon energy upscatter, one should use the full temperature dependent theories. Even as high as T = 25 keV, the error of the total Compton (Klein-Nishina) cross section is 3.6% or less (maximum ν' = 1000 keV) and of the differential cross section is of the order of or less than 10%. (Specifically at T = 25 keV, ν' = 25 keV the errors are +5.8% at θ = 45°, +8% at 90°, and -0.9% at 135°). At 1 keV temperature the error of the total Klein-Nishina cross section is 0.15% (ν' = 1000 keV) or less, and the errors of the Klein-Nishina differential cross section is 0.5% or less.

For higher temperatures (than say 10 keV or so), greater accuracies, or better specific detail, we recommend use of the exact equations as summarized above. This recommendation is only made with the proviso that an efficient computational algorithm can be found. Otherwise, we recommend the Wienke-Lathrop Isotropic Approximation summarized above with numerical integration over ϕ. Such approximation should be limited to $0 < T \leq 100$ keV and $1 \leq \nu' \leq 1000$ keV.

B. Mean Energy of Compton Scattered Photons from Electrons in Thermal (Maxwellian) Motion. Heating (J. J. Devaney)

In addition to the differential cross section for the Compton Scattering of photons from electrons in thermal motion (relativistic Maxwellian), one is of course interested in the energy of the scattered photon and the consequent energy deposition or heating of the electrons. We give the mean scattered photon energy and the mean heating of the electron gas by the photon scattering. Both quantities are given as a function of the photon scattering angle,

θ, the electron temperature, T, and the incident photon energy, ν'. We compare these means, $\langle\nu\rangle$ and $\langle H\rangle$, as calculated exactly, as calculated with the Wienke-Lathrop Isotropic and One-parameter Fitted Approximations, as well as with the unmodified, regular, T = 0, Compton Energy Equation results.

For the exact equation, averaging over the relativistic Maxwellian parameters, ϕ, α', and K' we obtain the mean heatings, $\langle H\rangle$:

$$\langle H\rangle_{\phi,x,\kappa} \equiv \langle H\rangle = \frac{m^3\nu'}{\gamma}\int_1^\infty \kappa d\kappa \cdot \sqrt{\kappa^2-1}\cdot e^{-(m\kappa/T)}$$

$$\times\left[(1-\mu) - \frac{1}{2\sqrt{\kappa^2-1}}\,(c+\kappa)(1-\mu) - c\right]\cdot \ell n\left|\frac{c+\kappa+\sqrt{\kappa^2-1}}{c+\kappa-\sqrt{\kappa^2-1}}\right| \quad , \qquad (186)$$

where the notation comes from the preceding article.

$$\gamma \equiv m^2\, T\, K_2\,(m/T) \qquad (187)$$

$$\kappa = 1 + (K'/m) \qquad (188a)$$

$$c \equiv (\nu'/m)(1-\mu) \quad . \qquad (188b)$$

The mean scattered photon energy is:

$$\langle\nu\rangle = \nu' - \langle H\rangle \quad . \qquad (189)$$

For the Wienke-Lathrop Isotropic Approximation[44] we obtain the heating:

$$\langle H_I\rangle = \nu'\left[1 - \frac{\kappa}{\sqrt{(c+\kappa)^2 - (\kappa^2-1)(1-\mu^2)}}\right] \quad , \qquad (190)$$

where κ is given by Eq. (180). The mean scattered photon energy is:

$$\langle\nu_I\rangle = \nu' - \langle H_I\rangle \quad .$$

We do not reproduce here the Fitted Approximation formulas which we do not recommend.

The regular Compton (T = 0) scattered photon energy is of course:

$$\nu = \nu'/(c+1) \tag{191}$$

and heating

$$H = \nu'-\nu \quad . \tag{192}$$

By the above formulas we calculated the mean energy of a photon scattered from a Maxwell distributed electron gas by four methods: Exactly; by the Wienke-Lathrop Isotropic and One-parameter Fitted Approximations; and by the standard (temperature T = 0) Compton Energy Equation. To about 4% error the simple Compton (T = 0) Equation is adequate up to 10 keV temperature. Above that temperature the Exact calculation is preferred if it can be efficiently coded for practical use. The Isotropic Approximation is a suitable compromise between simplicity and accuracy, but at the extreme end of the parameter range, we have considered (T = 100 keV incident photon energy ν' = 1 keV, scattering angle θ = 180°), the error is as high as -28%. For mid-range values like 10 to 25 keV, the errors are a percent or so up to 8%. The Fitted Approximation is generally found to have large errors and is consequently not recommended.

The energy deposited in the electron gas by the Compton scattering of the photon, i.e., the heating, is only adequately given for all parameters in the ranges $1 \leq T \leq 100$ keV and $1 \leq \nu' \leq 1000$ keV by the exact expression. For low depositions the heating is the difference between two large quantities, one approximate, and so can lead to order of magnitudes errors. However, for scattered photon energy $\nu \gg T$ the Isotropic Approximation does well, (0.13% error for ν' = 1000 keV, θ = 180°, T = 10 keV, ν = 790.7 keV, and 2.7% error for ν' = 1000 keV, θ = 90°, ν = 583.5 keV, T = 100 keV). The regular T = 0 Compton also does well for $T \leq 10$ keV and $\nu \gg T$. (0.7% for ν' = 1000 keV, θ = 180°, T = 10 keV, ν = 790.7 keV, and 0.08% for ν' = 1000 keV, θ = 180°, T = 1 keV, ν = 795.9 keV). The Fitted Approximation is without merit for heating.

REFERENCES

1. R. D. O'Dell, F. W. Brinkley, Jr., and D. R. Marr, "User's Manual for ONEDANT: A Code Package for One-Dimensional, Diffusion-Accelerated Neutral-Particle Transport," Los Alamos National Laboratory report LA-9184-M (February 1982).

2. R. E. Alcouffe, F. W. Brinkley, D. R. Marr, and R. D. O'Dell, "User's Manual for TWODANT: A Code Package for Two-Dimensional, Diffusion-Accelerated, Neutral-Particle Transport," Los Alamos National Laboratory Report (in preparation).

3. R. Douglas O'Dell, "Standard Interface Files and Procedures for Reactor Physics Codes, Version IV," Los Alamos Scientific Laboratory report LA-6941-MS (September 1977).

4. D. R. Ferguson and K. L. Derstine, "Optimized Iteration Strategies and Data-Management Considerations for Fast Reactor Finite Difference Diffusion Theory Codes," Nucl. Sci. Eng. 64, No. 2, 593-604 (1977).

5. W. F. Walters, R. D. O'Dell, and F. W. Brinkley, Jr., "THREETRAN (hex,z) User's Manual," Los Alamos Scientific Laboratory report LA-8089-M (October 1979).

6. W. F. Walters and R. D. O'Dell, "A Three-Dimensional Hexagonal-Z Difference Scheme for Discrete-Ordinates Codes," Proc. Am. Nucl. Soc. Top. Meeting on Computational Methods in Nuclear Engineering, Williamsburg, Virginia, April 23-25, 1979, Vol. 2, pp. 4-50, 4-63.

7. K. D. Lathrop and F. W. Brinkley, Jr., "TWOTRAN-II: An Interfaced, Exportable Version of the TWOTRAN Code for Two-Dimensional Transport," Los Alamos Scientific Laboratory report LA-4848-MS (July 1973).

8. K. D. Lathrop and B. G. Carlson, "Discrete-Ordinates Angular Quadrature of the Neutron Transport Equation," Los Alamos Scientific Laboratory report LA-3186 (September 1964).

9. Klaus Kufner and Renate Heger, "DIAMANT2 Ein Multigruppen Neutronen-transportprogramm fu Dreiecks- und Hexagonalgeometrie," Kernforschungs-zentrum Karlsruhe, Institut fur Neutronenphysik und Reaktortechnik, Projekt Schneller Bruter KFK report 3033 (September 1980) (in German).

10. R. E. Alcouffe, "Diffusion Synthetic Acceleration Methods for the Diamond-Differenced Discrete-Ordinates Equations," Nucl. Sci. Eng. 64, 344 (1977).

11. E. W. Larsen, "Diffusion Synthetic Acceleration Methods for the Discrete Ordinates Equations," Proc. of Top. Meeting on Adv. in Reactor Computations, Amer. Nucl. Soc., Salt Lake City, Utah, March 28-31, 1983, p. 705.

12. J. E. Morel and G. R. Montry, "Analysis and Elimination of the Discrete-Ordinates Flux Dip," Proc. of Top. Meeting on Adv. in Reactor Computations, Amer. Nucl. Soc., Salt Lake City, Utah, March 28-31, 1983, p. 796.

13. V. Y. Gol'din, "A Quasi-Diffusion Method for Solving the Kinetic Equation," USSR Comp. Math and Math Physics 4, 6, 136 (1967).

14. E. E. Lewis and W. F. Miller, Jr., "A Comparison of P_1 Synthetic Acceleration Techniques," Trans. Am. Nucl. Soc. 23, 202 (1976).

15. W. F. Miller, Jr., "Generalized Rebalance: A Common Framework for Transport Acceleration Methods," Nucl. Sci. Eng. 65, 226 (1978).

16. E. W. Larsen, "On Numerical Solutions of Transport Problems in the Diffusion Limit," Nucl. Sci. Eng. 83, 90 (1983).

17. R. D. O'Dell and R. E. Alcouffe, "Transport and Reactor Theory, January 1 through March 31, 1982," Los Alamos National Laboratory report LA-9451-PR (August 1982), p. 46.

18. E. W. Larsen, "A Sharper Version of the Cauchy-Schwarz Inequality for Real-Valued Functions," this progress report.

19. R. D. O'Dell and R. E. Alcouffe, "Transport and Reactor Theory, April 1-June 30, 1982," Los Alamos National Laboratory report LA-9533-PR (September 1982).

20. J. A. Fleck and J. D. Cummings, "An Implicit Monte Carlo Scheme for Calculating Time and Frequency Dependent Nonlinear Radiation Transport," J. Comp. Phys. 8, 313 (1977).

21. L. L. Carter and C. A. Forest, "Nonlinear Radiation Transport Simulation with an Implicit Monte Carlo Method," Los Alamos Scientific Laboratory report LA-5038 (January 1973).

22. G. H. Hardy, J. E. Littlewood, and G. Polya, Inequalities (Cambridge University Press, Cambridge, 1934).

23. E. F. Beckenbach and R. Bellman, Inequalities (Springer-Verlag, New York, 1965).

24. Los Alamos Monte Carlo Group, "MCNP - A General Monte Carlo Code for Neutron and Photon Transport, Version 2B," Los Alamos National Laboratory report LA-7396-M, Revised (April 1981).

25. American National Standard ANSI X3.9-1978, "Programming Language FORTRAN," American National Standards Institute, Inc., New York (April 1978).

26. American National Standard ANSI X3.9-1966, "USE Standard FORTRAN," American National Standards Institute, Inc., New York (March 1966).

27. Thomas E. Booth, "A Weight Window/Importance Generator for Monte Carlo Streaming Problems," Proc. of Sixth International Radiation Shielding Conference, Tokyo, May, 1983.

28. J. A. Halbleib, Sr. and W. H. Vandevender, "CYLTRAN: A Cylindrical Geometry Multimaterial Electron/Photon Monte Carlo Transport Code," Sandia Laboratories report SAND 74-0030 (1974).

29. "MOVIE: A General Purpose Computer Graphics System," Computer Graphics Document GR834, Los Alamos National Laboratory, August, 1982.

30. James C. Ferguson, "Dual Representation for Display of Complex Monte Carlo Geometric Configurations," Los Alamos National Laboratory document LA-UR-81-2508 (August 14, 1981).

31. Forrest Brown, William Martin, and Donald Calahan, "A Discrete Sampling Method for Vectorized Monte Carlo Calculations, Trans. Am. Nucl. Soc. 38, 354, (June 1981).

32. J. J. Tang, "Vectorized Sampling," Oak Ridge National Laboratory memorandum to W. A. Rhoades, July 1, 1981.

33. T. K. Basu, V. R. Nargundkar, P. Cloth, D. Filges, and S. Taczanowski, "Neutron Multiplication Studies in Beryllium for Fusion Reactor Blankets," Nucl. Sci. Eng. 70, No. 1 (1979).

34. Particularly Eq. (1) of B. R. Wienke, J. Quant. Spect. Rad. Transf., 19, (1978) 163. "Moment-Generated Radiative-Transfer Functions for Relativistic Maxwellian Electrons."

35. The derivation of the expression in Ref. 1 Eq. (1) is found in B. R. Wienke, "Relativistic Invariance and Photon-Electron Scattering Kernels in Transport Theory," Nucl. Sci. Eng. 52, 247 (1973).

36. B. R. Wienke, "Mean, Mean-Square, and Most-Probable Momentum for a Relativistic Maxwellian Ensemble," Am. J. of Phys. 43, 317 (1975).

37. B. R. Wienke, "Equivalence of Transformed and Invariant Radiative Transfer Kernels," Nucl. Sci. Eng. 60, 101 (1976).

38. B. R. Wienke, "Relativistic Compton Scattering from Moving Electrons and Angular Moments," J. Quant. Spect. Rad. Transf. 15, 151 (1975).

39. B. R. Wienke, "Electron Transport and Small Angle Collisions, "J. Quant. Spect. Rad. Transf. 22, 301 (1979).

40. B. R. Wienke, "Reduction of Azimuthally Symmetric Collision Kernels," J. Quant. Spect. Rad. Transf. 24, 385 (1980).

41. W. Heitler, The Quantum Theory of Radiation, 3rd ed. (Oxford University Press, New York, 1954), p. 219.

42. W. Pauli, "Uber die Intensitat der Streustrahlung bewegter freier Elektromen," Helv, Phys. Acta, 6, 279 (1933).

43. V. L. Ginzburg and S. I. Syrovat-Skii, "Gamma and X-Radiation Connected with Galactic and Metagalactic Cosmic Rays," Sov. Phys. JETP 19, 1255 (1964).

44. B. R. Wienke and B. L. Lathrop, "Fast Scheme for Photon-Maxwellian Electron Cross Sections," to be published in Trans. Am. Nucl. Soc.

45. G. E. Cooper and J. D. Cummings, "A Simple Fit for the Hot Compton Cross Section," Lawrence Livermore National Laboratory report UCID-15917 (September 28, 1971).

 ☆U.S. GOVERNMENT PRINTING OFFICE:1984—776-026 / 4075

Printed in the United States of America
Available from
National Technical Information Service
US Department of Commerce
5285 Port Royal Road
Springfield, VA 22161

Microfiche (A01)

Page Range	NTIS Price Code	Page Range	NTIS Price Code	Page Range	NTIS Price Code	Page Range	NTIS Price Code
001-025	A02	151-175	A08	301-325	A14	451-475	A20
026-050	A03	176-200	A09	326-350	A15	476-500	A21
051-075	A04	201-225	A10	351-375	A16	501-525	A22
076-100	A05	226-250	A11	376-400	A17	526-550	A23
101-125	A06	251-275	A12	401-425	A18	551-575	A24
126-150	A07	276-300	A13	426-450	A19	576-600	A25
						601-up*	A99

*Contact NTIS for a price quote.

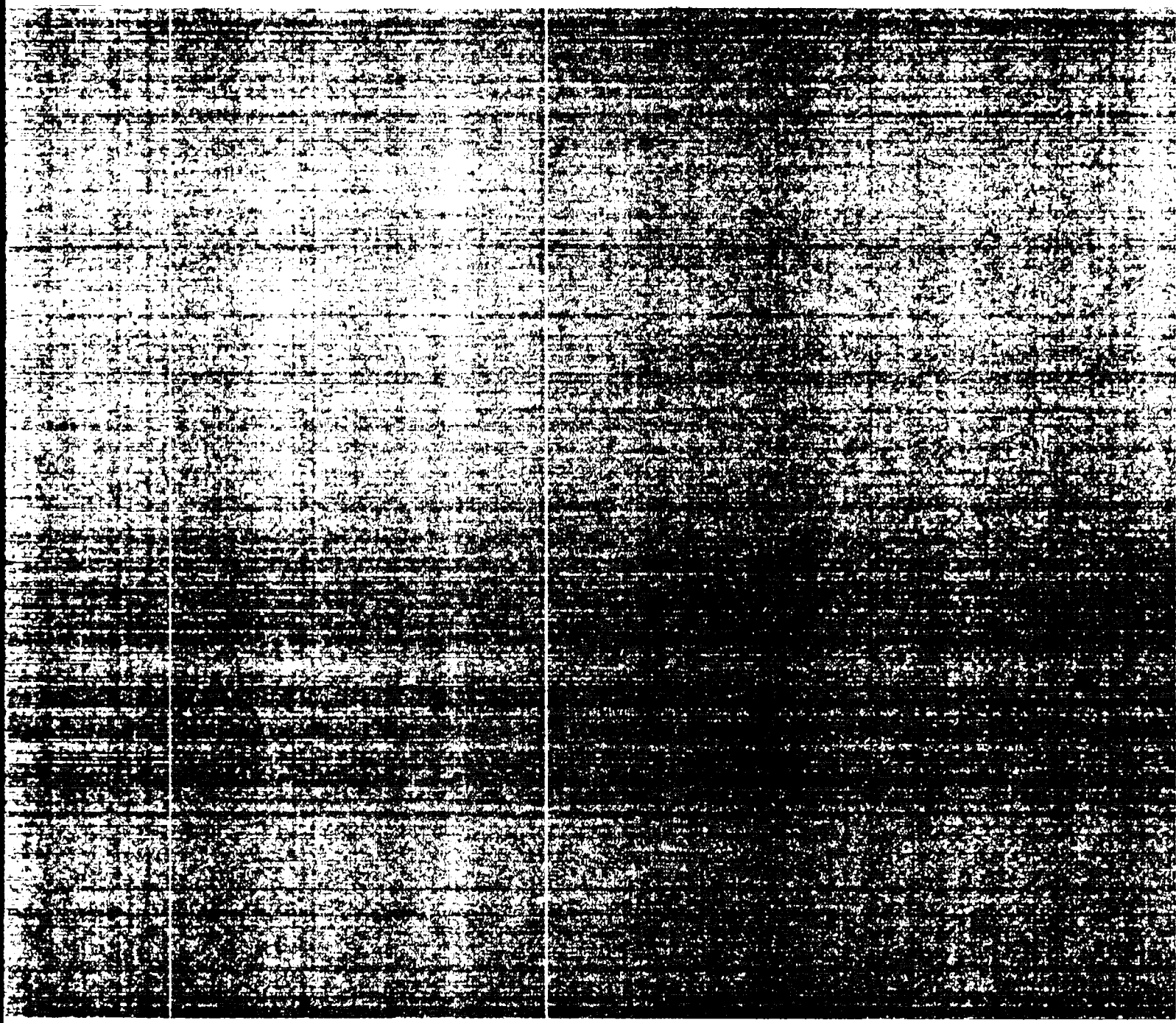

Los Alamos